THE DETERMINATION OF THE CROSS-SECTIONAL SHAPE AND AREA OF NORMAL AND HEALING LIGAMENTS USING LASERS

by

Daniel Kunbyul Moon

B.S. in Biomedical Engineering, Virginia Commonwealth University, 2002

Submitted to the Graduate Faculty of

The School of Engineering in partial fulfillment

of the requirements for the degree of

Master of Science in Bioengineering

University of Pittsburgh

2004

UNIVERSITY OF PITTSBURGH

SCHOOL OF ENGINEERING

This thesis was presented

by

Daniel Kunbyul Moon

It was defended on

August 31, 2004

and approved by

Richard E. Debski, Ph.D., Assistant Professor,
Department of Bioengineering

Zong-Ming Li, Ph.D., Assistant Professor,
Departments of Orthopaedic Surgery, Bioengineering, Occupational Therapy

Patrick J. McMahon, M.D., Assistant Professor,
Department of Orthopaedic Surgery

Thesis Advisor: Savio L-Y. Woo, Ph.D., D.Sc. (hon.), W.K. Whiteford Professor,
Departments of Bioengineering, Mechanical Engineering, Rehabilitation Science & Technology

THE DETERMINATION OF THE CROSS-SECTIONAL SHAPE AND AREA OF NORMAL AND HEALING LIGAMENTS USING LASERS

Daniel Kunbyul Moon, M.S.

University of Pittsburgh, 2004

The reported biomechanical properties of soft tissues are often dependent on the method used to determine specimen cross-sectional area as this is an important factor in tissue stress calculations. Cross-sectional shape is also important, especially for documenting morphological changes in the tissue during healing. Successful measurement of these geometric characteristics, however, has been hindered by the complex geometry of many biological tissues, as well as concerns regarding the deformability of these tissues under mechanical contact. The overall objective of this thesis was to evaluate the cross-sectional shape and area of normal and healing ligaments using laser-based devices. Lasers allow for measurements without inducing mechanical contact and deformation. Initially, the effects of treatment with a bio-scaffold, small intestinal submucosa (SIS), on the cross-sectional shape and area of healing ligaments were evaluated using the laser micrometer system. However, due to limitations of currently available methods such as the inability to detect concavities, a new system was also developed and evaluated.

The cross-sectional shape and area of non-treated healing and SIS-treated healing rabbit MCLs were assessed using a laser micrometer system 26 weeks after gap injury. No significant

changes in shape were detected between SIS-treated and non-treated MCLs ($p>0.05$). However, SIS-treatment significantly reduced the cross-sectional area at 26 weeks after injury in comparison to the non-treated group ($p<0.05$).

A charge coupled device (CCD) laser reflectance system was developed in order to determine the cross-sectional shape and area of tissues containing surface concavities. For this system, a CCD laser displacement sensor recorded distance measurements off a specimen while it rotated 360°. The area and shape could then be determined from this data. The system was evaluated using geometric shapes of known cross-sectional area before being applied to biological specimens.

This work demonstrated that cross-sectional shape and area measurements can be used to quantify tissue healing and remodeling. Additionally, the CCD laser reflectance system successfully detected concavities on the surfaces of tissues and therefore is a viable approach to biological tissue measurement. However, this system does not offer much improvement in accuracy over the laser micrometer system for tissues that do not have significant concavities.

TABLE OF CONTENTS

LIST OF TABLES

LIST OF FIGURES

PREFACE

Wow! What an interesting journey it's been so far. As my mind transcends back in time, I realize that these next hundred pages do not just reflect the work I did for these past two and a half years, but it reflects a culmination of my experiences these past 24 years: from the time when I, as a child would catch an assortment of wild animals from insects to turtles and try to raise them; to high school when I would fix luggage for my parent's business; to when I helped cardiothoracic surgeons do research in college; and now this. However, all of this would not have been possible, or as enjoyable, without having great teachers: my parents who were strict yet in the end stepped aside to let me do my own thing and kept believing in me; my teachers in high school who were frustrated with me and kept giving me detentions to try to put me back on the right track; my college professors (Dr. Miller, Dr. Bowlin, Dr. Wayne, Dr. Conway, Dr. Deanda and Dr. Tang) who helped foster my interest in bioengineering and research; and finally Professor Savio L-Y. Woo, my primary academic advisor and mentor, who is always helping me to try to reach my full potential and beyond. And how can I forget all the friendships that have been forged, especially these past couple years. I would especially like to thank my wonderful summer students, Kelly and Erik, who have helped me immensely and allowed me realize the joy of not only research but also teaching and mentoring. Steve, Yoshi, Danny, Jesse, Susan, Maribeth, Andy, Charu, Eric, Wei, Fengyan, Rui, Tom, Yuji, Dimos, Yunxia, Rob, Jens, Ryan and Tan, I really don't think I could have made it through this difficult ordeal and had so much fun at the same time without having you all around.

Finally, I would like to thank my committee members, Drs. Debski, McMahon and Li, for all their help and guidance along the way. As well as the Musculoskeletal Research Center, Dr. Borovetz, the Department of Bioengineering and NIH grant 41820 for their funding support.

1.0 MOTIVATION

Ligaments are bands of connective tissue which connect bones together and transfer tensile forces to help mediate diarthrodial joint motion. They perform this function by guiding joint motion at lower loads and then by limiting excessive displacements between the joint surfaces at higher loads due to their nonlinear mechanical properties. Injuries to ligaments resulting from excessively high loads experienced during accidents and sports can often lead to joint instability and absences from work and athletic activities. In addition, a joint with a ruptured ligament can overload other soft tissues in and around the joint and eventually cause more damage that leads to pain, morbidity and osteoarthritis.

With the increasing activity level and average life span of the general population, the incidence of ligament injuries has been on the rise. For young and active individuals participating in sports activities, the anterior cruciate ligament (ACL) and medial collateral ligament (MCL) of the knee are especially susceptible to injuries. Tears of these two ligaments account for as much as 90% of all sports related injuries to the knee ligaments [1]. It is estimated that nearly 150,000 new ACL injuries and as many as 95,000 new MCL injuries occur annually in the United States [2]. In addition, nearly 45,000 ACL-MCL combined injuries also occur annually. Injuries to the posterior cruciate ligament (PCL) are not as common, accounting for around 5% of all knee ligament injuries in the general population, but nearly 60% of the knee ligament injuries treated in emergency rooms involve the PCL [2].

Injuries to the MCL have been shown to heal and its function can return to near normal levels between 6 to 12 weeks with non-surgical treatment [3-5]. Laboratory studies have also shown that the structural properties of the femur-MCL-tibia complex become similar to that of the intact ligament while the mechanical properties, histomorphology and biochemical composition of the healing tissue remain far inferior to the intact MCL and can remain so for up to two years [6-10]. However, these studies also found that the MCL is able to restore its structural properties through a compensatory overgrowth of healing tissue, which is of inferior quality. Because of the MCL's ability to heal, a large amount of scientific research has been done to examine its healing process, as well as focusing on developing methods to improve the mechanical properties of the healing tissue.

The ACL and PCL on the other hand, cannot heal after a complete rupture in their midsubstance [11-13]. Therefore they are often surgically replaced by tendon grafts [14, 15]. Although these reconstructions help partially restore function to the knee and enable the patient to resume normal as well as sports activities, biomechanical studies have revealed that these reconstructions do not completely restore ligament function [16, 17]. Concomitantly, a percentage of patients with ligament reconstructions have experienced less than satisfactory results at both short and long-term clinical follow-up [18-22]. The factors that contribute to these failures are numerous and are not completely understood. Therefore, more laboratory as well as clinical studies will be needed to better understand the very complex function of the ACL and PCL as well as the its replacement grafts.

The primary function of ligaments is to transmit tensile forces between bones in order to maintain joint stability. Therefore uniaxial tensile tests of bone-ligament-bone complexes are done in the laboratory to characterize their biomechanical properties, as well as their contribution

to joint kinematics. Specifically, the mechanical properties of ligaments reflect their intrinsic properties that are based on the composition and organization and interaction of all the biochemical constituents, particularly type I collagen [23, 24]. Thus, changes of the tissue matrix constituents of a ligament during healing and remodeling will alter its mechanical properties.

It is well known that it is not straight forward to determine the mechanical properties of ligaments in the laboratory. Specifically, the measurement of the stresses and strains during a uniaxial tensile test involve significant care and requirement of very special instruments. Literature has shown that the tensile strains in the ligament midsubstance can be determined in a non-contact manner by the use of contrast markers or dye and optical tracking its elongation with video cameras [25, 26]. The Lagrangian stress, defined as tensile force divided by initial cross-sectional area, assumes that there is a uniform cross-sectional area and shape along the ligament. Thus, the accuracy of determining the Lagrangian stress depends on the accurate determination of the cross-sectional area of the ligament.

Further, the cross-sectional area and shape can be used to describe a tissue's anatomy and associated changes during healing and remodeling. In addition, knowledge of the three dimensional anatomy and geometry, i.e. the shape and area along the length of the specimen, has been used to correlate the shape with its properties and function [27] and its growth and remodeling during the healing process. In other words, these data can help with the selection of biological substitutes (e.g. tendon grafts) for reconstruction, as well as establishing mathematical modeling of these soft tissues. It will also be possible to assess whether a treatment can reduce excessive tissue hyper-proliferation of the healing ligament and whether its cross-sectional shapes are similar to that of a normal intact ligament.

In the literature, many methods have been developed and used to measure the cross-sectional shape and area of soft tissues. Some of the popular methods include calipers [28] and the constant pressure area-micrometer [29]. In addition to the assumption of a specific geometrical shape a priori, these methods can introduce error through mechanical contact with the soft tissue. Another technique, the "casting method" is labor intensive and time consuming since it involves the process of making molds of the ligament and casting with bone cement to create replicas which are then sliced and photographed to determine cross-sectional area [30]. Most importantly, this method has not been validated with objects of known cross-sections. Others have developed non-contact methods and these include the "shadow amplitude method [31] and the laser micrometer system [32, 33]. While these methods do not deform the cross-section of the ligament during measurements, they could not account for concavities of the cross-section. Also, the laser micrometer is quite expensive. Therefore, there is a need for a device that can measure the cross-sectional area and shape of soft tissues with concavities in order to more accurately study their mechanical properties and complex geometries. Additionally, such a device should be relatively inexpensive (under $5,000) in order for it to be easily adopted by other research laboratories, thereby allowing for comparison of data.

Thus, the major objective of this thesis was to accurately measure the cross-sectional shape and area of normal and healing ligaments. This was initially done on the rabbit MCL model using the laser micrometer system to assess the effects of treatment with a bioscaffold on the cross-sectional shape and area of the healing ligament. However, this first study raised some concerns on whether concavities in the healing MCL could cause error in the measurement of cross-sectional shape and area. Therefore, a new system was developed that could detect concavities in the cross-section so more accurate measurements of these properties could

potentially be taken on the MCL, as well as other ligaments and tendons such as the ACL, PCL and the patellar tendon.

2.0 BACKGROUND

2.1 GROSS ANATOMY

The knee is comprised of several diarthrodial joints, the patello-femoral joint, the tibiofibular joint and the tibiofemoral joint. The tibiofemoral joint, which allows relative motions between the thigh and shank, is the major joint in the knee and is formed between the two condyles at the distal femur and the tibial plateau of the proximal tibia. Both of these articulating surfaces are covered with cartilage to reduce friction and provide for a smooth gliding movement between the bones. The tibiofemoral joint is stabilized by several passive structures. The lateral and medial menisci are semicircular fibrocartilaginous wedges attached primarily to the tibial plateau. The menisci conform to the articulating surfaces of the femur and tibia to increase the contact area of the joint and distribute loads. Four major knee ligaments consisting of two extra-articular, the MCL and lateral collateral ligament (LCL) and two intra-articular ligaments, the ACL and PCL, connect the femur to the tibia (Figure 1).

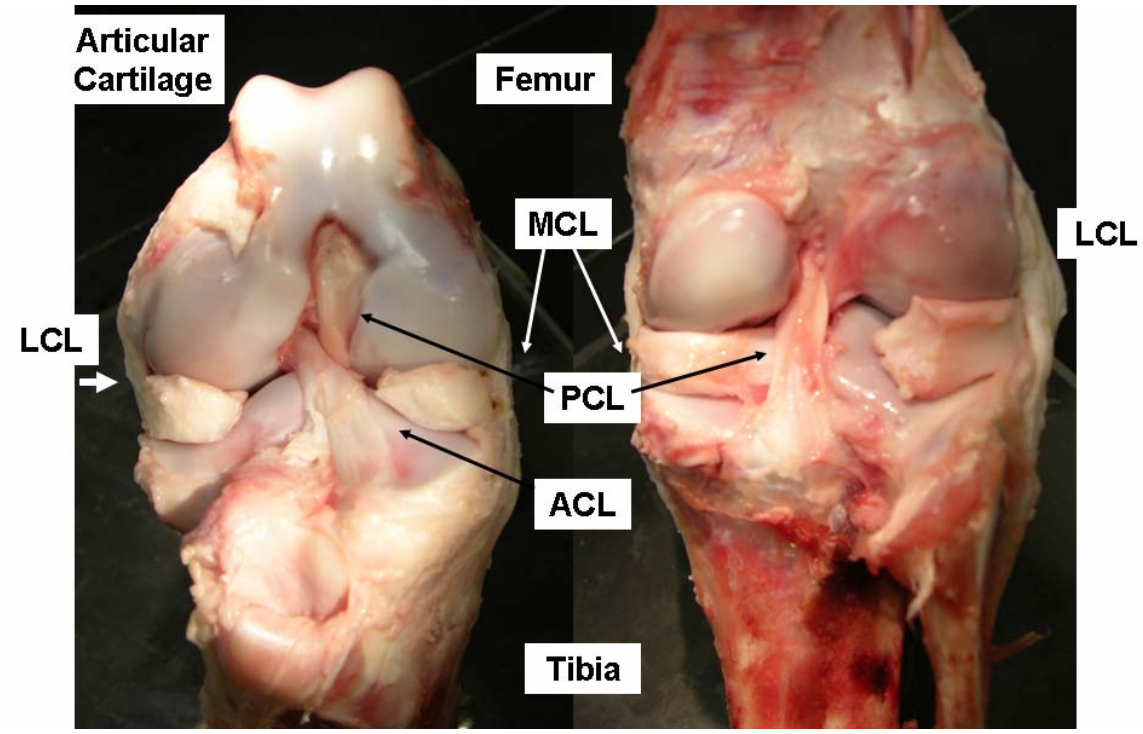

Figure 1: Anatomy of the porcine knee from an anterior and posterior view showing the position of the medial collateral ligament (MCL), anterior cruciate ligament (ACL), lateral collateral ligament (LCL), and posterior cruciate ligament (PCL) (the meniscofemoral ligaments have been removed to allow for unobstructed viewing).

The MCL has a relatively flattened shape and is attached to the medial epicondyle of the femur and inserts onto the anteromedial portion of the tibia. The ACL and PCL are located in the intra-articular space of the knee. The postero-convex femoral attachment of the ACL lies lateral to the vertical surface of the intercondylar fossa and its broad tibial attachment is located between the intercondylar spines of the tibia. The ACL has a complex geometry consisting of two bundles, the anteromedial (AM) bundle and the posterolateral (PL) bundle, which are distinguished based on tension patterns and named by the locations of their tibial insertions [34]. The PCL crosses the ACL intra-articularly with attachments on the lateral aspect of the medial

femoral condyle and posterior tibia and is the primary restraint to posterior tibial translation. The PCL also has a relatively complex geometry consisting of two bundles, the posteromedial (PM) and anterolateral (AL) bundles.

2.2 LIGAMENT BIOLOGY

Ligaments appear as shiny, white banded structures to the naked eye. However, close inspection under light microscopy reveals that ligaments have a highly organized extracellular matrix (ECM) of densely packed collagen fiber bundles that are nearly parallel with the long axis with fibroblasts interspersed between these fibers (Figure 2). These fibroblasts are responsible for the maintenance and remodeling of the ECM through the secretion of macromolecules such as collagen, elastin and proteoglycans.

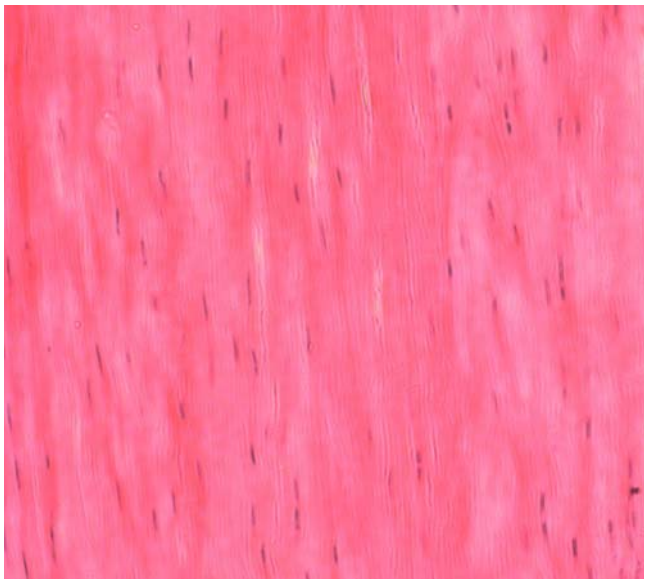

Figure 2: Histology slide (hematoxylin and eosin) shows the organization of the collagen fibers (pink) and fibroblasts (purple) aligned along these fibers within the midsubstance of the medial collateral ligament (Courtesy of Rui Liang, M.D.).

The collagen fibers within the ligament's extracellular matrix are composed of several types of collagen. Type I collagen (70-80% dry weight) is the major component of all ligament fibers; collagen types III, V, VI, and XII exist in small amounts [35]. Collagen is further organized into a cascade of levels with pro-collagen assembled into microfibrils which in turn aggregate to form subfibrils. Multiple subfibrils combine to form fibrils which are the elemental constituent of collagen fibers [36, 37]. Collagen fibers are the functional macrostructural element of ligaments and groups of these fibers form fascicular units which are readily observed upon inspection. These fascicular units are agglomerated together to form fasciculi, which in turn are bound together to form the ligament [36, 37]. In addition to collagen, small amounts of glycoproteins, proteoglycans, and elastin also exist in the extracellular matrix of ligaments and contribute to the ultrastructural anatomy and biomechanical behavior of ligaments.

Transillumination of the ligament midsubstance with polarized light reveals a crimp pattern of the collagen fibrils. This crimp pattern has implications in the nonlinear mechanical properties of ligaments. In addition, transitional zones are formed at the insertions of ligaments into bone in order to minimize stress concentration. Ligaments attach to bones through direct or indirect insertions [35]. In direct insertions, there are four distinct zones of transition: ligament, uncalcified fibrocartilage, calcified fibrocartilage, and bone. In indirect insertions, the surface of the ligament connects with the periosteum, whereas the deeper layers connect to bone via Sharpey fibers with little or no transitional zone. Indirect insertions can be found in ligaments that cross an epiphyseal (growth) plate, such as the tibial insertion of the MCL. Indirect insertions allow for constant remodeling of the oblique fiber and lengthening of the ligament in synchronization with bone growth at the epiphysis during skeletal maturation. The MCL of the knee is an example of a ligament that exhibits both types of insertions. Its femoral insertion is direct whereas the tibial insertion is indirect. In contrast, both of the ACL's insertions are direct.

2.3 BIOMECHANICS OF LIGAMENTS

Since ligaments function to resist tensile loads in joints, uniaxial tensile tests are performed on these tissues to characterize their biomechanical behavior, as well as their contribution to joint kinematics. It is important to understand the biomechanics of ligaments and tendons because the biomechanical properties correlate structure and biochemical composition of the tissue to its function. From uniaxial tensile tests of bone-ligament-bone complexes (Figure 3), the structural properties such as the load-elongation curve are obtained. Generally, a bone-ligament-bone complex exhibits a nonlinear load-elongation curve that has an initial nonlinear

region called the “toe region” that gradually stiffens into a “linear region” where the slope of the curve is constant before the specimen eventually fails (Figure 4). Parameters representing the structural properties are defined as follows:

- Stiffness (N/mm): The relationship between load and elongation measured as the slope of the linear portion of the load-elongation curve.
- Ultimate Load or Load at Failure (N): The highest load observed just before tissue failure during a tensile test.
- Ultimate Elongation or Elongation at Failure (mm): The maximum length a tissue can be stretched from its initial reference length until failure.
- Energy Absorbed at Failure (N-mm): The entire area under the load-elongation curve that represents the work exerted to fail the ligament.

The biomechanical properties of the bony insertion sites and substance of the ligament contribute to the shape of the load-elongation curve. This method also does not distinguish between differences in cross-sectional area of tissues when comparing specimens.

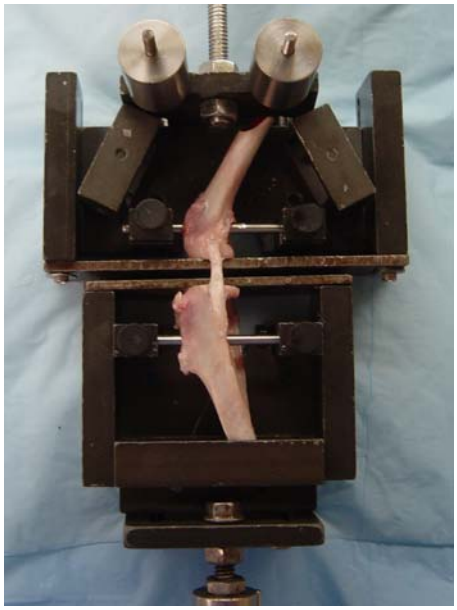

Figure 3: The femur-medial collateral ligament-tibia complex (FMTC) with the bones rigidly fixed by pins and plates to a clamp specially designed for tensile testing.

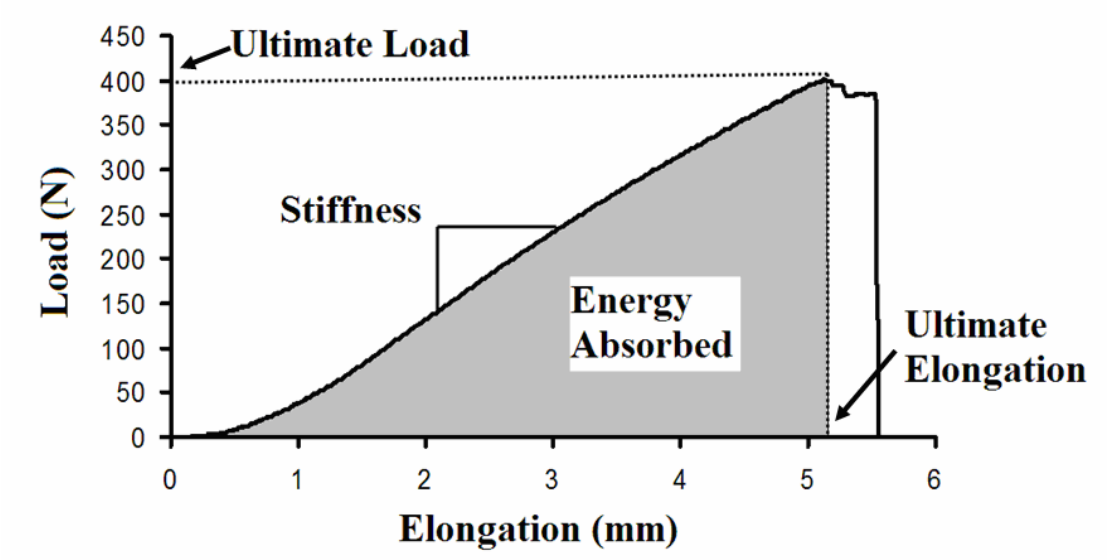

Figure 4: Typical load-elongation curve describing the structural properties of the bone-ligament-bone complex.

Stress-strain curves can be used to distinguish between the different regions and normalize for cross-sectional area. These curves of the ligament substance can be derived from the same tensile test used to obtain load-elongation data. These mechanical properties can provide a better understanding of the effects of biological factors and mechanical factors on the quality of tissue at the ligament or tendon substance by calculation of the stresses and strains of a defined region of the tissue. The stress is defined as the load per unit of cross-sectional area of tissue substance. The cross-sectional area of the specimen for stress calculations can be determined using a laser micrometer system or various other methods [32, 33]. Strain is defined as the change in length divided by the original length. Strain can be determined from a defined region of the ligament midsubstance using a video analysis system to track the position of reflective surface markers placed on the ligament during the test (Figure 5) [25]. A nonlinear stress-strain curve can then be obtained through mathematical calculations, from which parameters representing the mechanical properties can be determined (Figure 6). These parameters are

- Tangent Modulus (MPa): The relationship between stress and strain measured as the slope of the linear portion of the stress-strain curve.
- Ultimate Tensile Stress or Tensile Strength (MPa): The maximum stress observed on the stress-strain curve before failure of the tissue.
- Ultimate Strain (% or mm/mm): The strain at failure of the ligament substance.
- Strain Energy Density (MPa): The area under the stress-strain curve.

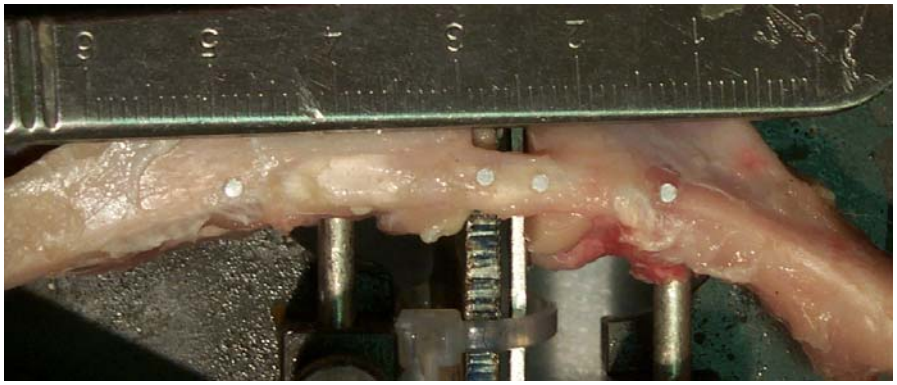

Figure 5: A close up view of the healing FMTC within tensile testing clamps showing the reflective markers placed on the ligament substance for motion tracking during testing. The relative positions of these markers are then used to calculate strain.

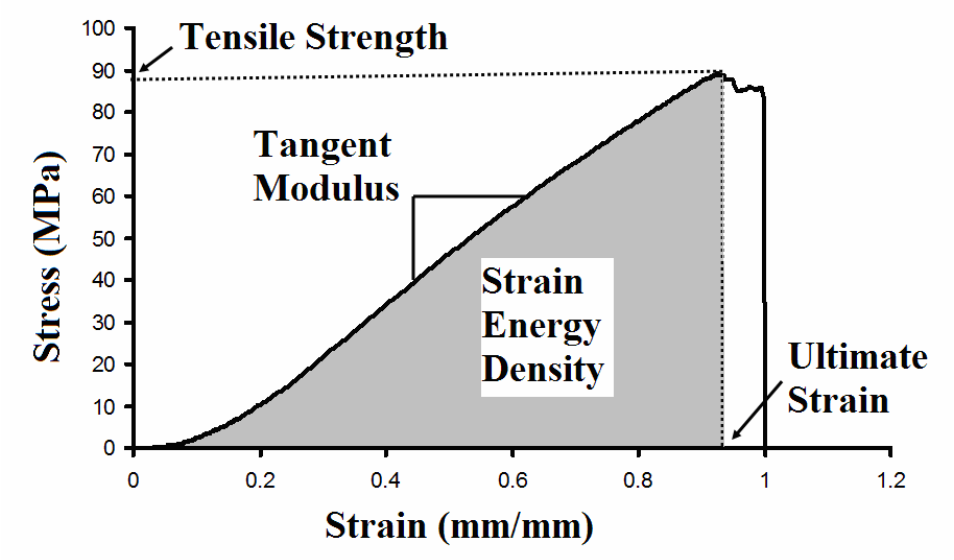

Figure 6: Typical stress-strain curve describing the mechanical properties of the ligament midsubstance.

Ligaments display time- and history-dependent viscoelastic properties that reflect the complex interactions between collagen, elastin, proteoglycans, and water [38, 39]. The loading and unloading curves of these tissues do not follow the same path but instead form a hysteresis loop representing internal energy dissipation (Figure 7). However, over the course of several cycles, the area of hysteresis is reduced and the loading-unloading paths become more repeatable. Other important viscoelastic characteristics of ligaments and tendons include creep (Figure 8A), an increase in deformation over time under a constant load, and stress relaxation (Figure 8B), a decline in stress over time under a constant deformation.

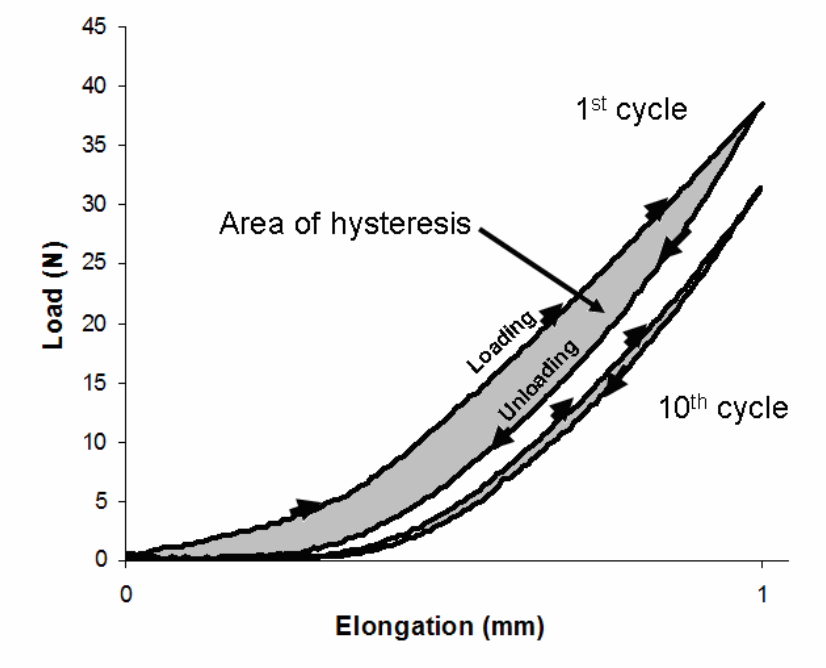

Figure 7: The loading and unloading curves for a medial collateral ligament do not follow the same path, forming a hysteresis loop. Note the decrease in the area of hysteresis by the tenth cycle of loading and unloading.

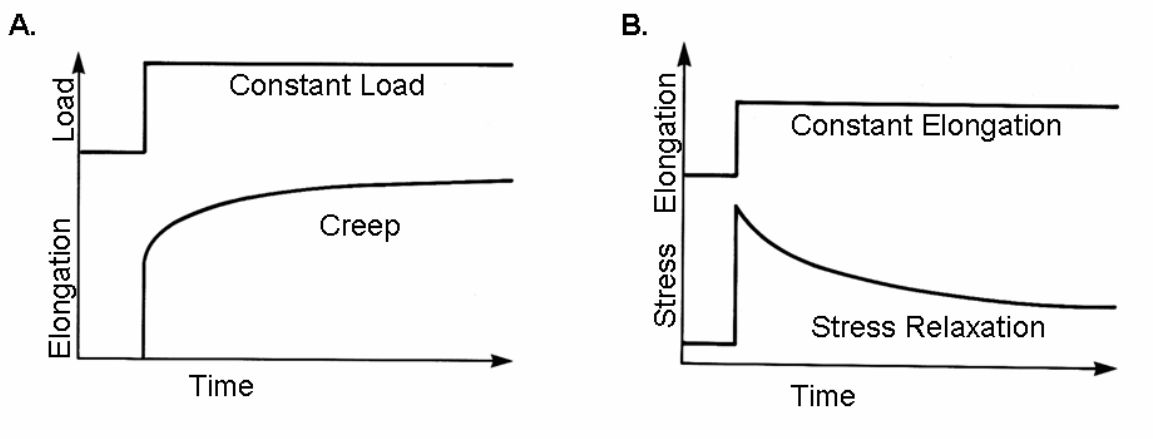

Figure 8: (A) Schematic representation of creep (increasing deformation over time under a constant load). (B) Schematic representation of stress-relaxation (decreasing stress over time under a constant deformation).

The viscoelastic behavior of ligaments has important clinical significance. For example during walking or jogging, cyclic stress relaxation (Figure 9) decreases a tissue's resistance to strain resulting in a continuous decrease in peak stress for each cycle [40]. This phenomenon may help to protect ligaments from fatigue failure and explains how stretching and warming up can help to prevent injury by increasing flexibility.

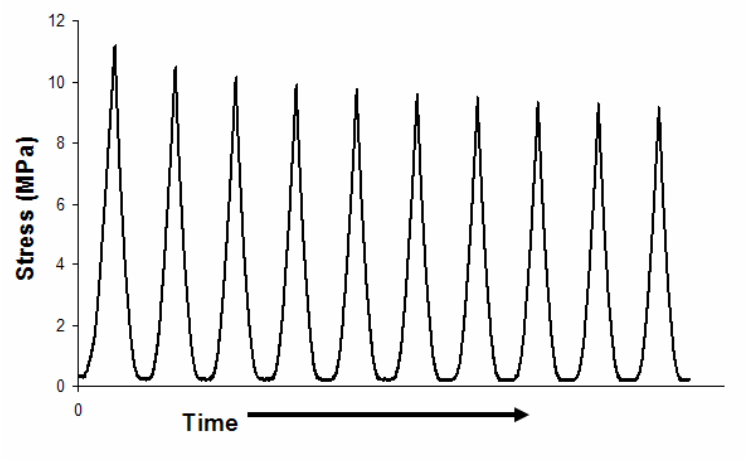

Figure 9: Cyclic stress relaxation behavior of the rabbit medial collateral ligament under cyclic elongations. Note the decrease in peak stress with each subsequent cycle of elongation.

2.4 CONTRIBUTIONS OF THE LIGAMENTS TO KNEE FUNCTION

Ligaments guide joint motion at lower load and limit excessive displacements between the articular surfaces at higher loads due to their nonlinear mechanical properties. Additionally, their geometry and anatomic orientation dictate their contribution to the function of the whole joint. In the tibiofemoral joint, the MCL provides restraint to valgus rotations of the knee and appear to become taut with knee flexion of 70 to 105 degrees. The MCL and its associated medial structures also act as restraints to anterior and posterior translations [41]. The AM and PL bundles of the ACL are important restraints to anterior tibial translation and rotational movements of the knee respectively [17]. Studies have shown that the *in situ* force of the PL bundle is higher in response to anterior tibial loads near full extension while the AM bundle is higher for greater flexion angles [42]. Furthermore, in response to a combined load of both

internal and valgus torque, the *in-situ* force of the AM bundle was greater at both 15 and 30º of knee flexion, but the PL bundle also experienced a significant level of *in situ* force [43]. In the PCL, the AL bundle becomes taut when the knee is flexed and the PM bundle becomes taut when the knee is near extension during passive knee flexion and extension [44]. These studies clearly revealed the complexity of the ACL and PCL and suggest that both bundles in these ligaments are important contributors to knee function. However information on the biomechanical properties of the cruciate ligaments and their bundles are difficult to study due to their complex anatomy and function. Hence there is a need for new technology to be developed in order to further study these intricate tissues.

2.5 LIGAMENT HEALING

The ability to heal varies from ligament to ligament, even within the same joint. The MCL can heal without significant dysfunction, whereas injuries to the ACL and PCL have significantly worse outcomes when treated non-operatively [3, 12, 13]. Therefore most ACL and PCL tears require surgical reconstruction after complete ruptures in order for the patient to return to sports [12, 15]. Differences in the healing potential between the collateral and cruciate ligaments may be attributed to the location of cruciate ligaments in the synovial joint space which receives relatively little blood supply and nutrition. Cell morphology [45], cell proliferation [46], biomechanical properties [35], physiological stresses [42] and overall ligament geometry have also been demonstrated to be markedly different.

Although methods of treating ligamentous injuries have seen substantial improvements in recent years, many questions remain about enhancing the rate, quality, and completeness of extra-articular ligament healing. In order to adequately address the intricacies of this process and improve upon techniques used in clinical practice, it is essential to derive knowledge on the basic science of ligament healing. Due to the accessibility, frequency of injury, and healing properties of the MCL, it has become a model for studying extra-articular ligaments in the body, as well as a primary focus for scientific research.

The healing of an MCL can be divided into four overlapping phases: hemorrhage, inflammatory, repair, and remodeling [35]. After a typical midsubstance tear of the MCL (characterized by the mop-end appearance of its torn ends), hemorrhage begins and a hematoma forms between the retracting ligament ends. Inflammatory and monocytic cells immediately migrate into the injury site to convert the clot into granulation tissue and phagocytose necrotic tissue. Within two to three days post injury, fibroblasts begin to proliferate rapidly and synthesize new matrix. A fibrous matrix containing high concentrations of water, glycosaminoglycans, and type III collagen thereby replaces the clot and necrotic tissue. Within about 2 weeks, the granulation tissue is replaced with a continuous network of immature, collagen fibers in the central region of the ligament, formed by randomly oriented fibroblasts.

During the next several weeks, the biochemical composition of the repair tissue changes as repair progresses. Water, glycosaminoglycans, and type III collagen concentrations decline, inflammatory cells disappear, and the concentration of type I collagen increases as newly synthesized collagen fibrils increase in size and begin to form tightly packed bundles. The tensile strength of the healing tissue also increases as the collagen content, especially type I collagen increases. The remodeling phase begins within several weeks of injury as the numbers of

fibroblasts and macrophages decrease, fibroblast synthetic activity decreases, and the fibroblasts and collagen fibrils assume a more organized appearance. In the months following injury the volume of the repair tissue decreases and the remodeling process is marked by increased alignment of collagen fibers along the long axis of the ligament and continued collagen maturation.

For patients with isolated MCL injuries, their prognosis is favorable with a return to pre-injury activity levels following limited weight bearing and physical therapy [3]. Concomitantly, investigators have documented in animal models that injuries to the MCL can heal with resulting structural properties of the FMTC equal to or almost equal to those of the normal ligament, thus providing the needed function for the involved joint [9, 10, 26]. However, these studies also found that the mechanical properties of the healing MCL remain inferior when compared with normal tissue for up to one year [8]. These differences have been correlated with a wide array of biochemical and histmorphological changes such as increased levels of collagen types III and V and a disorganized collagen matrix (Figure 10) compared to the intact state [6, 9, 10, 24, 47].

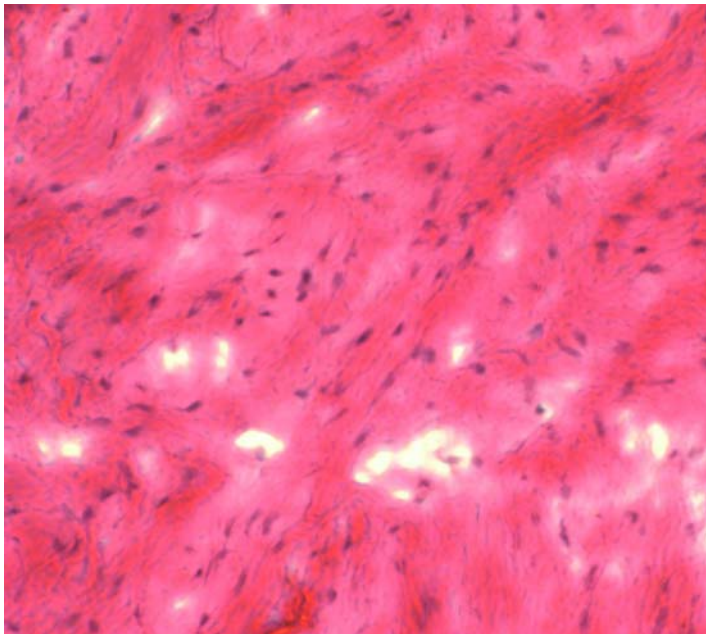

Figure 10: Histology (hematoxylin and eosin) of the midsubstance of the rabbit MCL at twelve weeks following gap injury showing disorganization of the collagen matrix and hyper-cellularity of the tissue (Courtesy of Rui Liang, M.D.).

Furthermore, it should be noted that the cross-sectional area of the healing MCL was much larger than that of the intact MCL regardless of injury model and treatment/rehabilitation regimen [9, 10, 48]. Compared with the preinjury state, the cross-sectional area of the healed ligament was significantly larger at 6 to 12 weeks and slowly continued to increase with time to reach structural properties of the normal ligament [49]. In some studies, the cross-sectional area of the healed MCL was up to 2.5 times larger than that of controls after 52 weeks [8]. In the case of combined MCL-ACL injuries, the quality of the healing tissue is far worse even when the ACL has been reconstructed [19, 50, 51]. Thus, healing of the MCL involves the production of a larger quantity of tissue, which is inferior in quality, thereby resulting in reduced mechanical properties.

2.6 FUNCTIONAL TISSUE ENGINEERING OF LIGAMENT HEALING

With the biomechanical, biochemical and histomorphological properties of the healing MCL failing to return to normal values and the quantity of healing tissue increasing to make up for the deficiency, researchers have been exploring new, improved methods of treatment that will improve the quality of the healing tissues and accelerate the rate of healing. Recent advances in the fields of molecular biology, biochemistry and functional tissue engineering offer new possibilities that could potentially lead to the modulation of cellular and biochemical mediators in order to improve the quality of the newly forming tissue while simultaneously restricting the cross-sectional area growth of the healing tissue. Current research has been focused on combining mechanical stimuli with biological and synthetic scaffold materials in order to create tissue engineered implants [52] or directly applying these scaffolds *in vivo* [48, 53, 54] to treat ligament defects.

It has also been well recognized that mechanical stimuli can induce changes in the biochemical composition and structural properties of connective tissues. Applying tension to a healing rabbit MCL four weeks after surgical transection improved the organization of collagen fibers and the alignment of the fibroblasts [55]. *In vitro*, the mechanical stretching of fibroblast populated-collagen gels induced realignment of the fibroblasts and collagen fibrils along the direction of stretching [56, 57].

The cellular environment has also been shown to affect cell orientation and matrix organization by contact guidance. A cell exhibiting contact guidance is characterized as having a "bi-directional" orientation, meaning that the cell has the maximum probability of migrating in opposite directions [58]. These preferred directions can be correlated with chemical, structural and/or mechanical anisotropies of the substratum [59]. Contact guidance can be demonstrated by

fibroblasts cultured on microgrooved surfaces [60]. Fibroblasts, when cyclically stretched in culture on smooth silicone surfaces, were oriented perpendicular to the direction of stretching, while cells cultured on microgrooved silicone surfaces elongated and oriented themselves in alignment with the direction of stretching [61]. The latter more closely resembles the *in vivo* condition where fibroblasts are aligned along the collagen fibers and hence the direction of stretching. Static culture of cells on microgrooved surfaces also produced an organized collagen matrix with fibers that were aligned parallel to the microgrooves while those cells grown on smooth silicone surfaces were randomly oriented and produced a disorganized collagen matrix [62]. This suggests that orienting cells along the longitudinal direction of the ligament midsubstance may lead to production of aligned matrix that more closely resembles the intact state. This may help enhance the mechanical properties of the healing tissue. Therefore, to improve the quality of the healing ligament midsubstance it is suggested that both cell orientation and mechanical loading of the healing ligaments be taken into consideration.

Functional tissue engineering approaches utilizing synthetic and biologic scaffolds have the potential to restore the healing ligament to its normal state. Scaffolds can provide the structural template for guiding tissue development by distributing mechanical stresses and controlling cell orientation through contact guidance. The ideal scaffold will also be designed to gradually degrade while new functional tissue forms until the scaffold has been completely replaced with tissue *in vivo*.

Porcine small intestinal submucosa (SIS) is a potential scaffolding material that could be used to enhance ligament healing. SIS is a cell-free biomaterial that has been applied as a scaffold for repair for various tissues of the musculoskeletal systems [53, 54, 63, 64]. SIS, which

is predominantly composed of collagen type I, has been shown through small angle light scattering analysis to have a preferred orientation ± 28 degrees to the longitudinal direction [65].

In our research center, SIS was found to enhance healing in the rabbit MCL at 12 weeks after gap injury. Specifically, the SIS-treated MCLs were found to have a tangent modulus and tensile strength that was nearly two times greater than the non-SIS treated group [48]. Additionally, the histological appearance of the healing tissue improved, with the SIS-treated group showing increased cellularity, greater collagen density, and improved collagen fiber alignments compared to the non-treated group. However, the average cross-sectional area between the SIS-treated and non-treated groups were not significantly different and the properties of SIS-treated MCLs remained inferior to their sham operated controls. It has been postulated that SIS enhances MCL healing by inducing the migrating cells to align themselves along the scaffold's fibers by contact guidance, thus the collagen matrix produced will be more organized and the mechanical properties of the tissue will be improved. In addition, the scaffold may provide mechanical stimulation to the healing tissue during remodeling, which may further improve matrix organization. However, if the collagen matrix is more organized, then the cross-sectional shape and area of the SIS-treated healing ligament should resemble that of the intact tissue. It is possible that this could happen after a longer period of remodeling, therefore more in depth studies of the healing tissue's shape and area are needed.

2.7 OVERVIEW OF PREVIOUS METHODOLOGIES FOR CROSS-SECTIONAL SHAPE AND AREA MEASUREMENT OF SOFT TISSUES

The accuracy of determining tensile stresses depends on the accuracy of the methodology used to measure the cross-sectional area of the specimen. Determination of the cross-sectional area of soft tissues has had a long history that began as early as 1936 when Cronkite cut sections of tendon, projected the shadow of the sections on a screen, and then measured the cross-sectional area [66]. Other early methods included imbedding the specimen before sectioning [31], immersing the specimen in liquid and measuring the volume displaced divided by length [66, 67], as well as using rulers or calipers to measure specimen width and thickness [28]. Since then various other methods have emerged and have been used to describe the anatomy as well as for materials testing studies of biological tissue. However, many of these methods can introduce errors due to preparation, contact during the measurement process, or the inherent assumption in the method that the specimen is convex.

All methods of cross-sectional area measurement for soft tissues can be grouped into two general categories (Figure 11): (1) destructive, and (2) non-destructive. Although the cross-sectional shape and area can be determined with destructive methods [31, 66], the specimen cannot be subsequently used for any other purposes such as biomechanical testing. In contrast, non-destructive methods leave the specimen intact so that other tests can be performed. However, most non-destructive methods do not allow for the determination of the cross-sectional shape of the specimen.

Within the non-destructive approaches, a further division into contact and non-contact methods of cross-sectional area measurement can be made. The drawback with contact methods is that they easily deform soft biological tissues, which are pliable in nature, thus introducing

error into the measurements. Once the shape of a specimen has been altered, it is difficult to determine the original configuration. In addition, some of these methods assume the shape of the specimen a-priori. Within the non-contact group, methods can be classified into those which assume a convex surface and those which can be applied for general shapes. Methods which assume a convex specimen cannot detect concavities along the specimen surface. Although this may be acceptable for some specimens, many soft tissues contain concavities in their cross-section. Therefore, methods which can be applied to general shapes and can detect concavities on the surface are better suited for measurement of these tissues.

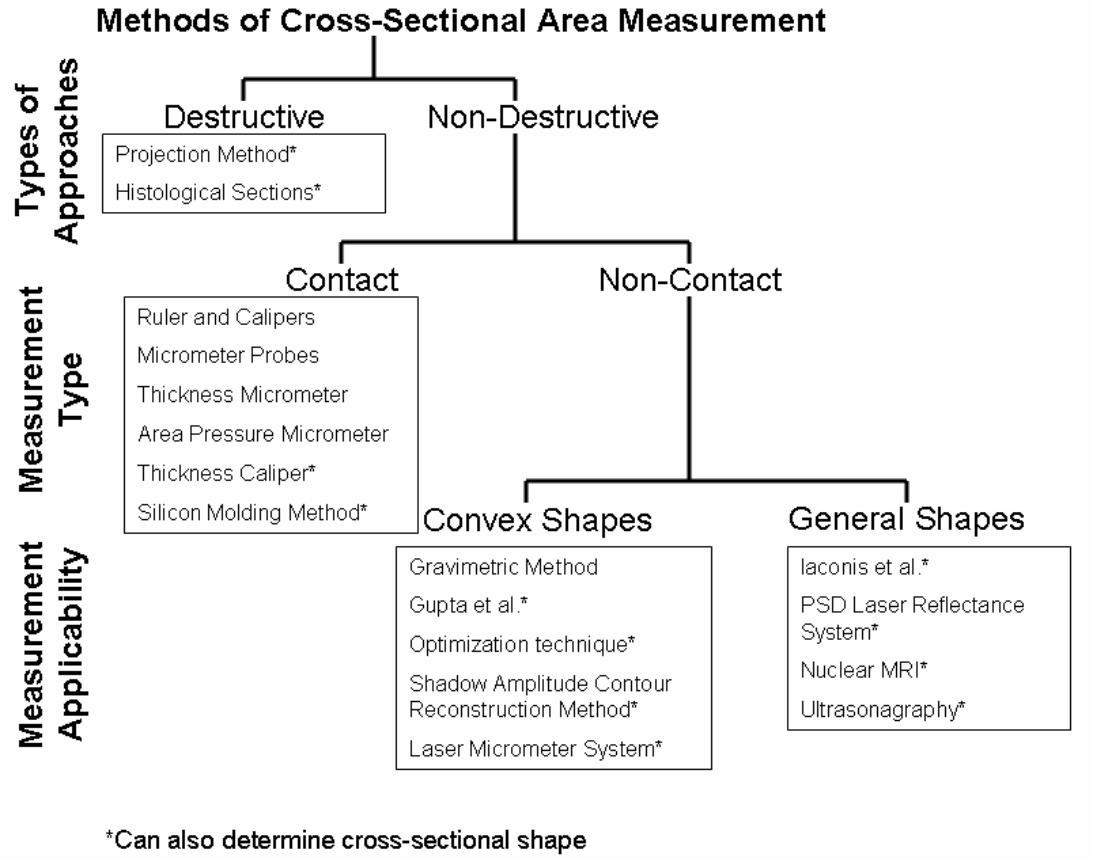

Figure 11: Flow diagram of previously developed cross-sectional area measurement devices. Adapted from [68].

2.7.1 Destructive Methods

Two destructive methods for determining the cross-sectional shape and area are the projection method [66] and histological sectioning [31]. As previously described, Cronkite cut 0.5 - 1.0 mm thick sections of tendon, projected the shadow of the sections on a sheet of paper, the outline was carefully traced with a sharp pencil and then the cross-sectional area was measured using a planimeter [66]. For histological sectioning, the specimen can be either (1) embedded in paraffin and stained with hematoxylin and eosin, or (2) suspended between two ends of a specially designed fluorocarbon boat and dehydrated through a graded series of ethanol solution after which the specimen is embedded in nitrocellulose and stained with Van Gieson's stain [31]. Photographs are taken of the specimens after sectioning and enlarged. Measurements are made using a polar planimeter on the photomicrographs. The major limitation of destructive methods is that the specimen is destroyed and cannot be used for other purposes. Also, for histological sectioning, there is some shrinkage of the specimen due to the preparation process, especially during the dehydration process.

2.7.2 Non-Destructive Methods

Since specimens are often needed for biomechanical testing following measurement, many non-destructive methods have been used. These range from contact methods such as the use of a simple ruler or calipers, and various micrometers to non-contact methods such as the gravimetric methods, optimization techniques, shadow, and optical methods. For convenience, the devices were reviewed in terms of contact and non-contact methods. The non-contact

methods were further divided into methods that assume convex shapes and methods that can detect and account for concavities in the specimen (general shapes).

2.7.3 Contact Methods

The simplest contact method of cross-sectional area measurement uses a ruler or calipers to measure the dimensions of a specimen and calculate the area assuming a rectangular or elliptical shape. Wright and co-workers [69] used this method to measure the cross-sectional area of the human plantar fascia. The width and depth were measured with a ruler and calipers at three levels after each specimen was mounted in the testing machine. These three measurements were then averaged. The limitations to this method are that it assumes a rectangular or elliptical shape, when in fact, soft tissues have irregular shapes. In addition, the instrument is in direct contact with the specimen and may distort it, thereby making the measurements dependent on the skill of the user. Also concavities cannot be detected. However, this method is simple and quick to use.

A variation on the previous method is the micrometer method as described by Haut and Little [67]. A special set of micrometer probes were designed for easy access into the intact joint and attached to a 2-3 inch micrometer. Major and minor diameters of the ACL were measured and the area was calculated assuming an elliptical shape. The limitations to this method are similar to the previous method in that it assumes a geometric shape and there is contact with the specimen. Although this technique is vulnerable to user error, it can be implemented *in situ*.

A micrometer with an electrical sensor circuit was designed by Woo and coworkers following Professor Y.C. Fung for use with cartilage and tendons (Figure 12) [70]. This device consists of a vertical rod with a flat surface at the foot supported by a double cantilever spring

system which was initially set down on the specimen. The purpose of this self-balancing system was to place minimal vertical force on the tendon. The first reading is taken after the spindle of the micrometer was lowered to contact the sharp point on the top of the vertical rod and an electrical circuit is used to indicate the time of contact. After the specimen was removed, the foot of the vertical rod is placed onto the stage and the micrometer spindle was lowered to contact the top of the rod for a second reading. The difference between the two readings yielded the thickness of the specimen. The cross-sectional area is determined after measuring the width of the specimen with a cathetometer. Disadvantages to this method include the assumption of rectangular shape and direct contact with the specimen; although contact was minimized since an electrical circuit was used to indicate contact rather than visual observation.

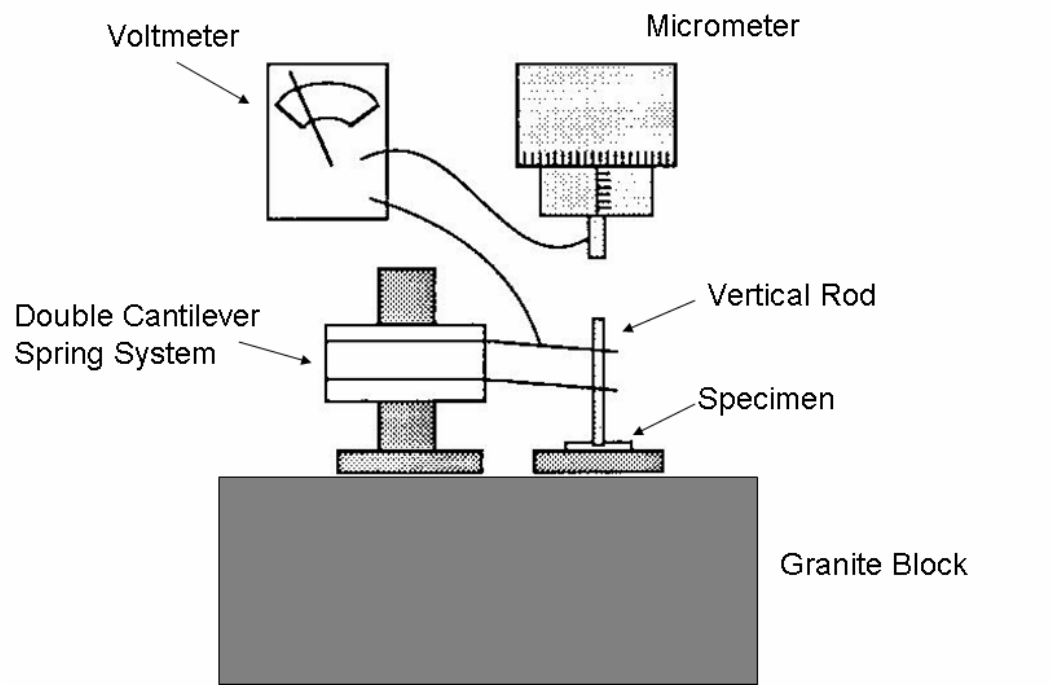

Figure 12: A thickness micrometer instrument used to measure the thickness of soft tissues (designed after Y.C. Fung) [70]. A voltmeter is used to indicate contact between the vertical rod and the micrometer spindle.

A device commonly used in cross-sectional area measurement is the area pressure micrometer, of which there are many variations (Figure 13) [29, 31, 69, 71]. In general, the specimen is forced to assume a rectangular shape with or without a constant pressure applied. The height of the specimen is then measured and the cross-sectional area determined by multiplying the width of the rectangle by the height of the specimen. A drawback of this method is that it assumes that the specimen has a rectangular shape. In addition, this is a contact method where there is compression of the specimen, which can alter the shape and/or the structure of the specimen [72].

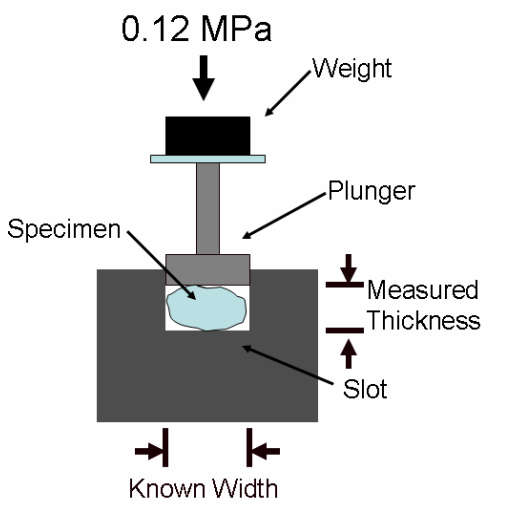

Figure 13: A general schematic of the area pressure micrometer based on the device used by Butler et al. [29]. Tendon and ligament specimens were forced to conform to a rectangular slot of known width while a constant pressure of 0.12 MPa was applied.

A thickness caliper with strain gauges was developed by Shrive et al. [73]. This system measures the thickness of the tissue as a function of position along the width of the tissue. The device uses a thickness caliper consisting of stainless steel tension arms and a linear potentiometer which measures the position of the caliper (between the tips of the tension arms) along the width direction of the specimen. The tension arms have strain gauges on their inner and outer surfaces which indicate the relative distances between the tips (the thickness of the specimen). As the tension arms are dragged across the specimen, the thickness versus location on the tissue is plotted on an x-y recorder. The cross-sectional area is determined by calculating the area under the curve produced by the plotter. With this technique, there is an applied stress of approximately 0.1 MPa to the contact area. Unfortunately, the laxity of the specimen affects the readings and therefore a 5% preload is applied to the specimen in order to obtain repeatable

readings. This method also cannot obtain a true pictorial representation of the cross-sectional area.

Race and Amis [72] developed the casting method, which is based on the destructive histological sectioning method. A silicon rubber mold of the specimen is made and then a polymethylmethacrylate replica is fashioned from that mold. This replica is then sectioned, stained with black ink, and photographed. Once enlarged, the cross-sections are traced onto graph paper and cross-sectional area is determined by counting the squares in the enclosed area. This is considered a contact method because the specimen is touched by the silicon during curing. There are also unknown variables associated with this method such as heat dispersed by the silicon while it is curing, shrinkage of the mold and any after effects to the specimen from the entire process. The viscosity of the silicon determines whether or not some of the concavities are captured. Despite this, the shape of the specimen, including the concavities, can be clearly determined, although the reported method of cross-sectional area calculation is not the most sophisticated. Finally, the entire process is time consuming and involves a great deal of handling; therefore there is the possibility of error at multiple steps.

2.7.4 Non-Contact Methods for Convex Shapes

Non-contact methods of cross-sectional area measurement range from very simple methods, such as gravimetric methods, to the more sophisticated, such as traveling microscopes, optimization techniques, shadow methods, optical methods, and the laser micrometer system. Some of these methods are capable of detecting and accounting for concavities on the surface of the specimen while others are not, depending on the manner that the measurements are taken. Thus, discussion of these non-contact methods has been divided into two sections. This section

will review methods, which cannot detect concavities and were developed for use with convex shapes.

One of the earlier non-contact methods of determining cross-sectional area is the gravimetric method [31, 66], which utilizes the tissue's density-volume relationship. The specimen is weighed in air before it is immersed into a cylinder of distilled water. Due to Archimede's principle, the specimen will displace a volume of water, which is weighed to find the volume displaced. The cross-sectional area is then calculated by dividing the volume of water displaced by the specimen's length. This method can be performed on either moist or dry specimens, but unfortunately is neither accurate nor reproducible. Although it is not a contact method, it assumes constant cross-sectional area along the length of the specimen, and the shape of the specimen cannot be determined. Another concern with this method is that the specimen's immersion in fluid may alter the shape, volume and density of the specimen. However, this method is relatively simple to use.

A unique concept developed by Gupta and co-workers [74], consists of a microscope set on a vernier scale that is used to measure the width of a specimen at 10° angular increments. The measurements of the different diameters were then plotted on graph paper. A smooth curve was drawn to connect the points and the squares enclosed by the curve were counted to determine the cross-sectional area. With this method, concavities cannot be detected and the accuracy is very user dependent. Further, although an idea of the cross-sectional shape can be determined, it is more of an approximation, with all the edges rounded and the concavities removed.

The optimization technique developed by Njus and Njus [75] uses the profile widths of the specimen as obtained from photographs and a video dimension analyzer (VDA). The profile widths are then fitted to a mathematical model and the area is obtained by integration. Concerns

with this method are that the user needs to assume a simple shape which may not match all tendons and ligaments and the method of reconstruction may not be entirely optimal as it requires at least one plane of symmetry in the cross-section of the specimen.

Ellis and co-workers [31] developed a shadow amplitude contour reconstruction method for the determination of cross-sectional area. This method creates a partial shadow of the specimen using a light beam which provides the basis for the reconstruction of a specimen contour which is then integrated to give the cross-sectional area. The center of rotation needs to be located on the edge of the light beam due to the reconstruction approach.

In our laboratory, the laser micrometer system (Figure 14) was developed as an accurate non-contact method of determining the cross-sectional area of soft tissues [32, 33]. This system works under a similar principle to the shadow amplitude contour reconstruction method detailed previously, however it incorporates a laser micrometer instead of a VDA. In this system, collimated laser beam is rotated 180° around the specimen while diameter and reference distance are measured in 3° increments. Using these parameters, an algorithm is then used to reconstruct the cross-sectional shape. The area of the resulting shape is then calculated using Simpson's rule. The entire system is automated, except for the mounting of the specimen, therefore making it easy to use. It is also possible to measure different locations on the same specimen and the cross-sectional shape reconstructions accurately depict the cross-sections of tissues with relatively simple geometries such as the rabbit MCL [33].

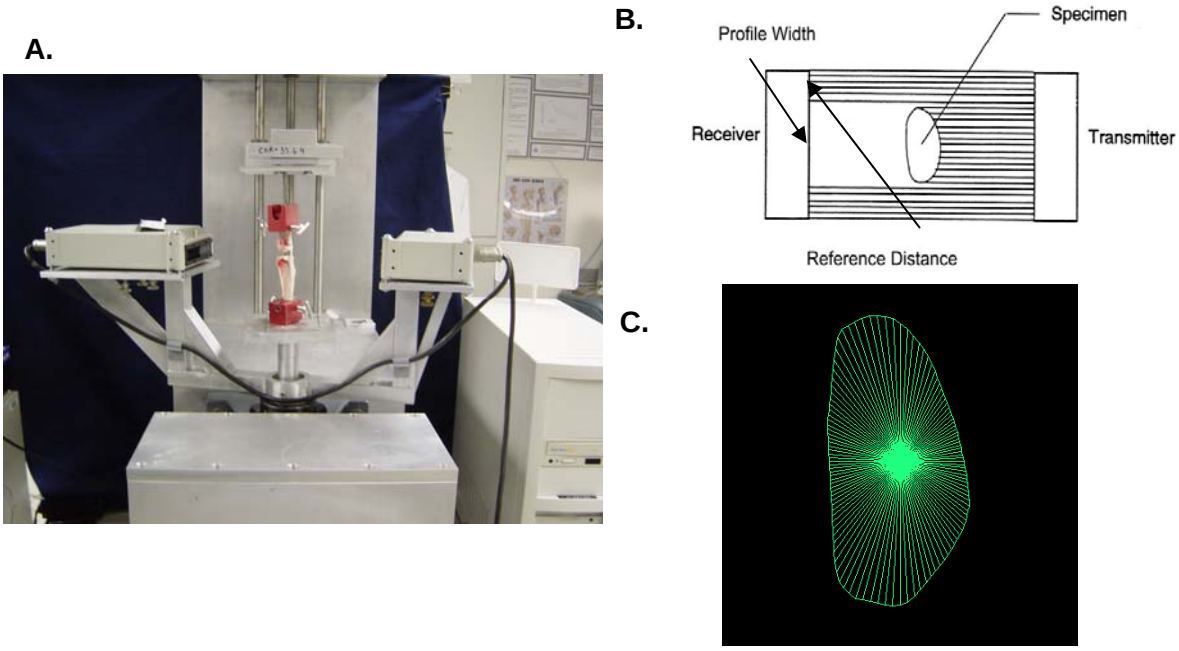

Figure 14: A) Photograph of the laser micrometer system with a femur-MCL-tibia complex; B) A schematic showing the laser transmitter and receiver with parameters profile width (width of shadow created by specimen) and reference distance (distance from the edge of receiver to beginning of shadow) with respect to the specimen [32]; and C) a sample output of cross-sectional shape from the system showing the typical shape of the normal rabbit MCL midsubstance.

2.7.5 Non-Contact Methods for General Shapes

Tissues with complex geometries require more sophisticated methods of non-contact measurement due to concavities on their surfaces in order to reduce error in cross-sectional shape and area determination. An optical method developed by Iaconis and co-workers [76], position sensitive device (PSD) laser reflectance system developed in our research center [68], the ultrasonography method [77], nuclear magnetic resonance imaging (MRI) [78] are non-contact

methods that are capable of detecting concavities on the surface of the specimen. The optical method and laser reflectance system are similar in that electromagnetic beam(s) were used to triangulate a location on the surface of the specimen in order to reconstruct its perimeter. However, in the ultrasonography method, ultrasound is passed through the specimen in order to reconstruct its shape.

The optical method developed by Iaconis and coworkers, involves aligning two light beams with a triangular spot on the surface of the specimen [76]. Since the origin and direction of each of these light beams is known, the distance of the surface of the specimen from its center of rotation can be calculated. By collecting measurements around the entire specimen, the outline can be reconstructed and the cross-sectional area calculated. This method can detect concavities, but irregular surfaces reduce the accuracy of the measurements and can introduce an error of 3-7%. Also the device is user dependent as the operator is required to line up the two light beams properly.

The position sensing detector (PSD) laser reflectance system (Figure 15) was previously developed by our laboratory for measuring the cross-sectional shape and area of ligaments with complex cross-sections. The PSD laser transducer generates a beam of laser radiation at a known wavelength which strikes the specimen, and collects reflected radiation in the same wavelength to determine the distance to a target's surface. In this system, the transducer was rotated 360° around a specimen while distance from the transducer to the specimen's surface was measured at 3° increments. The resulting data on the angular position and distance to the specimen's surface are then combined to reconstruct the cross-sectional shape of the specimen in polar coordinates which are then converted to Cartesian coordinates. The area of the specimen is determined by calculating the area under the curve using a trapezoidal approximation [68]. This

system was able to successfully reconstruct the cross-sectional area of specimens and is relatively simple to use. However the accuracy of the PSD laser reflectance system can be affected by the surface conditions of the specimen and by the position of the specimen within the system.

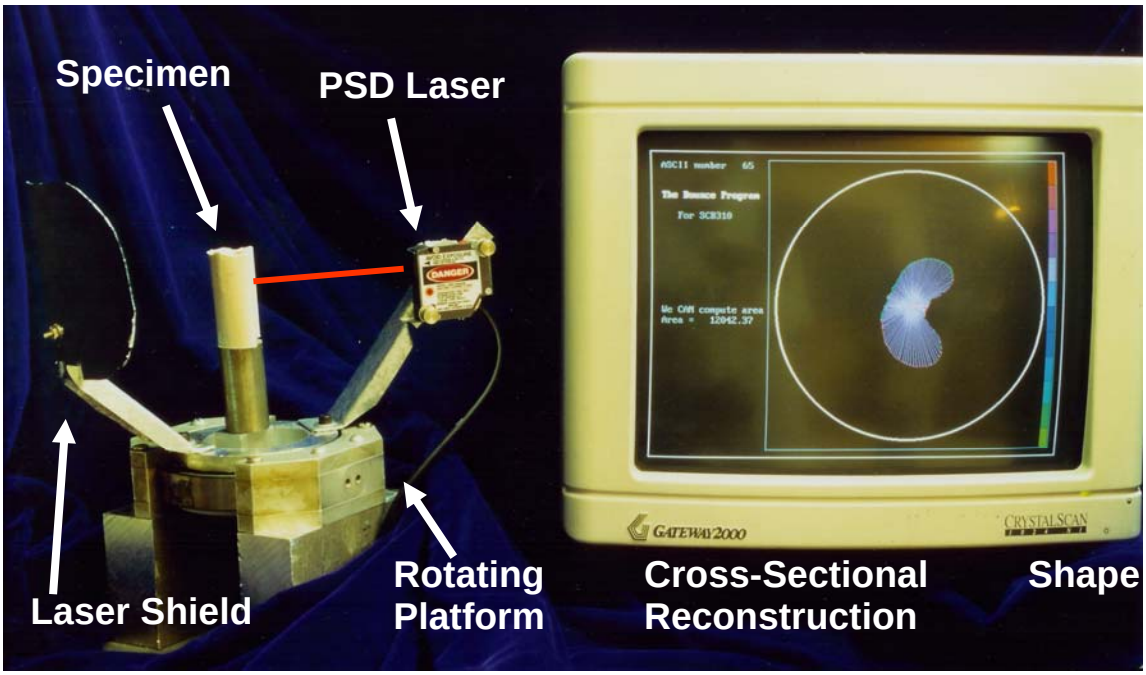

Figure 15: The PSD Laser Reflectance System with a sample cross-sectional shape reconstruction shown on the computer monitor.

Recently, ultrasonography has been applied as a means of determining the cross-sectional shape and area of ligaments [77]. For this method, an ultrasound probe was used to make a scan of a specimen. The resulting image is then manually traced using the ultrasonograph trackball and analyzed using image analysis software to find the number of pixels within the enclosed

area. Although this method is non-contact and fairly quick, there are concerns about the manual tracing of the specimen and the ultrasound machines can be expensive to purchase and operate.

Nuclear magnetic resonance imaging (MRI) has been used to measure the physiological cross-sectional area of muscles in response to strength training [78]. For this method, an MRI scan is taken and the contours of the desired tissue on the image are digitized using a graphic tablet, which would enable determination of the number of pixels enclosed. Pixels are then converted to square millimeters by a scale conversion algorithm. Although this technique is fairly sophisticated and can measure the area of tissue *in vivo*, the digitization of muscle contours was carried out manually, which can be time consuming and introduce error. Nuclear MRI machines and scans are also expensive to purchase and to use and require an experienced technician to operate.

3.0 OBJECTIVES

3.1 BROAD GOALS

The objective of this study was to more thoroughly describe the cross-sectional shape and area of the normal and healing ligaments. This was initially done on the rabbit MCL model using the laser micrometer system [33] to assess the effects of treatment with a bioscaffold on the cross-sectional shape and area of the healing ligament. However, this first study raised some concerns on whether concavities in the healing MCL could cause error in the measurement of cross-sectional shape and area. Therefore, a new laser based system; the charge coupled device (CCD) laser reflectance system was developed for future studies. This new system can detect concavities in the cross-section so that cross-sectional shape and area can be more accurately measured on the MCL, as well as other ligaments and tendons such as the ACL, PCL and the patellar tendon. Non-contact methods were chosen for measuring cross-sectional shape and area in order to prevent any errors due to mechanical contact and deformation during measuring.

3.2 SPECIFIC AIMS AND HYPOTHESES

Specific Aim I: To determine whether the cross-sectional shape is altered when small intestinal submucosa (SIS) is used as a bioscaffold to treat the gap injury in comparison to non-treated healing MCLs. The shape of the tissue will be quantified by finding the minor and major axis as determined by the laser micrometer measurement system.

Hypothesis I: SIS-treated MCLs will be more similar in shape to the intact MCL and therefore will have a smaller major and minor axises than the non-treated group possibly due to contact guidance and mechanical stimulation provided by the scaffold.

Specific Aim II: To determine whether the cross-sectional area is reduced when SIS is used as a bioscaffold to treat the gap injury in comparison to non-treated healing MCLs.

Hypothesis II: SIS treated MCLs will have significantly reduced cross-sectional areas than non-treated healing MCLs possibly due to contact guidance and mechanical stimulation provided by the scaffold.

Specific Aim III: However, due to limitations of the current system in measuring the shapes and areas of the MCL, a new system with the capacity to detect concavities on the specimen will possibly allow for more accurate cross-sectional shape and area measurements. With a more accurate system, smaller differences can be detected between different treatments in future studies. Therefore a new laser-based system, which can detect concavities in the cross-sections of tissues, was developed and evaluated.

4.0 SPECIFIC AIMS I AND II: EFFECTS OF BIOSCAFFOLD TREATMENT ON THE CROSS-SECTIONAL SHAPE AND AREA OF HEALING MCLS

The MCL is able to restore its structural properties after injury through a compensatory overgrowth of healing tissue, which is of inferior quality [6, 8, 9]. SIS, a bioscaffold, has been previously shown to enhance the quality of the healing rabbit MCL at 12 weeks in the gap injury model [48]. More detailed studies of the changes in cross-sectional shape and area of the MCL that occur with SIS treatment could provide insight into the mechanisms by which the bioscaffold alters the MCL healing and remodeling process.

4.1 EXPERIMENTAL MODEL

Inanimate models are unsuitable for investigations of the healing process of the MCL, and invertebrate animals lack mammalian-type knee joints and MCLs. Different vertebrate species (including rabbits, dogs, and goats) have been used in our laboratory to study various aspects of the normal and healing MCL [9, 38, 48, 79]. However, the New Zealand White rabbit is of sufficient size to allow surgery to be performed easily and is relatively inexpensive. Furthermore, specimens from these animals have been shown to provide tissue samples large

enough for successful biomechanical testing. Hence, this animal model was used to accomplish the first two specific aims of this thesis.

4.2 SURGICAL PROCEDURE

All surgical procedures were performed using well-established protocols developed in our research center. Twenty two skeletally mature, female New Zealand white rabbits with an average body mass of 5.0 ± 0.5 kg (range 4.3–5.6 kg) were used for this study. After a five day acclimation period the animals were taken to the operating room. An initial intramuscular injection of xylazine and ketamine was given as a preanesthetic. The fur was then shaved from the hind limbs, and the exposed area was sterilized with betadine solution. General anesthesia was maintained with 1.5-2.0% isofluorane supplemented by oxygen and nitrous oxide.

The MCL was exposed by making an anteromedial incision, centered over the joint line and carried down to the deep fascia using a #15 scalpel blade and electrocauterizer to minimize bleeding. The fascia was incised, exposing the MCL, which was undermined. The knee was positioned at approximately 60 to 75° of flexion during the whole procedure. For the gap injury model used in this study, a piece of the MCL midsubstance 6 mm in length was transected and removed using a #15 scalpel blade in the right MCL of all animals [48]. After transection, the ends of the ligament recoiled to produce a gap in the midsubstance around 8 mm in length (Figure 16). This model provided a reproducible and consistent injury to the midsubstance without injuring the insertion sites at the time of surgery. The left MCLs were sham operated,

whereby the ligaments were exposed but not injured. The specimens were divided equally in SIS-treated and non-treated groups. In the SIS-treated group (n=11), a single strip of SIS (Cook® Biotech Inc., Bloomington, IN) was secured on top of the gap (luminal side faced down) with the use of a non-resorbable suture (6-0 silk) at each of the four corners. The non-treated group (n=11) received no treatment to their gap injuries and the corners of the loose ends of the gap were marked using non-resorbable suture (6-0 silk). For all specimens, the wound was then irrigated with saline and the fascia and skin were closed using 5-0 ethibond suture and 5-0 nylon suture respectively. This surgical procedure has been approved by the University of Pittsburgh Institutional Animal Care and Use Committee (IACUC; Protocol Number 0302394).

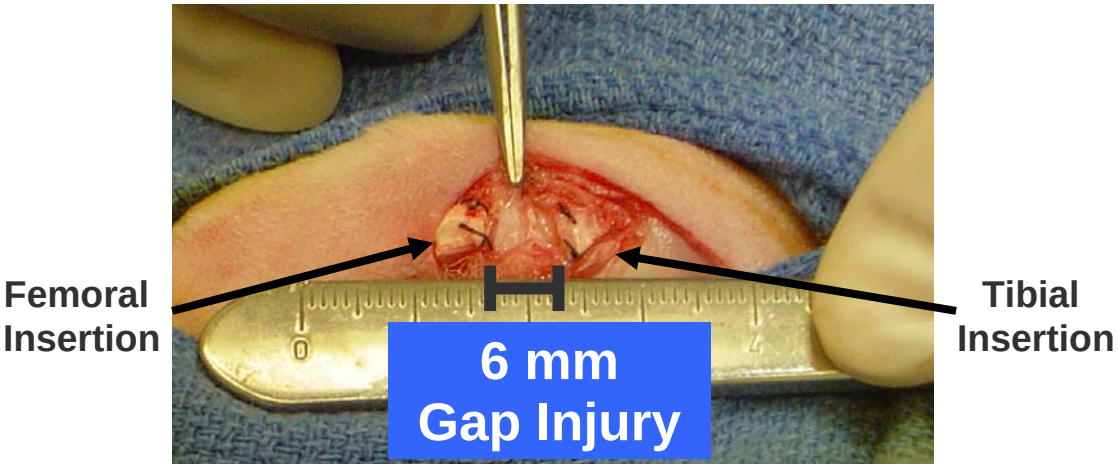

Figure 16: The photograph on the top shows the gap injury model in the rabbit medial collateral ligament (MCL) with suture markers at the loose ends of the gap.

Postoperatively, all animals were allowed free cage activity. No immobilization was used. The status of weight bearing, general health condition, as well as food and water intake of all animals was monitored by an experienced veterinary technician. Cephazolin (20-25 mg/kg) was administered twice a day for five days post-operatively for infection prophylaxis. Pain was assessed by monitoring changes in level of cage/pen activity and eating habits.

After 26 weeks, a lethal injection of sodium pentobarbital was given intravenously (50-100 mg/kg) while under sedation to humanely euthanize the animals at the time of sacrifice. This time point was selected for comparison with a previous study which looked at MCL healing and SIS-treatment at 12 weeks after gap injury [48]. After sacrifice, bilateral hind limbs were disarticulated at the hip joint. All hind limbs were wrapped in saline-soaked gauze, and immediately packed in plastic bags and stored at -20°C [80]. These methods are consistent with the recommendations of the Panel on Euthanasia of the American Veterinary Medical Association (University of Pittsburgh Assurance Number A3187-01).

4.3 CROSS SECTIONAL SHAPE AND AREA MEASUREMENTS

On the day of testing, each limb was thawed at room temperature and an orthopaedic surgeon examined specimens for joint abnormalities during dissection. All extraosseous and periarticular connective tissues around the knee were dissected leaving only the femur-MCL-tibia complex (FMTC) intact. To provide a clear path for the laser beam of the laser micrometer system, approximately 2 to 3 mm of the femoral and tibial condyles were cut parallel to each

other with the knee flexed at approximately 60 to 75°. Care was taken to avoid damage to the ligament at the tibial and femoral insertion sites.

The cross-sectional shape and area of the MCL substance was measured using the laser micrometer system [32, 33]. The laser micrometer system projects a collimated laser beam across a specimen and takes profile width measurements at 3° increments as it rotates 180° around the specimen. Measurements were obtained approximately at the ligament midsubstance (joint line), 5 mm proximal and 5 mm distal to the joint line. The cross-sectional shape obtained at the midsubstance was then quantified by finding the minor and major axis of the shape obtained by assuming a rectangular cross-section (Figure 17). The minor axis is defined as the minimum profile width measured by the laser micrometer system, and represents the thickness of the MCL. The major axis was the profile width measured at 90° from the angular position at which the minor axis was found. This value represents the width of the MCL. The cross-sectional area of the ligament was determined through an algorithm incorporated into the computer program that controls the system which utilizes Simpson's rule.

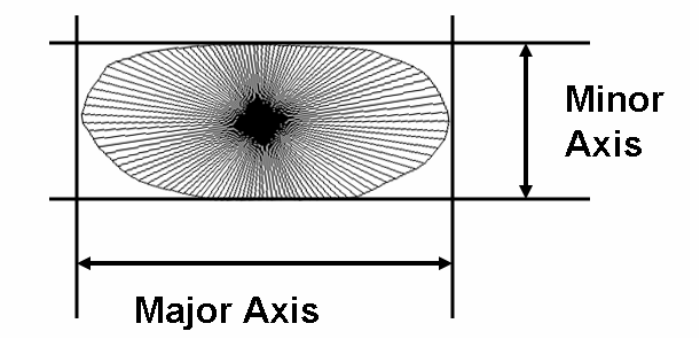

Figure 17: The minor and major axis of the ligament cross-section as determined by the laser micrometer system.

An unpaired t-test was performed to test the effects of treatment on the major and minor axis and average cross-sectional area of non-treated and SIS-treated healing MCLs. Each group was then compared to their respective sham-operated controls using a paired t-test. A significance level was set at $p \leq 0.05$.

4.4 RESULTS

No abnormal behavior was observed in the rabbits after surgery. All animals were healthy and ate well. In addition, no fatalities occurred during the 26 week period before sacrifice. At dissection, it was observed that all gap injuries of the MCLs healed with continuity of neoligamentous tissue and appeared to be without signs of inflammation in both SIS-treated and non-treated groups (Figure 18). For the sham-operated sides, gross inspection revealed no significant swelling or inflammation.

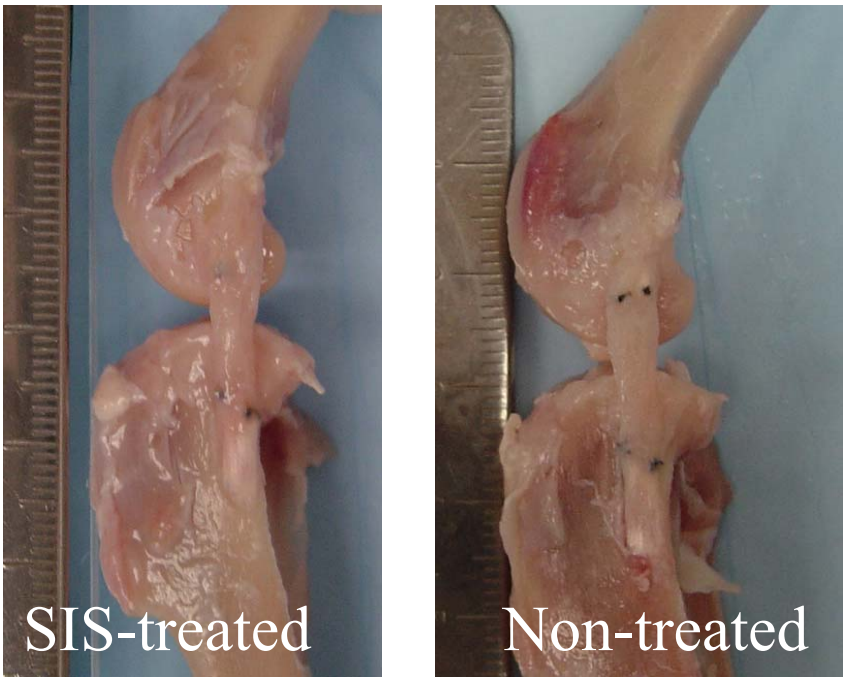

Figure 18: Photograph showing the typical healing medial collateral ligaments in the SIS-treated and non-treated groups respectively. The gap injuries in both groups healed with a continuity of neoligamentous tissue.

The cross-sectional shape as determined by the laser micrometer system showed that the SIS-treated group appeared less rounded than the non-treated group (Figure 19). Further analysis revealed that the SIS-treated group's cross-sections had a smaller minor axis (1.9±0.3 mm) than the non-treated group (2.2±0.4 mm), however this difference was not found to be significant ($p>0.05$). The major axis of the SIS-treated ligaments' cross-sections (3.4±0.5 mm) were also slightly smaller than the non-treated ligaments (3.7±0.5 mm), but this was also not significant ($p>0.05$). The cross-sections of the sham-operated control ligaments were more flattened in shape than the SIS-treated and non-treated groups (Figure 20). Their minor axis (1.5±0.2 mm) was significantly smaller that of the SIS-treated and non-treated groups ($p<0.05$). No significant

differences were found in the major axis for the sham-operated controls (3.5±0.3 mm) in comparison to the treatment groups ($p>0.05$).

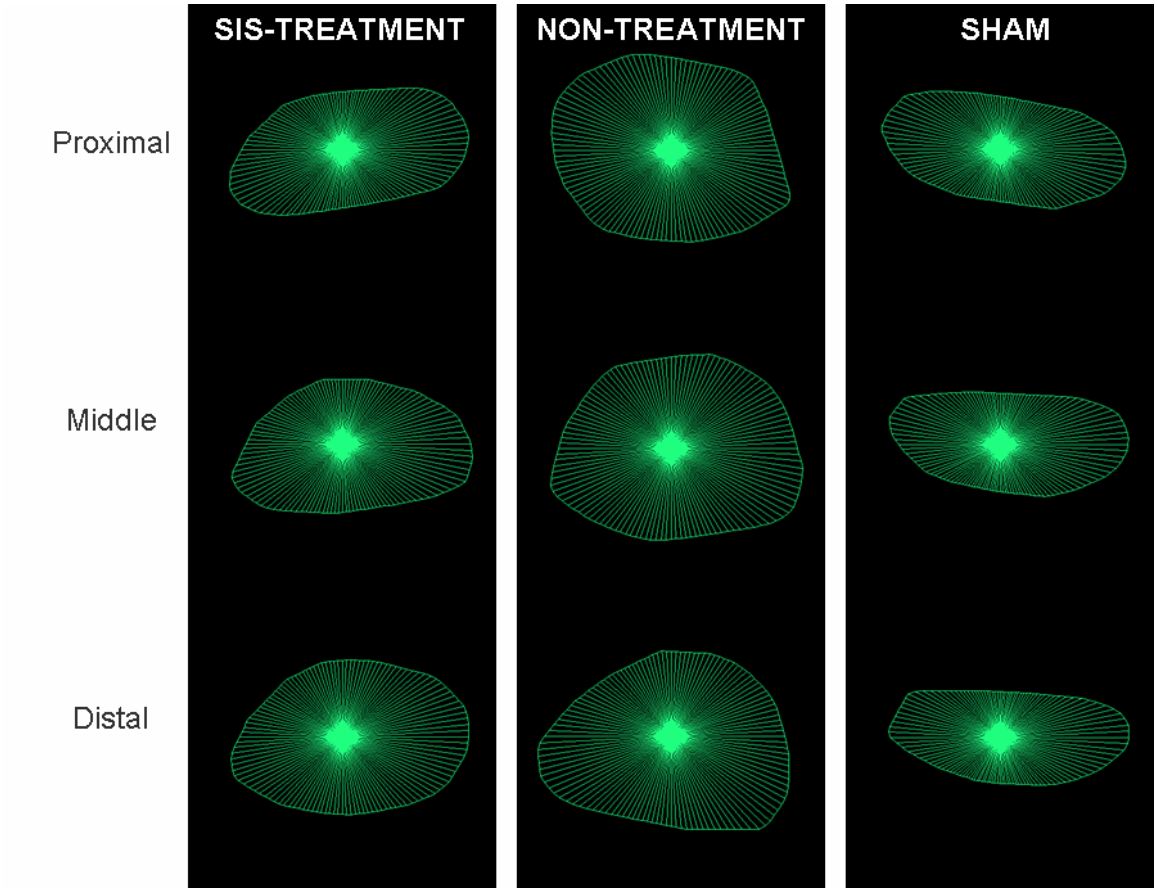

Figure 19: Representative cross-sectional shapes between the SIS-treated, non-treated, and sham-operated control groups.

Laser micrometer system measurements further revealed that SIS-treated ligaments (4.9±1.3 mm^2) had significantly smaller cross-sectional area than non-treated ligaments (6.4±1.4 mm^2, $p<0.05$). However, SIS-treated ligaments still had significantly larger cross-sectional areas

than their respective sham operated sides (4.1±0.7 mm^2, $p<0.05$). The cross-sectional areas of the non-treated group were nearly 50% greater than their respective sham-operated sides (4.2±0.4 mm^2, $p<0.05$). Furthermore, when the cross-sectional areas at the proximal, middle and distal sections of the substance were compared between groups (Figure 20), it was observed that the cross-sectional area for the SIS-treated and non-treated groups decreased from the proximal to the distal section. The cross-sectional areas for the SIS-treated group decreased 0.7 mm^2 and 0.2 mm^2 from the proximal to middle sections and from the middle to the distal sections, respectively. The cross-sectional areas for the non-treated group experienced larger decreases in area than the SIS-treated group with decreases of 1.0 mm^2 and 0.6 mm^2 from the proximal to middle sections and from the middle to the distal sections, respectively. On the other hand, the areas for the sham-operated control ligaments remained relatively constant throughout the section with a decrease of 0.5 mm^2 from the proximal to the middle section and a subsequent increase of 0.2 mm^2 from the middle to the distal section of the ligament substance.

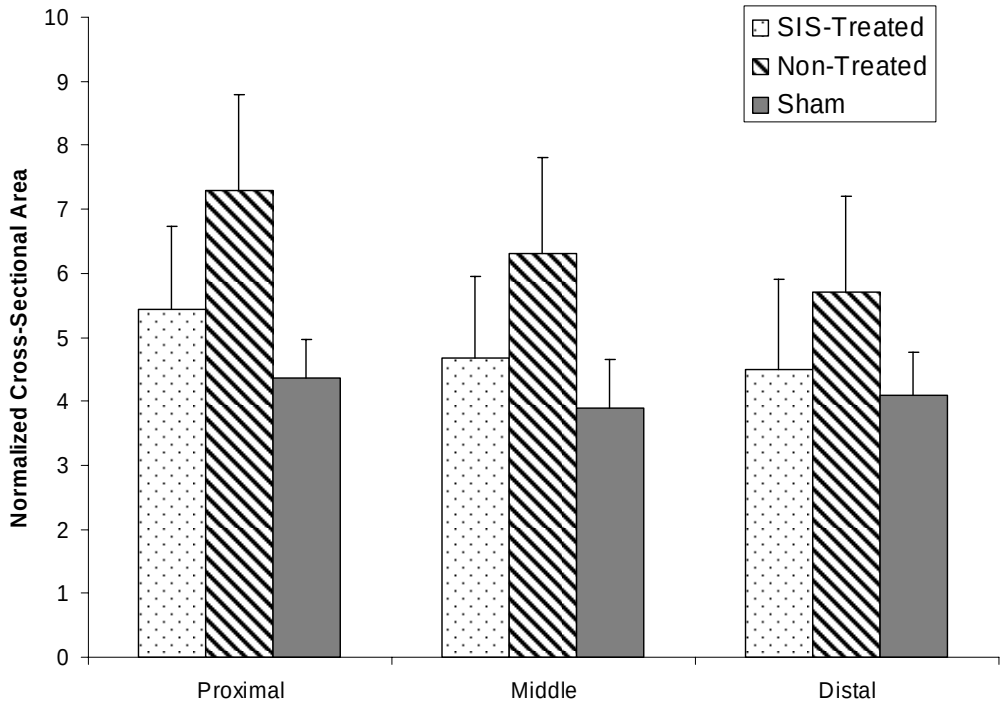

Figure 20: Comparison of the cross-sectional areas at the proximal, middle and distal sections of the medial collateral ligament for SIS-treated, non-treated and sham-operated control groups (data expressed as mean±S.D.).

4.5 DISCUSSION

In this study, treatment with a single layer of SIS collagen scaffold to enhance healing of a 6 mm MCL gap injury in the rabbit knee model was compared to a non-treated group after 26 weeks of healing. Although, SIS-treated MCLs appeared more flatter and similar in appearance to non-treated groups, no significant differences were found in their major and minor axis. SIS-treatment significantly reduced the cross-sectional area of the healing ligament in comparison to non-treated healing ligaments. These findings suggest that SIS may aid ligament healing by

contact guidance, helping the healing tissue more closely resemble intact tissue in terms of cross-sectional area.

The findings reported here are consistent with previous reports for non-treated MCLs, i.e. the healing process produces a large quantity of tissue at the injury site. In comparison to a previous shorter term study on SIS-treatment of MCLs, the cross-sectional area had reduced from 7.9 ± 4.7 mm^2 at 12 weeks (Musahl et al. 2004) to 4.9±1.3 mm^2 at 26 weeks after injury. The cross-sectional areas for the non-treated group were also reduced (7.2±4.7 mm^2 and 6.4±1.4 mm^2 respectively) but to a lesser extent. This finding suggests that SIS promotes remodeling of the healing MCL which may further improve its mechanical properties. It is also interesting to note that in this gap model, the cross-sectional areas of the healing MCLs decreased with time, where as in the rupture model they were increased (Ohland et al. 1991). This observation may reflect a difference between the injury models, but further investigation would be necessary.

One of the major limitations of this study is that the laser micrometer system is unable to detect concavities on the surface of the ligament. Not accounting for these concavities could result in a decrease in the accuracy of measurements for the minor and major axis of the cross-sectional shape, as well as the cross-sectional area. Additionally, one group may tend to have larger concavities than the other. Thus the size of the concavities could be considered a source of variability affecting shape and area measurements. However, in this study the differences between the groups were large enough that concavities did not to affect the comparisons of cross-sectional area. But the same cannot be assumed for the major and minor axis measurements, which may be more sensitive to variability in the data. Therefore, a more accurate method capable of detecting concavities within the cross-sections of MCLs is needed to

reduce this possible source of variability and allow for improved comparisons between experimental groups.

5.0 SPECIFIC AIM III: DEVELOPMENT OF A NEW SYSTEM FOR MEASURING THE CROSS-SECTIONAL SHAPE AND AREA OF LIGAMENTS

Due to limitations of the current system in measuring the shapes and areas of the MCL, a new system with the capacity to detect concavities on the specimen will possibly allow for more accurate cross-sectional shape and area measurements. With a more accurate system, smaller differences can be detected between different treatments (e.g. comparing treatment with different scaffolds) in future studies.

The determination of the cross-sectional shape and area of soft tissues has been a subject of interest for many decades in the field of biomechanics. Even to this day, there are no widely accepted methods for the determination of these parameters. However, with a standard method and device available, the tensile properties of soft tissues such as ligaments and tendons could be accurately obtained on the same basis by different research laboratories, thereby allowing for improved comparison of data. The mechanical properties for more complex tissues such as the cruciate ligaments could also be more accurately determined with the new device.

The charge coupled device (CCD) laser reflectance system is a device that can determine the cross-sectional shape and area of complex tissues and be easily adopted by other laboratories. The development of this device closely parallels that of its predecessor, the PSD laser reflectance system [68]. Development work included research in four distinct areas: (5.1) characterization of the CCD laser displacement sensor (influence of surface characteristics on accuracy), (5.2) development of a method for cross-sectional shape reconstruction and calculation of cross-

sectional area, (5.3) validation of the method and comparison to existing methods and (5.4) application to ligaments. In addition, a sensitivity analysis (5.5) was performed to investigate the effect of different factors on the accuracy of the system and alternative configurations (5.6) were also considered.

Before the system can be designed, some criteria which the device should meet need to be set forth. In order to set these criteria, some information must be obtained on the tissues that the device may possibly be used on. Therefore, several histological cross-sections of normal rabbit MCLs were analyzed using image analysis software (Scion Imaging Software, Scion Corp., Frederick, MD) (Appendix A). From this analysis, it was found that the concavities in the rabbit MCL can contribute approximately 5% error in the cross-sectional area measurements. The MCL's cross-section was also found to contain shallow concavities that could be up to 0.2 mm deep. The new system should be able to account for these concavities in order to improve the accuracy of measurements. The system should also be relatively fast in order to prevent dehydration during measurements and should not damage the tissue so that they can undergo biomechanical testing afterwards. Therefore, the developed device should meet the following design criteria:

1. Non-destructive
2. be accurate to less than 2% error,
3. making no contact with the specimen during measurement,
4. be able to measure the cross-sectional shape,
5. be able to detect shallow semicircular concavities that are common in ligaments,
6. be simple to use,
7. allow quick measurements (no more than 1 minute per cross-section), and

8. be relatively inexpensive (less than $5,000).

Satisfying these requirements will also permit the device to be easily adopted by other laboratories doing similar research as well as for application to measuring other tissues with more complex cross-sections (e.g. the cruciate ligaments, acromioclavicular ligaments, etc.) in addition to the rabbit MCL.

5.1 CHARACTERIZATION OF CCD LASER DISPLACEMENT SENSOR

Currently available laser scanning systems on the market are very expensive and not designed for use with biological tissue but rather for rapid prototyping and reverse engineering applications. In many cases, the lasers used in these systems require a dull surface on which to take measurements due to the sensitivity of the laser. Therefore objects are often spray painted or covered in talc powder to overcome this problem, thus these systems cannot be applied to biological tissues. Previous systems designed for biological tissues used PSD laser transducers to measure the distance between the sensor and the specimen's surface [68, 81]. However, the accuracy of these sensors can be affected by surface conditions and changes in the slope of the surface.

Since ligaments have glistening white surfaces, an ideal tool for measuring these distances would be a CCD laser displacement sensor because its accuracy is not compromised by surface conditions that are characteristic of ligaments. CCD laser displacement sensors are not sensitive to surface conditions such as color, reflectivity, and tilt because the CCD element reacts to light intensity, not light quantity, as is true with the PSD element, resulting in more stable

measurements. Therefore a CCD laser displacement sensor (650 nm wavelength, Class II red visible diode, Model AR-200-50M, Schmitt Measurement Systems, Inc., Portland, OR), which has a stand-off distance of 42 mm, a measurement range of ±25.4 mm and an accuracy of 0.1 mm was chosen for this new system (Figure 21). The sensor generates a 0.05 mm wide beam (at its stand-off distance) which strikes the specimen, while its receiver collects the reflected laser radiation to obtain distance measurements. A sensor with a 0.05 mm wide beam was chosen because it was suitable for detecting the concavities in the rabbit MCL as shown in sample histological sections (Appendix A).

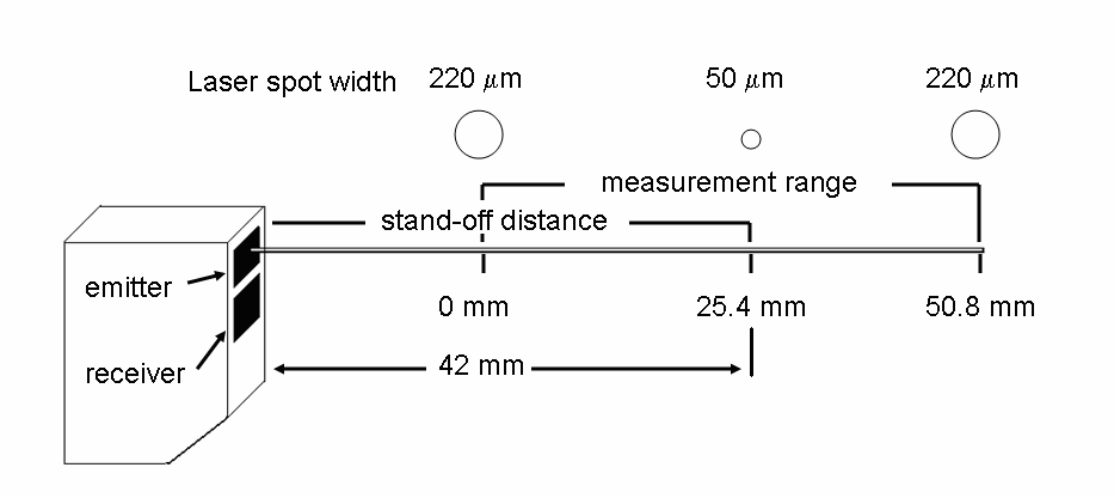

Figure 21: CCD laser displacement sensor (650 nm, Class II red visible diode) with design specifications.

The CCD laser displacement sensor uses the principle of triangulation to determine the distance from a target surface to the laser. A laser triangulation system consists of a laser source

(diode); a receiver lens; and a detector (CCD receiver). The diode projects a laser beam that illuminates a spot on the object of interest, and the receiver lens projects an image of light reflected from that spot onto the detector (Figure 22). When a point of light falling on an object moves, the spot's position on the detector changes as a result. The distance from the sensor to the surface can then by determined by taking the position of the imaged spot and calculating the angles involved.

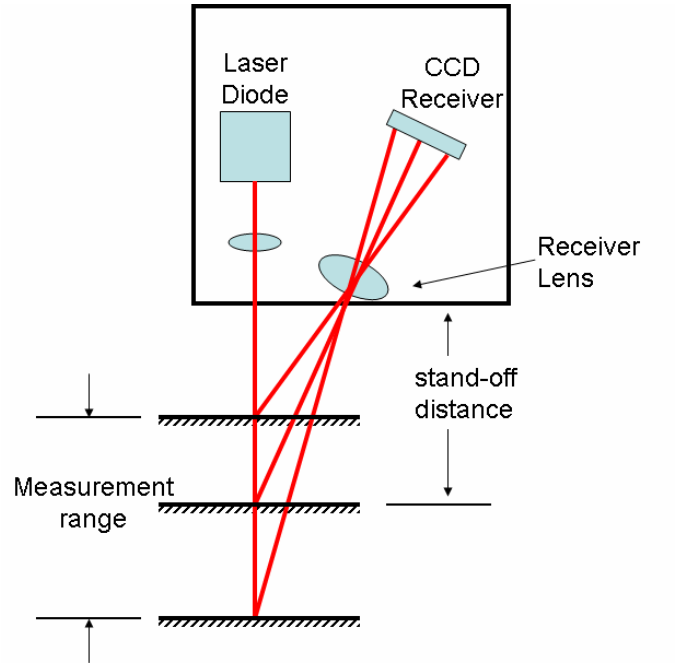

Figure 22: The CCD laser displacement sensor works on the principle of triangulation. A laser diode emits a laser beam onto a target, and the reflected light is captured by the CCD receiver.

Linear and rotary positioning tables (Parker Daedal 106006BT and 20601RT) were used to move and rotate the laser and the specimen in relation to one another (A schematic of how

these devices are connected to the computer has been provided in Appendix B). The linear positioning table has a reported positional accuracy within 24 μm and the rotary positioning table has a reported positional accuracy of 0.2 arc minutes. Laser interferometer measurements revealed that the linear positioning table has a positional accuracy within 7.5 μm of the target displacements. These positioning tables were then used to evaluate the effect of measurement distance, relative incidence angle, and surface characteristics on the accuracy of the laser. The accuracy of the CCD laser's displacement sensor was evaluated by comparing displacement readings taken from the laser and the linear motion table at 1 mm increments between 0 and 50 mm of the laser's measurement range. A dull gray colored surface was used initially to obtain a baseline evaluation of the sensor's readings (Figure 23). It was shown that the measurements of the laser sensor and displacements of the motion table corresponded well to one another since the differences between the two devices were less than 0.1 mm. The surface was later changed to white, black and rabbit MCL in order to evaluate the effects of surface conditions on the sensor. In addition, the rotary tables were used to rotate the gray, white and black surfaces 15, 30, 45, 60 and 75 degrees with respect to the laser sensor to evaluate the effects of incidence angle on the sensor's accuracy (Figure 24).

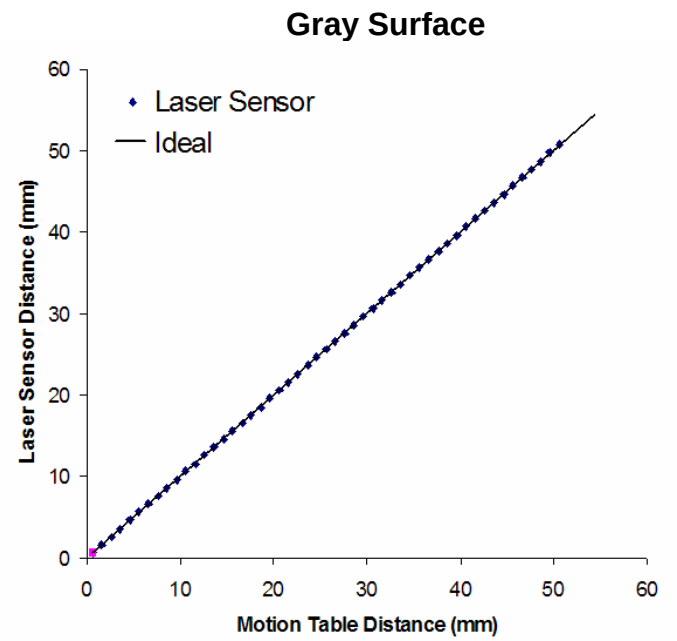

Figure 23: Motion table distance vs. laser sensor distance to illustrate the effect of measurement distance on a gray surface, which is the ideal surface for the laser sensor (r^2=0.999).

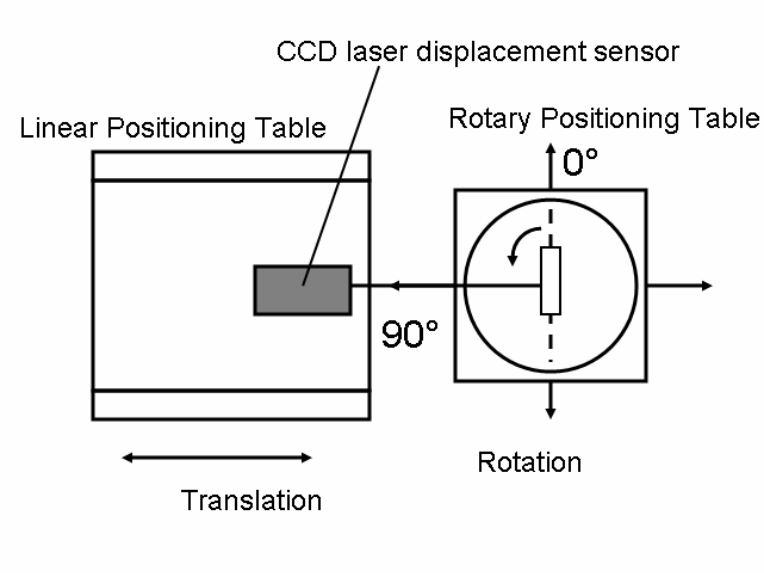

Figure 24: Experimental set-up to evaluate the effect of measurement distance, surface conditions and relative incidence angle

Surface conditions did not appear to affect the sensor's accuracy as the differences between the displacement of the target and the sensor were also within the accuracy of the laser sensor (less than 0.1 mm) on the different surfaces (white, black, rabbit MCL) (Appendix C). The angle of incidence also did not appear to affect the sensor's accuracy at 15, 30, 45, 60 and 75 degrees for the gray, white and black surfaces as differences between the displacement of the target and the sensor were also within the accuracy of the laser sensor (less than 0.1 mm) (Appendix D).

5.2 METHODOLOGY

A rigid aluminum frame was constructed to measure the cross-sectional shape and area of specimens (Figure 25). In this frame, a linear positioning table was mounted upright and used to control the location of the laser sensor. A shaft is connected to the rotary table and coupled to two gears via a gear belt. The gears will be used to rotate the specimen, which will be mounted perpendicular to the laser sensor. All positioning and measurement is automated using computer controlled stepper motors and data acquisition.

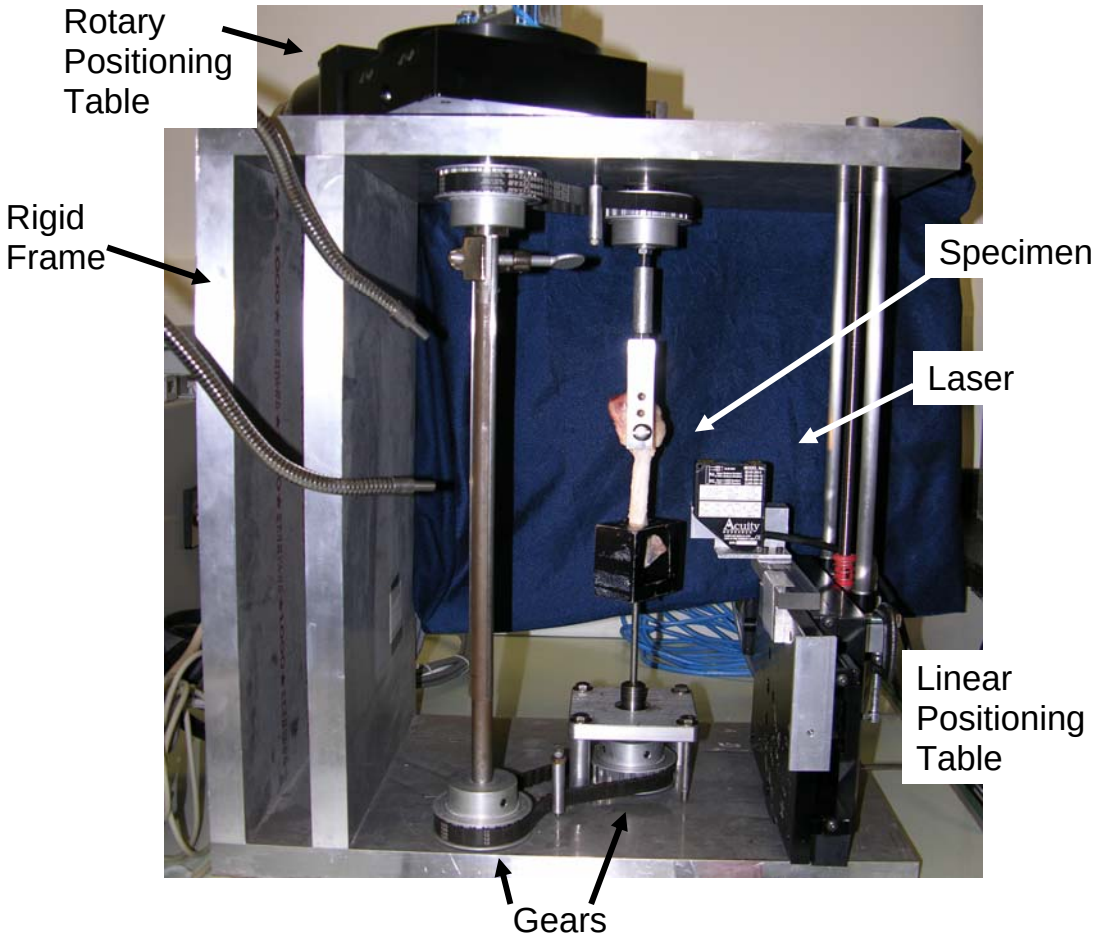

Figure 25: Frame used to position and rotate specimen within path of laser during measurements.

Two system configurations by which the laser sensor would collect measurements around the perimeter of the specimen were initially considered, the circular and octagonal system configurations [68]. In the circular system configuration, the specimen rotates 360° in the path of the laser while measurements are taken at defined angle increments (Figure 26). Due to limitations of the circular system such as the effect of specimen placement [68], the octagonal system was also considered. For the octagonal system configuration, data for the specimen

profile from one view is collected in a pass along one side of the specimen; then the specimen is rotated 45° and another pass is done; these steps are repeated until eight passes have been completed from which the cross-sectional shape and area can be determined (Figure 27). Although, specimen placement does not have an effect on measurements, a major drawback to this configuration is that it is very slow (9 minutes per cross-section) while the circular configuration was a great deal faster (72 seconds per cross-section). In addition, it was previously found for the PSD laser reflectance system that the values obtained for porcine ACL were not significantly different from one another between the two system configurations [68]. The octagonal configuration was also found to give less repeatable measurements, possibly due to the lengthy data reduction process incorporated. Since dehydration is a major concern when taking measurements of tissues, the circular system configuration was ultimately chosen for its speed.

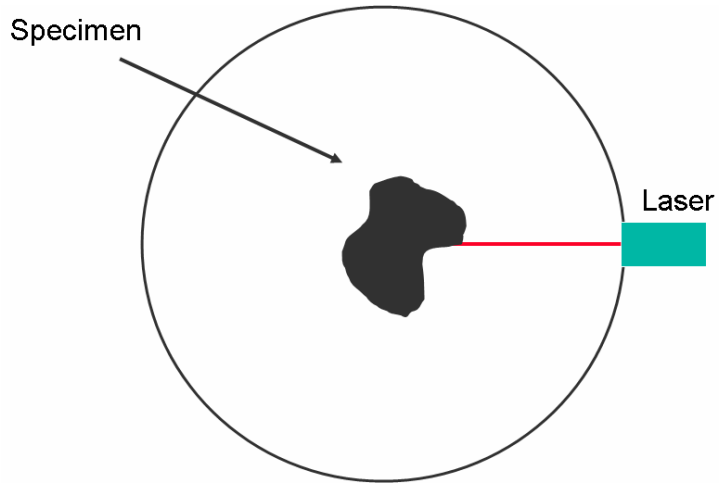

Figure 26: In the circular configuration, the laser sensor follows a circular path around the specimen while collecting measurements at defined angle increments [68].

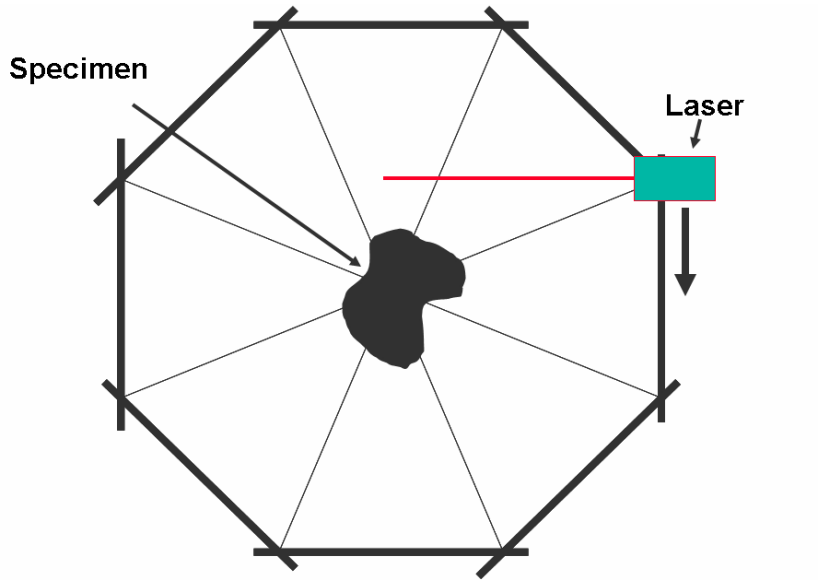

Figure 27: In the octagonal system, the laser sensor takes a pass along a side of the specimen at 45° increments, for a total of eight passes, while collecting measurements [68].

For the circular configuration, a series of measurements were taken using a circular object (D = 19.02 mm) in order to determine the center of rotation (COR) of the frame in a manner similar to that of Lee and Woo [32] (Figure 28). Since the object is circular, it was assumed that the minimum reference distances recorded for a linear scan across the object at 0° (parameter A) and 180° (parameter B) would correspond to opposite points on a chord going directly through the center of the circle. Once these two values and the diameter of the circle (D) are known, the COR is calculated by the following formula:

$$COR = (A+B+D)/2 \qquad (1)$$

In order to align the laser itself with the COR, The position of the laser on the linear positioning table corresponding to this COR was found by calculating the average of the corresponding

linear positions for the minimum reference distances (parameters C and D). The laser via the linear positioning table was then moved to this position.

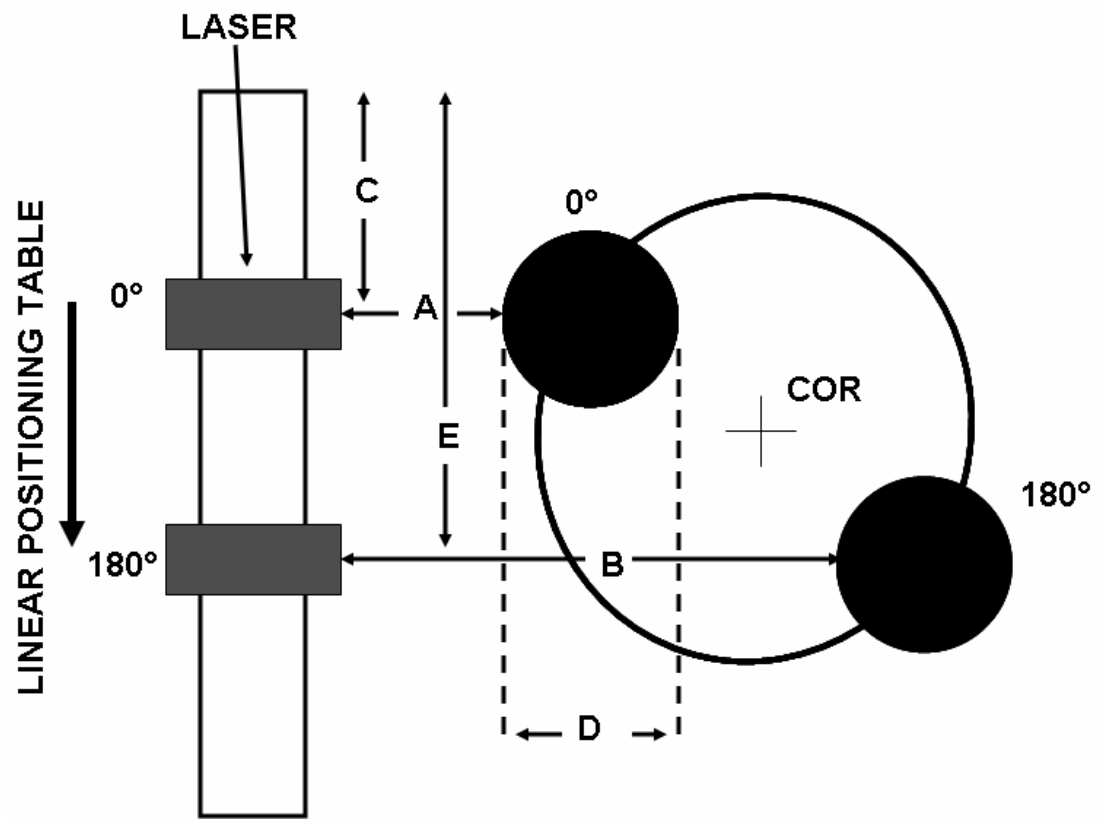

Figure 28: An off-centered circular object was used to determine the location of the center of rotation (COR) of the frame by taking linear scans at 0 and 180 degrees. A, B, and D are described in the text. The bold circle indicates the path of the off centered circular object around the COR.

Once the COR is determined and the laser aligned with the COR, a rotary positioning table was used to rotate the specimens 360° at 5°/sec within the path of the laser using Motion Planner software (Parker Hannifin Corp., Irwin, PA). The distance measurements of the surface of the specimen to the laser sensor were collected using Accurange Laser Sensor Interface

software (Schmitt Measurement Systems, Inc., Portland, OR) at a sampling rate of 100 Hz. Thus, a measurement was taken every 0.05° of rotation. This was the smallest angle increment possible at this speed. Smaller angle increments have been previously shown to result in more accurate cross-sectional shape and angle measurements [68]. Since the diameter and radius (R) of the path of rotation around the specimen is known (Figure 29), the distance to the edge of the specimen (r) from the center of rotation of the device at a particular angle (θ) can be determined as the difference between the outer radius and the distance to the surface,

$$r = R - d. \qquad (2)$$

In order to reconstruct the shape in a plot, the points representing the specimen perimeter are then converted from the polar coordinate system to the global X-Y coordinate system using the following formulas:

$$x = r \cos \theta \qquad y = r \sin \theta. \qquad (3)$$

Using the collected data and equations (2) and (3), the cross-sectional shape of the specimen was then reconstructed and graphed using Excel® spreadsheets (Microsoft Corp., Redmond, WA).

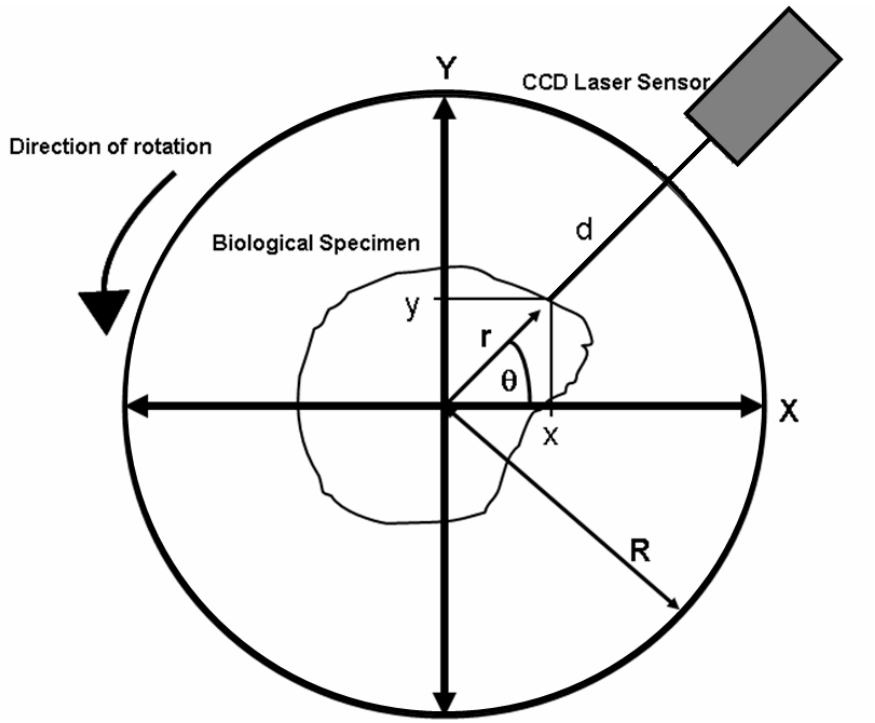

Figure 29: Top view of the CCD laser system configuration and cross-sectional shape reconstruction

The area of the resulting shape was then determined using Simpson's rule (3). This method takes two successive specimen radiuses (r) and averages them together to define the radius of the "pie-piece" shape between them. The area of this shape is calculated. This is repeated for each successive pair of points in a clockwise direction of rotation. Once the complete circumference of the specimen has been traverse, the cross-sectional area is determined by summing the area of all of the pie shapes.

$$\text{Area} = \sum_{\Phi = 0.05}^{360} \frac{0.05\pi \left(r(\Phi) + r(\Phi+0.05)\right)/2)^2}{360} \qquad (3)$$

Simpson's rule has also been used previously to find the areas of shapes obtained using the laser micrometer system [32]. All area calculations were done using Excel® spreadsheets (Microsoft Corp., Redmond, WA).

5.3 VALIDATION AND COMPARISON TO EXISTING METHOD

The accuracy and repeatability of the CCD laser reflectance system was evaluated using standardized shapes of known cross-sectional area (i.e. triangle, square, hexagon, circle, circle with square keyway, circle with triangle keyway, and circle with two half circle cutouts). These shapes were precision machined to a tolerance of 0.01 mm from acetyl Delrin (with the exception of the circle, which was made of stainless steel). Each specimen possessed a constant cross-section along the length. Because of the accurate machining, the cross-sectional area of the convex shapes could be accurately calculated from digital caliper measurements. Illustrations of the cross-sectional shapes of each specimen and their cross-sectional areas are included in Appendix D. Each shape was measured ten times by the CCD laser system. Each shape was also measured ten times in the laser micrometer system for comparison [32].

The CCD laser reflectance system was able to capture the concavities in the geometric shapes and give accurate representations of their cross-sections (Appendix E). The laser micrometer system, on the other hand, could not detect these concavities and as a result gave higher values for the cross-sectional area of geometric shapes with concavities (Appendix E). The results for the determination of cross-sectional area using the CCD laser reflectance system are shown in Table 1.

Table 1: Cross-sectional area calculation of standard geometric shapes of known cross-sections

Shape	Area (mm^2)	% Error
0.75" Dia. Circle	283.9±0.6	-0.3
Hexagon	410.7±1.5	-2.6
0.5" Square	150.72±0.1	-7.6
Triangle	202.5±0.2.6	-4.0
1" Circle w/ 2 half circle cutouts	462.0±0.6	-1.9
0.5" Circle w/ 2 half circle cutouts	114.2±0.4	-6.0

One of the limitations of using precision machined shapes is that they have sharp corners and angular indentations, which hardly mimic the biological condition. Therefore, a more rounded "kidney bean" shaped specimen constructed out of epoxy putty was also assessed. The cross-section of this specimen was photographed and the area in square pixels was found using image analysis software. Further analysis of the image for this shape revealed that not accounting for the concavity would result in approximately an 8% increase in area. Afterwards, the area of this specimen was measured ten times in the CCD laser reflectance system and then the laser micrometer system.

The CCD laser reflectance system was able to detect the shallow concavity within the "kidney bean" shaped specimen while the laser micrometer system was not (Figure 30). The cross-sectional area found using the laser micrometer system (177.2±0.7 mm^2) was 9.8% greater than that of the CCD laser reflectance system (160.6±0.4 mm^2). Thus, the CCD laser micrometer system was found to give reasonable measurements for the "kidney bean" shape.

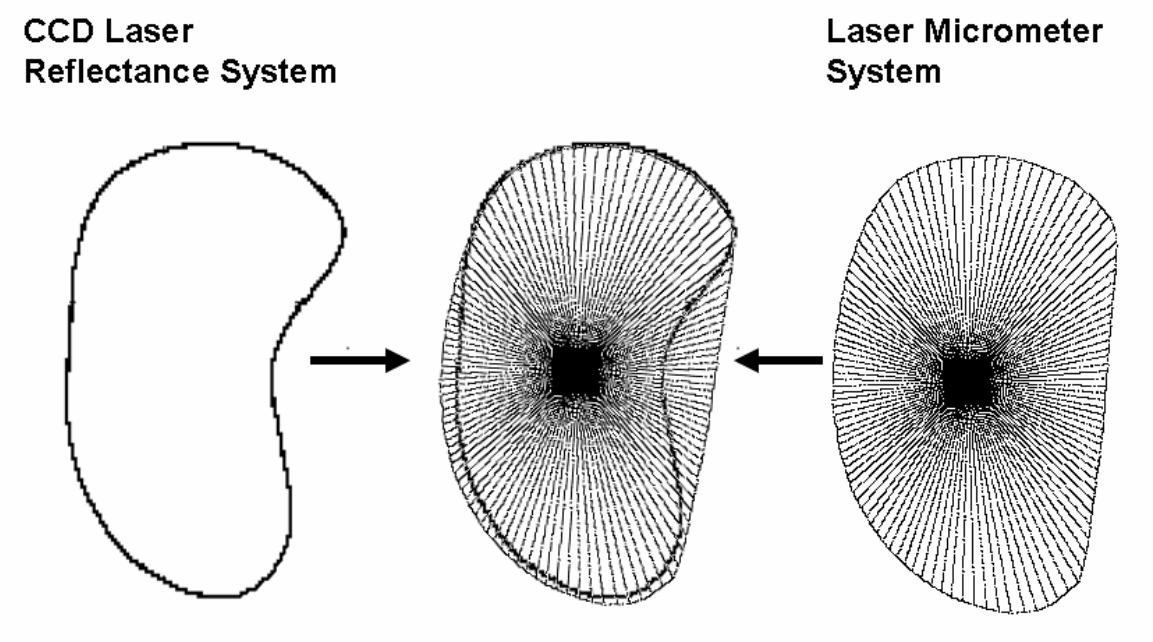

Figure 30: The cross-sectional shapes for the "kidney bean" shaped object showing the differences in the shape obtained for the CCD laser reflectance system and the laser micrometer system with the two shapes overlapping in the middle.

5.4 APPLICATION TO BIOLOGICAL SPECIMENS

The application of the CCD laser reflectance system was evaluated using porcine ligament and tendon specimens. Measurements of rabbit MCLs were attempted, but were not successful because the specimen kept leaving the path of the laser beam due to the small size of the specimen. Therefore the cross-sectional shape and area of the midsubstance for a porcine MCL, patellar tendon, ACL and PCL were evaluated using the CCD laser reflectance system and compared to measurements taken using a previously established method, the laser micrometer system [32]. Ligaments and tendons other than the MCL were tested in order to see how the

system could be applied to other tissues. The cross-sectional area and shape measurements were taken in the same location in the specimen for each device.

Ligament and patellar tendon specimens were harvested from porcine knees with their insertions intact within tibial and femoral bone blocks. These specimens were mounted in the laser reflectance system frame using clamps in an orientation where the fibers were aligned. Saline was used to ensure hydration was maintained between tests. Ten cross-sectional area measurements were obtained for one section of each specimen in both the CCD laser reflectance system and the laser micrometer system.

Valid measurements of the cross-sectional shape and area of the porcine MCL could not be taken using the CCD reflectance system because the tissue was relatively thin and therefore it was difficult to position the specimen so that it remained within the path of the laser beam for all 360° of rotation. For the other tissues measured, the CCD laser reflectance system was able to detect concavities within the cross-sections of the patellar tendon, ACL and PCL (Figure 31). The laser micrometer system, on the other hand, was unable to detect the surface concavities and the shapes obtained tended to appear more rounded off (Figure 31). Overall, the shapes obtained using these two systems compared well to each other in that the corresponding regions where concavities were detected using the CCD laser reflectance system appeared as flat regions in the laser micrometer system. In terms of cross-sectional area, the CCD laser reflectance system consistently yielded much lower values compared to the laser micrometer system (Table 2). The percent differences between the two systems was also higher than expected considering the sizes of the concavities, thus a sensitivity analysis was performed to investigate the effects of some of the possible sources of error on the accuracy of the system.

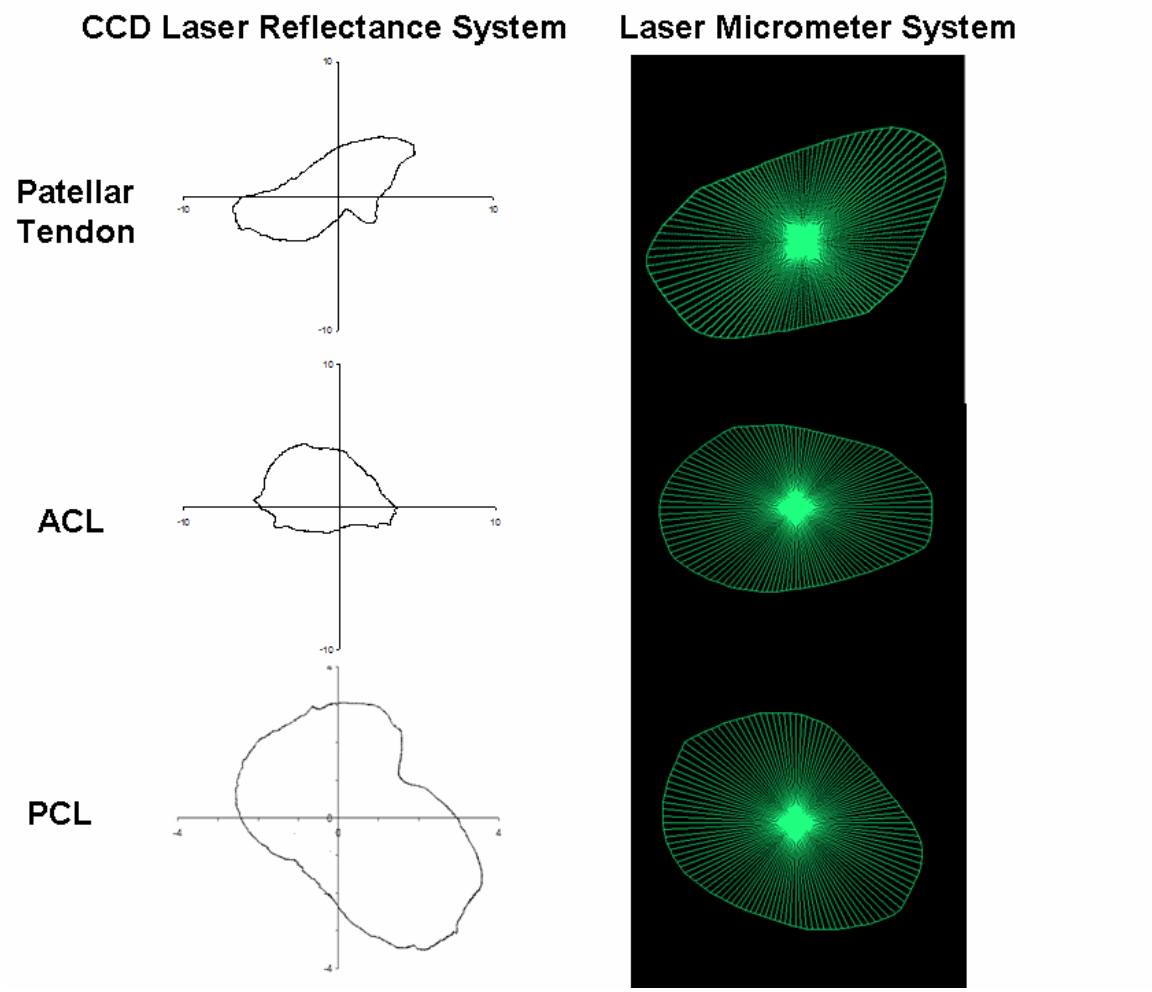

Figure 31: Comparisons of cross-sectional shapes obtained from the CCD laser reflectance system and the laser micrometer system for the A) patellar tendon, B) anterior cruciate ligament and C) posterior cruciate ligament.

Table 2: Comparisons between the cross-sectional areas obtained using the CCD laser reflectance system and the laser micrometer system for biological tissues

Tissue (area in mm^2)	CCD Laser Reflectance System	Laser Micrometer System	% Difference
Patellar Tendon	48.6±1.3	63.1±0.3	26.0
ACL	40.7±1.7	50.8±0.2	22.2
PCL	26.3±1.3	38.6±0.4	38.0

5.5 SENSITIVITY ANALYSIS

The percent errors for some of the geometric shapes and the percent differences for the biological tissues were higher than what is to be expected. However, it should be noted that the system presented here is a prototype, and therefore needs to have some refinements incorporated. The most significant of these involves the accuracy with which the system was constructed, and it is believed that tighter tolerances will improve the accuracy and repeatability of measurements. One possible source of error in the system is the angular deviation of the laser from the ideal alignment (Figure 32). An angular deviation will result in an erred value for the radius of the circular system configuration, "R", and the laser beam will also be offset from the COR of the system due to misalignment of the laser sensor (Figure 32). For example, an angular deviation of 1° can result in an "R" value being overestimated by 0.0064 mm and an offset of 0.7331 mm from the COR at the laser sensor's standoff distance (42 mm). Errors in "R" and misalignment of the laser beam with the COR of the system can also occur due to reasons other than angular deviation of the sensor. The impact these errors have on the resulting cross-sectional shape and area measurements may also be dependent on the size of the specimen being measured. Therefore a sensitivity analysis was conducted to look into the effects of these errors on subsequent measurements. The results of this analysis were then used to decide within what tolerances the frame would be machined in order for the CCD laser reflectance system to meet the requirements for accuracy.

A) Ideal Alignment of the Laser Sensor

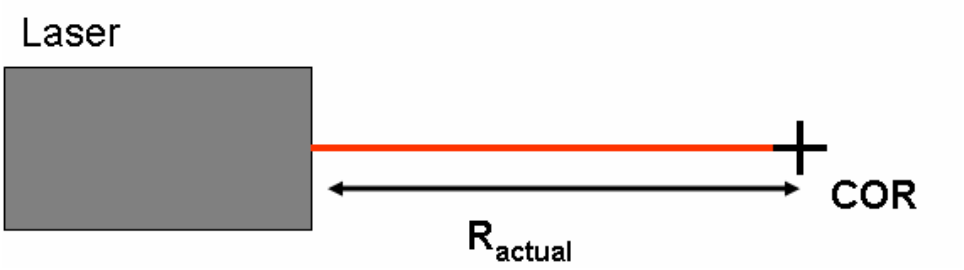

B) Misalignment of the Laser Sensor Due to Angular Deviation

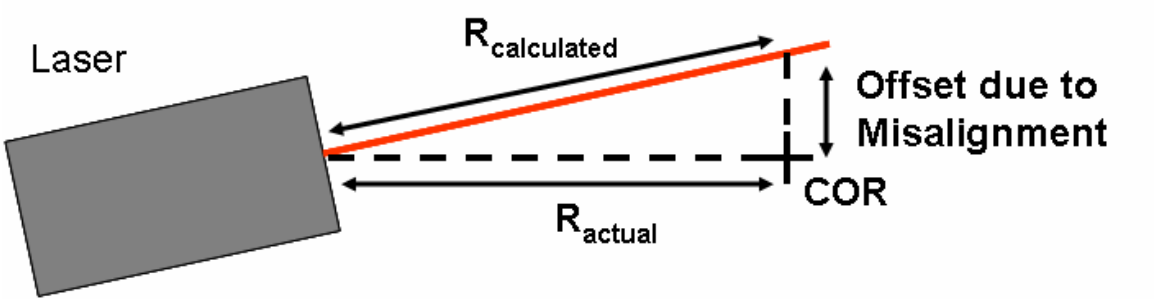

Figure 32: (A) In the ideal configuration, the laser sensor is aligned with the center of rotation (COR), however (B) an angular deviation of the laser can result in the laser sensor being offset from the COR and a miscalculation of "R".

In order to conduct a sensitivity analysis, hypothetical data sets were created which described a perfectly centered circle and square. No experimental data was used and the sensitivity analysis was performed computationally using spreadsheets so that each variable could be easily controlled. First the effect of offsetting "R" by ±0.1, ±0.05, ±0.025 and ±0.01 mm with respect to "R_{actual}" (i.e. the effect of miscalculating "$R_{calculated}$" relative to "R_{actual}") was evaluated on theoretical circle and square shapes of varying sizes. The size of the shapes varied from being within the size range of the rabbit MCL (3.14 mm^2 and 4.0 mm^2 for the circle and square, respectively) to the size of the standard shapes that were used for validation (201.06 mm^2

and 256 mm^2 for the circle and square, respectively). The effects of misaligning the laser with the center of rotation of the system by ±0.1, ±0.05, ±0.025 and ±0.01 mm were also evaluated on theoretical circle and square shapes of various sizes.

When "R" is miscalculated by -0.1 mm relative to "R_{actual}", the resulting cross-sectional shape becomes larger; as a result the cross-sectional area is overestimated for the circle (Figure 33). When "R" is miscalculated by +0.1 mm, the resulting cross-sectional shape becomes smaller and therefore the cross-sectional area is underestimated (Figure 33). Further analysis looking at the effects of miscalculation of "R" by ±0.05, ±0.025 and ±0.01 mm showed similar trends to what was previously demonstrated with ±0.1 mm, however the percent errors became smaller as the "R" value became more accurate (Figure 34). The percent error was found to decrease as the area of the circular cross-section increased (Figure 35). The absolute percent error due to a miscalculation of "R" by ±0.1 mm ranged from 21% (circle with area = 3.14 mm^2) to 2.5% (circle with area = 201.06 mm^2). Sensitivity analysis revealed that a tolerance of 0.01 mm is required for all sizes of this shape in order to meet the requirements for accuracy (less than 2% error for all sizes). For complete results of this analysis please refer to Appendix G.

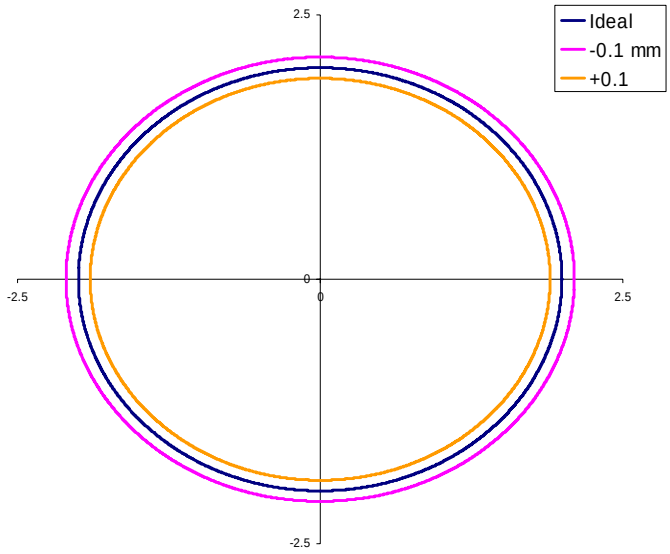

Figure 33: An offset by -0.1 mm relative to "R_{actual}" results in a larger cross-sectional shape (magenta) and thus an overestimation of the cross-sectional area for the circle. While an offset of the value for "R" by +0.1 mm relative to "R_{actual}" results in a smaller cross-sectional shape (orange) and thus an underestimation of the cross-sectional area for the circle.

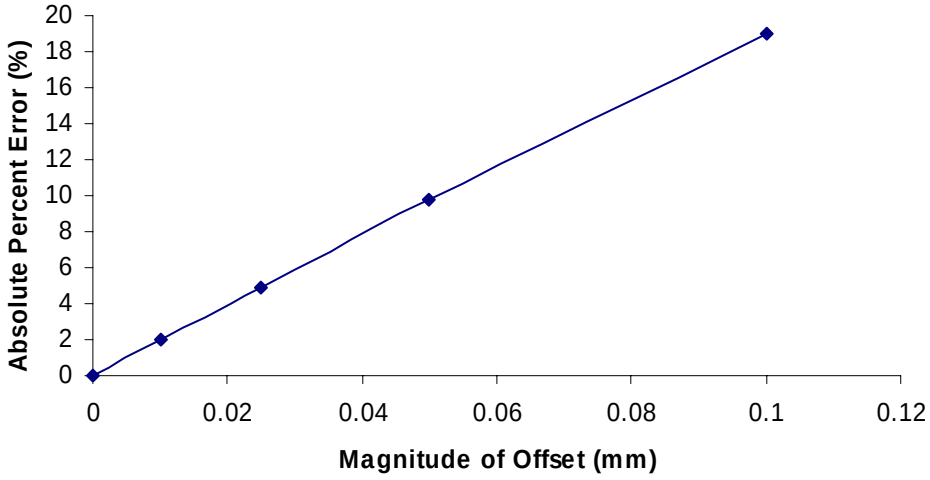

Figure 34: The effects of the offset magnitude on the absolute percent error of the cross-sectional area for a circle (area = 3.14 mm^2).

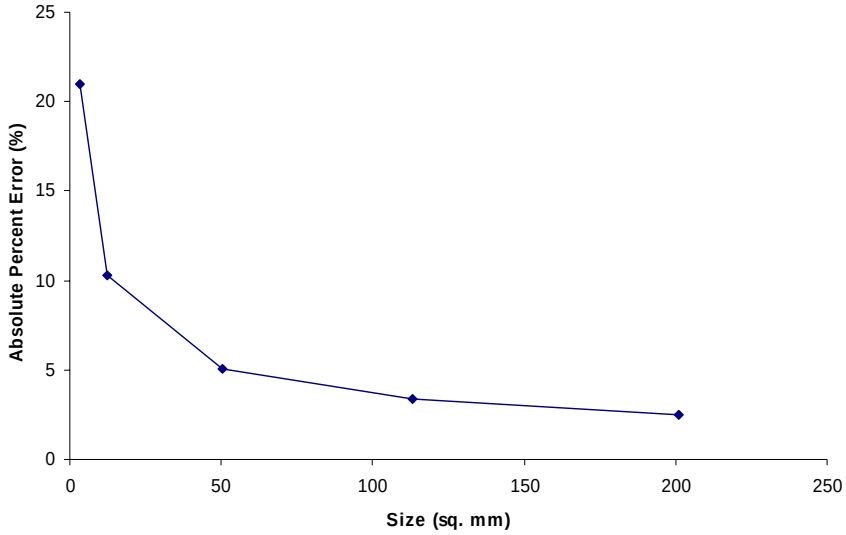

Figure 35: This graph demonstrates the effects of specimen size on the absolute percent error of the cross-sectional area measurement when the value for "R" is offset by +0.1 mm relative to "R_{actual}". The percent error decreases as the size of the circle increases.

When this analysis was done for square cross-sections of varying sizes, similar results were obtained to those for the circular shapes, however the flat edges of the squares tended to bend inwards or outwards compared in comparison to the ideal situation, where the edges were straight (Figure 36). Further analysis looking at the effects of miscalculation of "R" by ±0.05, ±0.025 and ±0.01 mm showed similar trends to what was previously demonstrated with ±0.1 mm, however the percent errors became smaller as the "R" value became more accurate (Figure 37). The absolute percent error due to a miscalculation of "R" by ±0.1 mm ranged from 18.4% (square with area = 4.0 mm^2) to 2.2% (square with area = 256.0 mm^2). The percent error was found to decrease as the area of the square cross-section increased (Figure 38). Sensitivity analysis also revealed that a tolerance of 0.01 mm is required for all sizes of this shape in order

to meet the requirements for accuracy (less than 2% error for all sizes). For complete results of this analysis please refer to Appendix H.

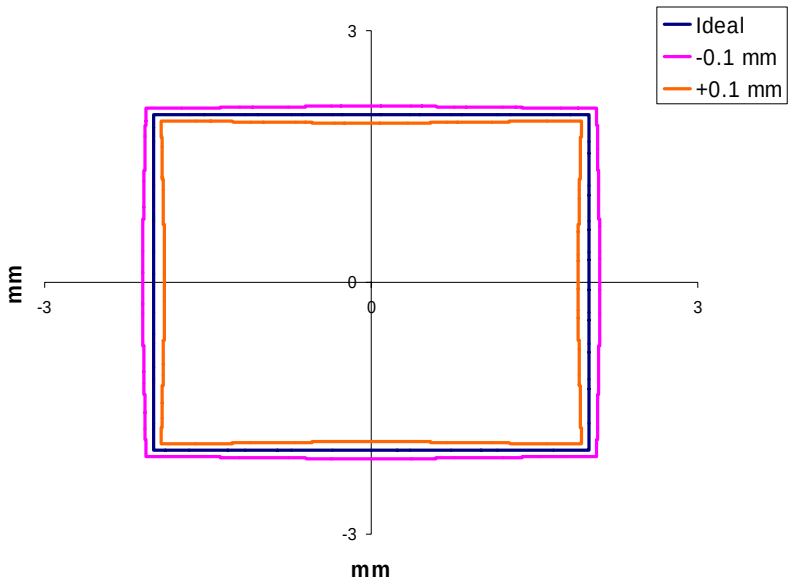

Figure 36: An offset by +0.1 mm relative to "R_{actual}" results in a smaller cross-sectional shape (orange) and thus an underestimation of the cross-sectional area for the square. While an offset of -0.1 mm relative to "R_{actual}" results in a larger cross-sectional shape (magenta) and thus an overestimation of the cross-sectional area.

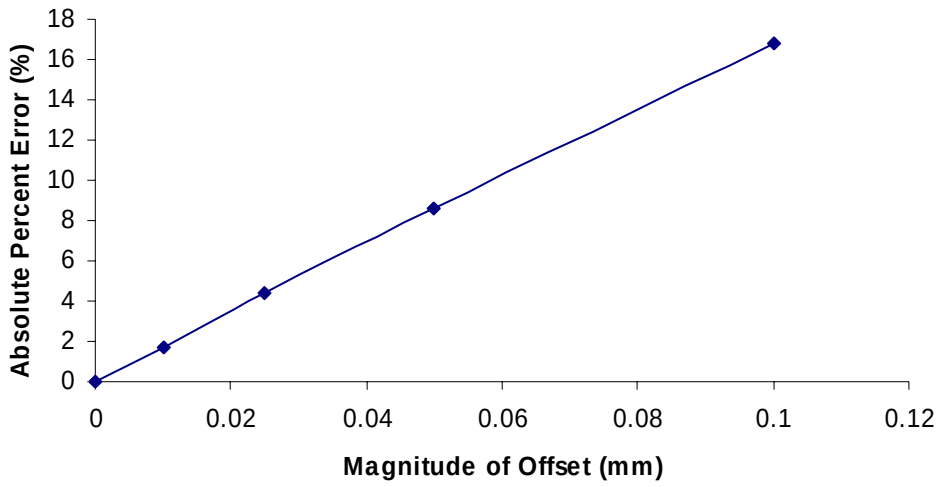

Figure 37: The effects of the offset magnitude on the absolute percent error of the cross-sectional area for a square (area = 4.0 mm^2).

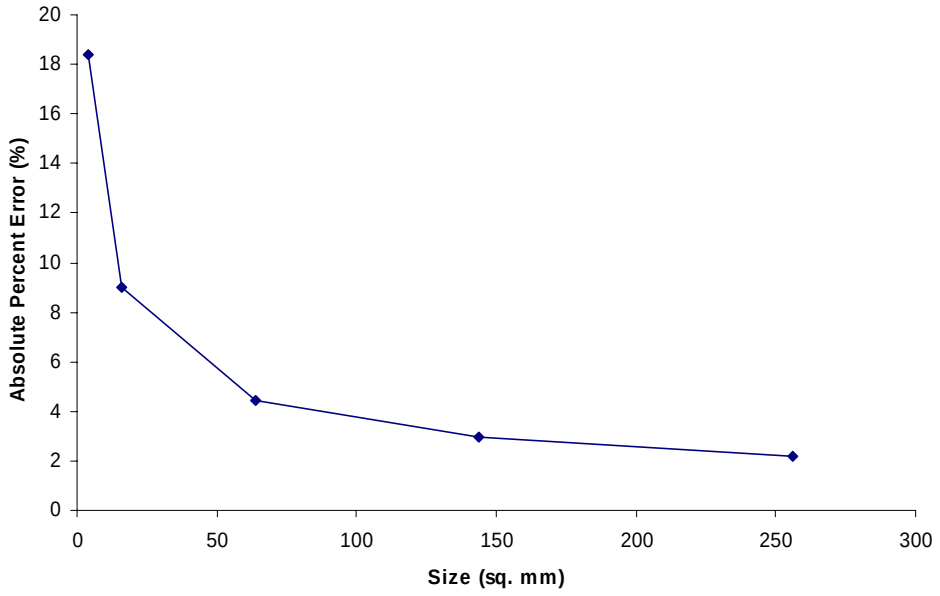

Figure 38: This figure shows the effects of specimen size on the absolute percent error of the cross-sectional area measurement when the value for "R" is offset by +0.1 mm relative to "R_{actual}". The percent error decreases as the size of the square increases.

The misalignment of the laser sensor with the center of rotation by ±0.1 resulted in no significantly noticeable differences in the cross-sectional shape of the circle (Figure 39). The misalignment of the laser sensor with the center of rotation by ±0.1, ±0.05, ±0.025 and ±0.01 mm resulted in less than 1% error for circular cross-sections of all sizes investigated (Figure 40). These percent errors due to misalignment of the laser decreased as size increased (Figure 41). Therefore in this case, a tolerance of ±0.1 mm would be acceptable for the alignment of the laser sensor in order to meet the requirements for accuracy with circular cross-sections of various sizes (less than 2% error for all sizes). For complete results of this analysis please refer to Appendix I.

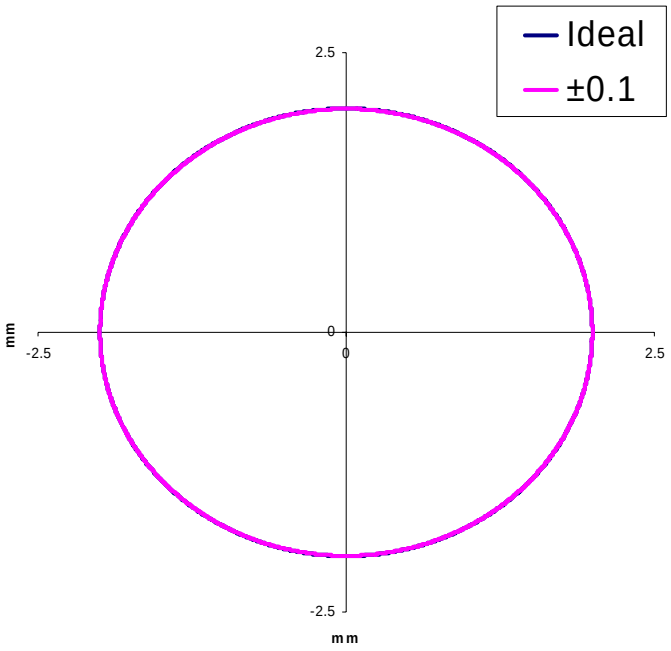

Figure 39: A misalignment of the laser by ±0.1 mm results in a slightly smaller cross-sectional shape (magenta) and thus an underestimation of the cross-sectional area for the circle. However the percent error resulting from this misalignment was less than 1% for circular cross-sections of all sizes and misalignments investigated.

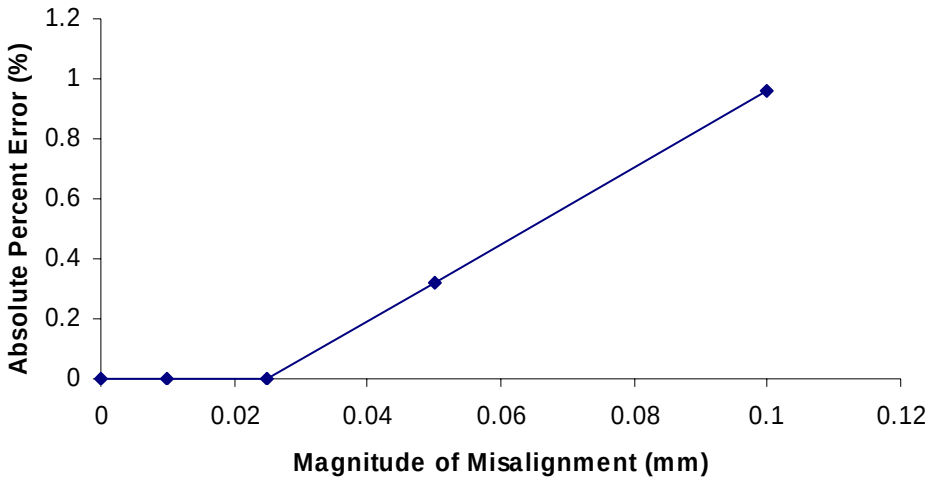

Figure 40: The effects of the magnitude of the misalignment of the laser relative to the COR on the absolute percent error of the cross-sectional area for a circle (area = 3.14 mm^2).

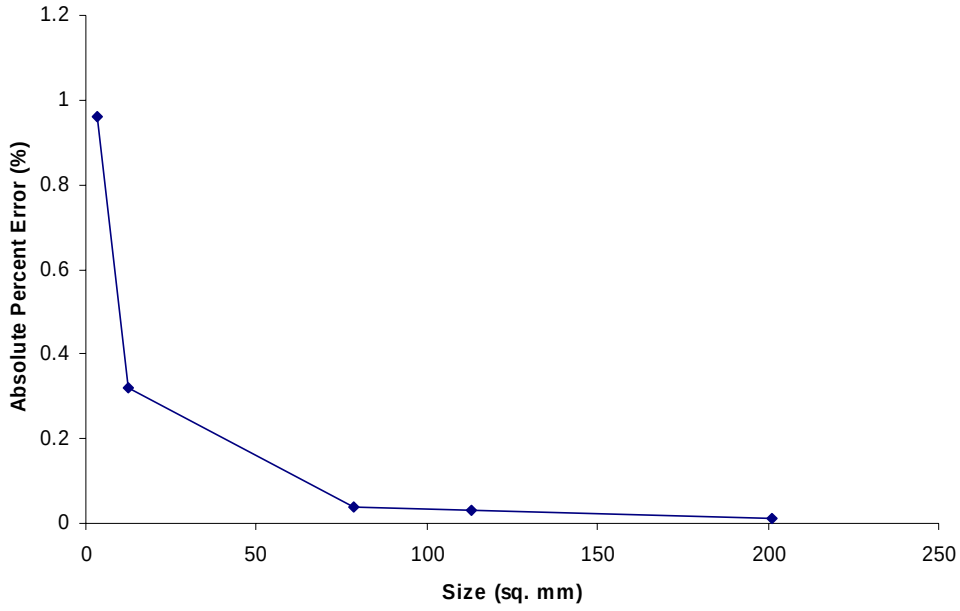

Figure 41: This figure shows the effects of specimen size on the absolute percent error of the cross-sectional area measurement when the laser is misaligned with the COR by ±0.1 mm. The percent error decreases as the size of the square increases.

Misalignment of the laser with the COR by ±0.1 mm had a more significant impact on the shape reconstruction of the square cross-sections (Figure 42). As a result, the cross-sectional area of the shape was underestimated. The absolute percent errors for the squares of various sizes ranged from 8.0% (square with area = 4.0 mm^2) to 1.0% (square with area = 256.0 mm^2). Theses errors decreased as the magnitude of misalignment decreased (±0.05, ±0.025 and ±0.01 mm) (Figure 43). In addition, the percent errors due to misalignment of the laser decreased as size of the square increased (Figure 44). From this sensitivity analysis, a tolerance of ±0.025 mm for the alignment of the laser would be acceptable in order to meet the requirements for accuracy with square cross-sections of various sizes (less than 2% error for all sizes). For complete results of this analysis please refer to Appendix J.

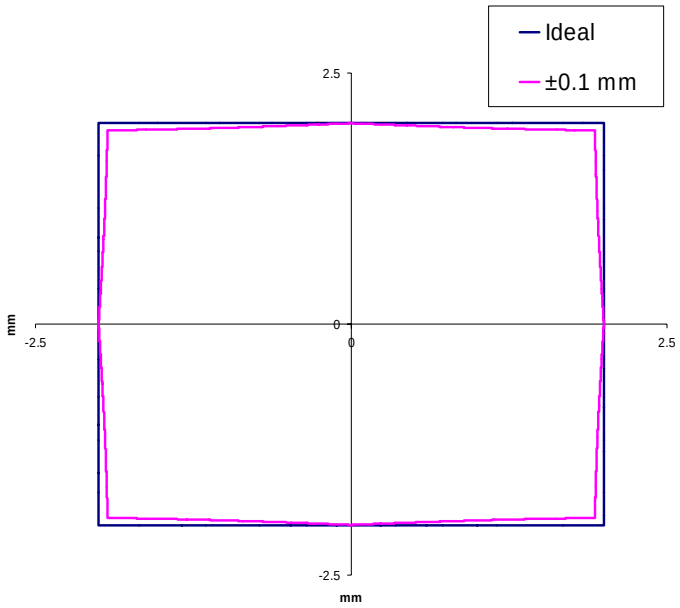

Figure 42: A misalignment of the laser with the COR by ±0.1 mm results in a smaller cross-sectional shape (orange) and thus an underestimation of the cross-sectional area for the circle.

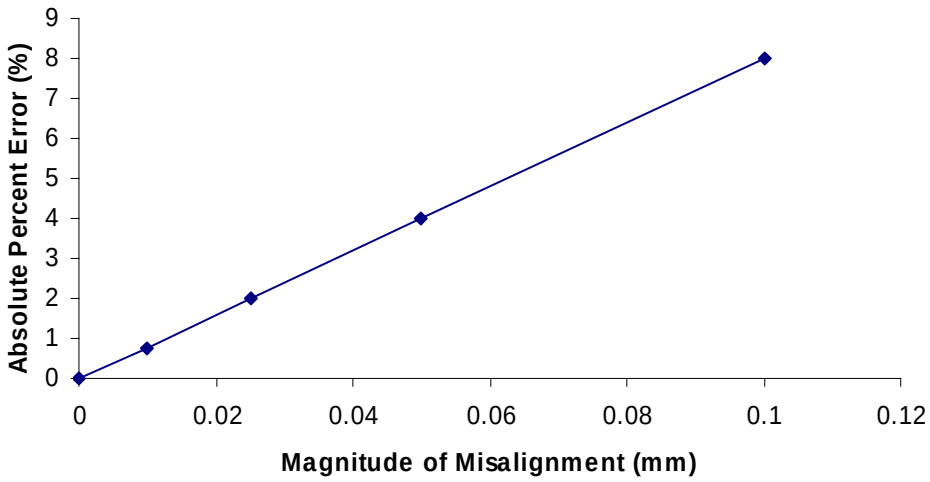

Figure 43: The effects of the magnitude of the misalignment of the laser relative to the COR on the absolute percent error of the cross-sectional area for a square (area = 4 mm^2).

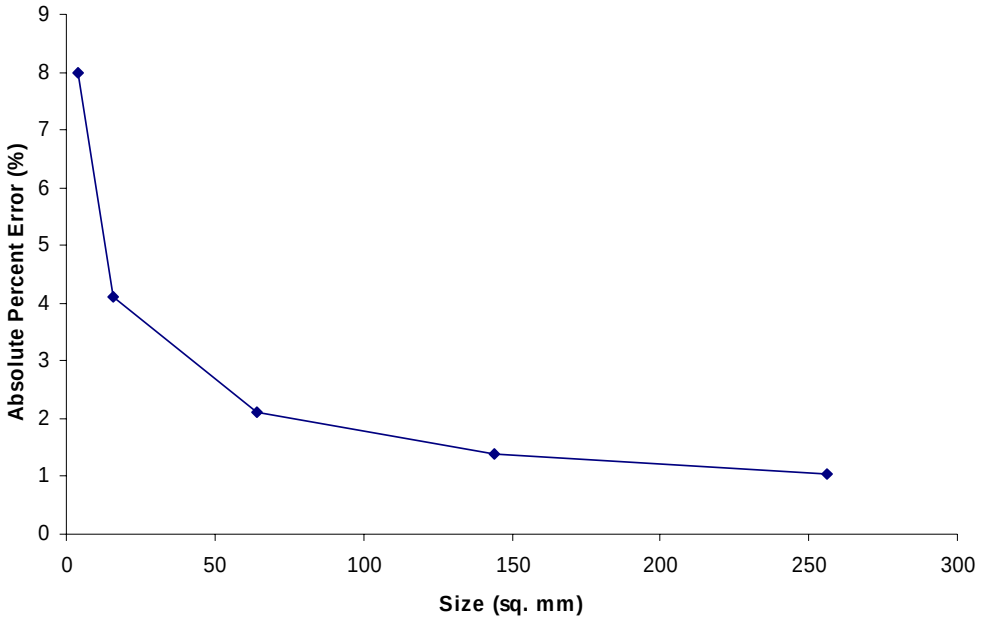

Figure 44: The effects of specimen size on the absolute percent error of the cross-sectional area measurement when the laser is misaligned with the COR by ±0.1 mm. The percent error decreases as the size of the square increases.

From the sensitivity analysis, it was determined that the CCD laser reflectance system would have to be constructed within a tolerance of 0.01 mm in order to provide accurate measurements (less than 2% error) for specimens as small as rabbit MCLs. Sensitivity analysis using theoretical data demonstrated that if the laser is not positioned and aligned perfectly, then the accuracy in the cross-sectional area measurements should decrease as the size of the specimen decreased. In order to investigate whether experimental data would support the findings of the sensitivity analysis, several metal objects with circular cross-sections of various sizes were measured in the CCD laser reflectance system, as well as the laser micrometer system (Table 3). The accuracy of the CCD laser reflectance system decreased (percent errors increased) as the size of the shapes became smaller. The accuracy of the laser micrometer

system remained relatively consistent (within 0.6% error) regardless of the size of the circle. In addition, the amount of error in the measurements caused by inaccuracies in the positioning and alignment of the laser can be dependent upon the shape being measured. For instance square shapes had more error than circular shapes. Experimentally this was shown because the square (area = 163.2 mm^2) had a -7.6% error while a circle of a similar but smaller size (area = 127.7 mm^2) had an error of -1.25%.

Table 3: The Effects of Size of Circle on the Accuracy of the CCD Laser Reflectance System and the Laser Micrometer System

Diameter of Circle (mm)	Actual Area (mm^2)	CCD Laser (mm^2)	% Error	Laser Mic (mm^2)	% Error
19.03	284.7	283.7	-0.35%	283.5	-0.42%
12.75	127.7	126.1	-1.25%	127.1	-0.47%
7.98	50.0	48.2	-3.60%	50.0	0.00%
6.32	31.4	30.7	-2.23%	31.4	0.00%
4.67	17.1	16.3	-4.68%	17.0	-0.58%

The sensitivity analysis performed computationally had the objects placed at the ideal position, perfectly centered over the COR. However for the experimental measurements, the objects were not ideally positioned, and a combination of a miscalculated "R" value and misalignment of the laser sensor could have contributed to the errors in the measurements performed. In addition, the decrease in percent error observed for the CCD reflectance system between the circles with diameters of 7.98 mm and 6.32 mm suggest that there may be other factors contributing to the errors and variability in the measurements such as the positioning of the specimen in relation to the COR (Figure 45). One of the limitations of the circular

configuration as previously described (Chan et al. 1995) is that if the specimen's center is not located on the COR of the system (Figure 45-B), then the side of the specimen closer to the laser sensor will have readings taken at larger intervals around the perimeter. In addition, the laser might possibly have to take measurements off the surface at extreme angles of incidence.

For the CCD laser reflectance system used in this study, the increment angles were made very small (0.05°) compared to the previous PSD laser reflectance system (3°) [68] in order to reduce the possible effects of specimen location within the system. However the position of the specimen relative to the COR may still have an effect and this effect may be size dependent. Thus a sensitivity analysis was performed to see if this was the case.

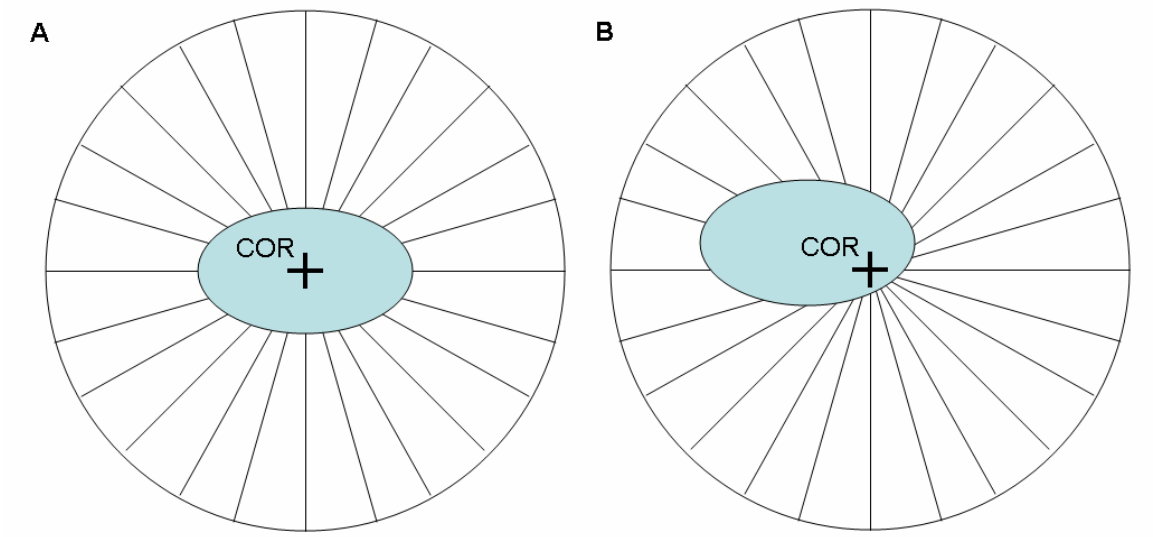

Figure 45: A) When the center of the specimen is on the COR of the device, the measurements taken around the perimeter are more evenly spaced apart compared to B) where the side of the specimen located farther from the sensor will have readings taken at smaller intervals around the perimeter than the other sides.

The square was used as a model to assess whether the position of the specimen's center relative to the COR had any significant effect on the cross-sectional shape and area measurements. This shape was chosen because it was much easier to control the position of its center relative to the COR by using spreadsheets. No errors were detectable (percent error = 0.00%) when squares of various sizes (4 x 4 mm, 5 x 5 mm and 6 x 6 mm) were offset by 1 mm relative to the COR (Figure 46). The 4x4 mm square was then used to investigate whether if the magnitude of the offset could affect the accuracy of the measurement. No errors were also detected when the center of the square was offset 0.5 mm, 1 mm, 1.5 mm, 1.75 mm and 1.9 mm relative to the COR of the circular configuration (Figure 47).

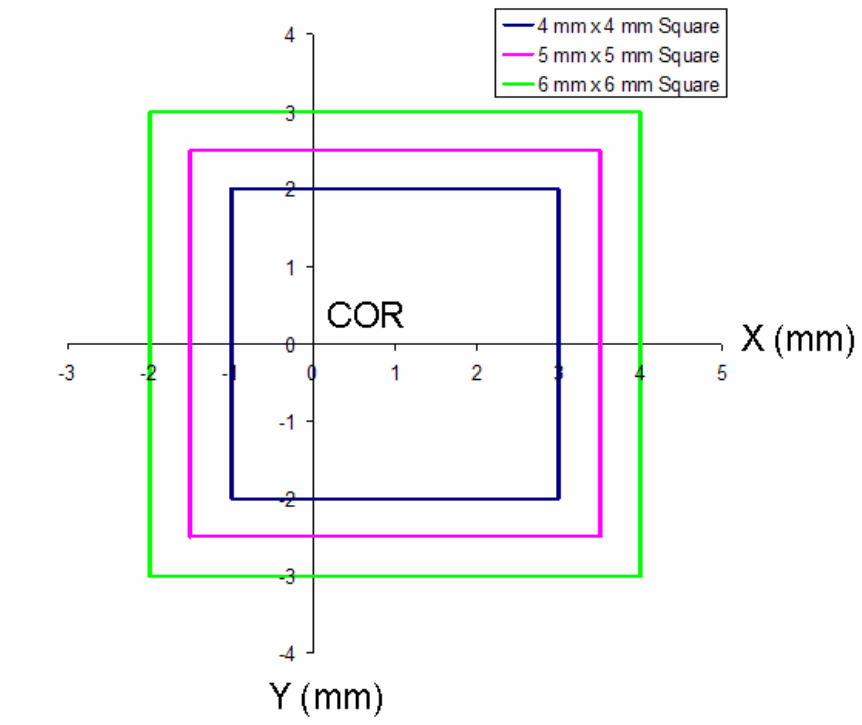

Figure 46: A 1 mm offset in the X direction relative to the COR did not produce any errors for the square shapes of various sizes (4 x 4 mm, 5 x 5 mm and 6 x 6 mm).

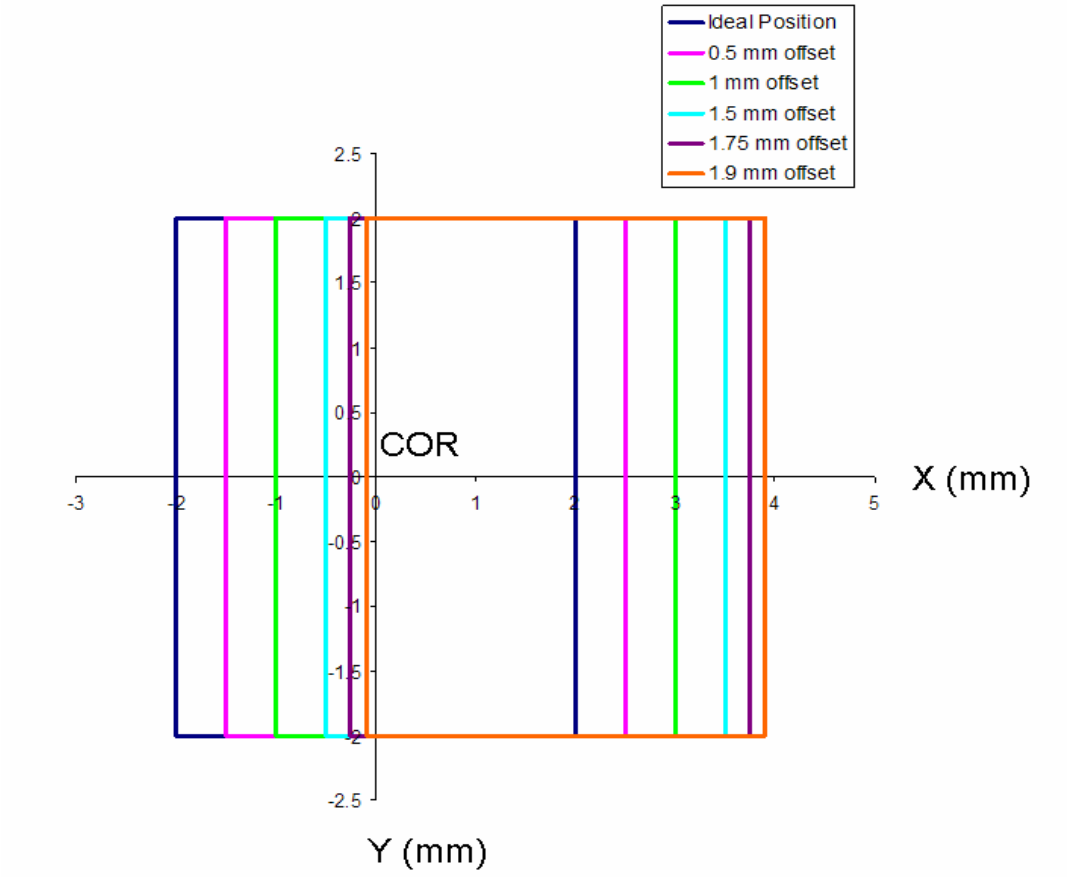

Figure 47: Offsetting the center of the square by 0.5 mm, 1 mm, 1.5 mm, 1.75 mm, and 1.9 mm did not have any effect on the measurement of the cross-sectional shape and area.

Using the square shape as a model, it was found that the position of the specimen relative to the COR may not have an effect on the accuracy of measurements of cross-sectional shape and area, except in extreme cases when the COR is not within the specimen's cross-section. The specimen's position should not have an effect on these measurements as long as the COR is well within the specimen's cross-section, because the increments at which laser sensor readings are taken are very small. However, this analysis could not take into account the error due to taking laser sensor readings when the specimen's surface is oriented at extreme angles (greater than

75°) in relation to the sensor. These extreme surface angles are more likely to occur when the specimen's position is off centered relative to the COR.

5.6 ALTERNATIVE CONFIGURATIONS

The CCD laser reflectance system in the circular system configuration was found not to be suitable for measuring the cross-sectional shape and area of rabbit and porcine MCLs, mainly due to their size and shape. The small size of the rabbit MCLs and the elongated shape of the MCL cross-section in general make measurements in the circular configuration difficult because the specimen keeps leaving the path of the laser if it is not ideally positioned within the system. The octagonal system configuration, on the other hand, was found not to be suitable because it takes a long amount of time to take one measurement, which may lead to dehydration and shrinkage of the specimen (Chan 1995). With the octagonal system configuration, however, it is easier to position the specimen since the specimen does not have to always be within the path of the specimen. The major reason why the octagonal system takes a long time to complete a measurement is because it requires eight separate scans along eight different paths around the specimen. These scans make the measuring process lengthy and tedious due to the large amount of data points generated. However, the amount of time and the data points taken by the measuring process can be reduced by utilizing less scans at fewer planes around the specimen. A hexagonal (six scans at 60° increments), square (four scans at 90° increments) or triangular (three scans at 120° increments) configuration could be utilized. Or an even simpler

configuration utilizing two scans at 180° apart from one another might be sufficient for small and relatively flat tissues such as the MCL.

However, a major problem encountered when measurements are taken at a linear path along one side of a specimen is that an irregularity is noticed at the first edge encountered by the laser sensor. For example, when a linear scan is taken across a cylinder, a symmetrical semicircular profile should be generated, but instead the profile is asymmetric due to the irregularity at the beginning of the scan (Figure 48). This problem must be resolved before any linear scans can be taken of specimens.

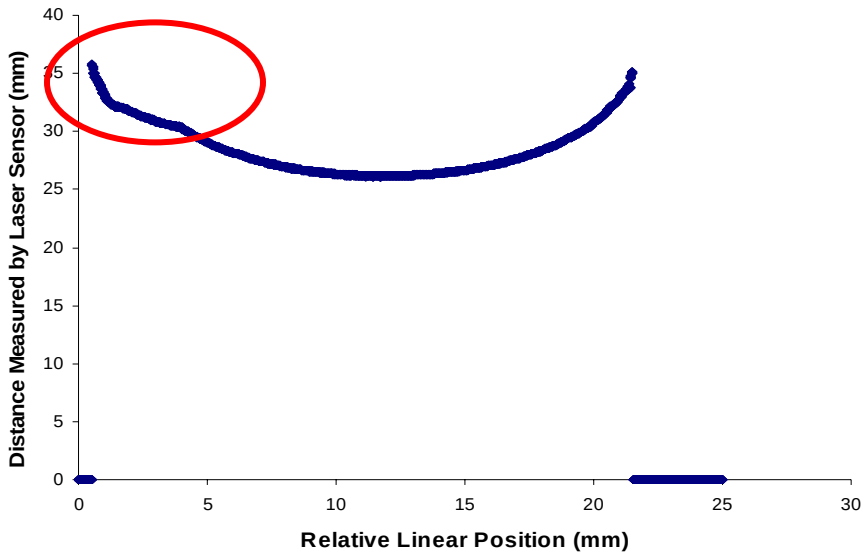

Figure 48: A sample scan by the laser sensor across the surface of a cylinder showing the irregularity in the data at the edge of the cylinder (circled in red).

It was suspected that the irregularity observed in the linear scan of the cylinder was due to instability in the laser sensor. This instability may have been due to the jump in measurements

that occurs when the laser sensor goes from detecting nothing in its path (therefore reading 0 mm) to all of a suddenly detecting an object. In order to see if this is true, a linear scan was taken of the cylinder with and without a flat surface in its background (Figure 49). When a surface was provided in the background, the stability of the laser sensor improved and the irregularity previously observed at the edge of the semicircle disappeared, resulting in a smooth, symmetric semicircle (Figure 50). Therefore, the instability of the laser sensor was due to the sudden jump in the measurements being taken. Thus, when taking linear scans across an object, a surface must be provided in the background for the laser sensor to detect when it is not measuring the surface of the specimen.

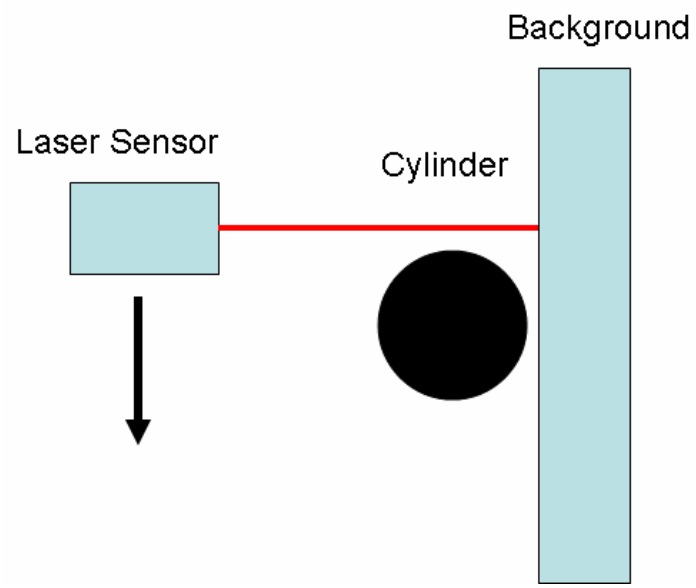

Figure 49: In order to see if a sudden jump in measurements would affect the stability of the laser sensor, a linear scan of a cylinder was taken with and without a background surface.

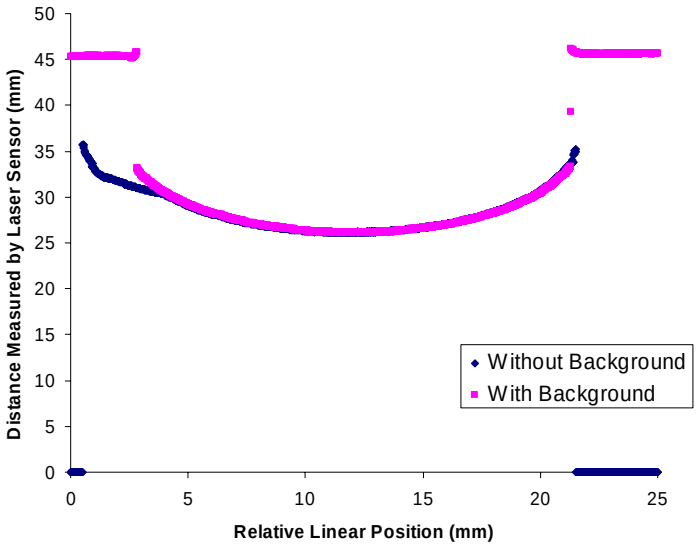

Figure 50: When a linear scan of the cylinder is taken with a background surface, the stability of the laser sensor improved and the irregularity previously observed when a scan was taken with no background disappeared. Note: For the scan without the background, the laser sensor gives an output of "0 mm" when it does not detect a target within its measuring range.

In order to choose the appropriate configuration for measuring MCLs, the general shape of and the characteristics of the concavities on the tissue must be considered. Histological cross-sections of rabbit MCLs revealed that these tissues tended to have one long shallow concavity on one side of the tissue [33]. This concavity is visible to the naked eye and occurs on the side where the tissue was originally attached to the joint capsule of the knee. Since these tissues have elongated, relatively thin cross-sections with few concavities, two linear scans of the tissue 180° apart from one another may be sufficient for measuring the cross-sectional shape and area of these tissues. This methodology is based on an instrument developed by Shrive and coworkers which utilizes thickness calipers and a linear displacement cam to measure the thickness of a specimen as a function of position along its width [73]. This instrument was specifically

designed for rabbit MCLs, but it is a contact method and the specimen must be placed under 5 N pre-load. However, by utilizing the CCD laser displacement sensor, contact during measurements can be avoided and a preload would not be necessary in order to obtain repeatable results.

To find the thickness of a specimen as a function of position along its width, the previously constructed frame was utilized. But instead of taking distance readings to the specimen's surface at 0.05° increments, the new configuration collects distance readings to the specimen's surface along its width at an initial position (0°) and after the specimen is rotated 180° (Figure 51). In the current setup, the laser translates via the linear positioning table at a speed of 1 mm/second while collecting distance readings at 100 Hz, thus a reading is taken every 0.01 mm of translation. In this configuration, the laser does not need to be aligned with the COR, however, the distance from the sensor to the COR, "R", still needed to be determined (same as for circular configuration). In order to reconstruct the shape of the specimen, the difference between the distance measurement of the laser and "R" is found for all points at 0° and 180°. These points with their corresponding position along the width of the specimen are plotted and the area enclosed by the resulting curve is calculated by using the trapezoidal rule at 0.01 mm intervals. In order to test whether this configuration would be feasible, the cross-sectional shape and area of a circle and triangle were measured in this manner. When the shapes of these objects were reconstructed, major gaps were noticed in the perimeter between the linear scans at 0° and 180° (Figure 52). These gaps are due to the failure the laser sensor to take accurate readings, if any readings at all, at the edges of the width of the specimen. This error may be due to the extreme angles of incidence encountered by the sensor the edges of the shapes

and specimens. In terms of cross-sectional area, measurements of the circle had 0.1% error while the triangle had 12.9% error.

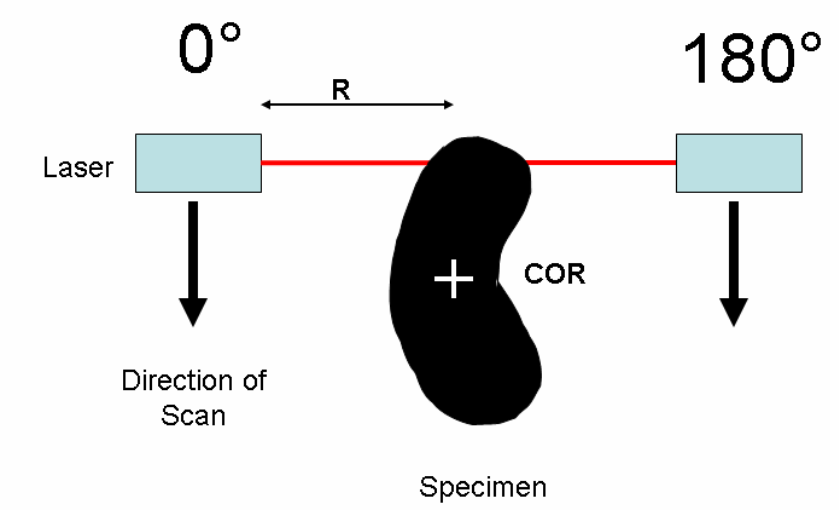

Figure 51: Two scans are taken across the surface of the specimen at 0° and 180° to obtain thickness measurements as a function of the specimen's width.

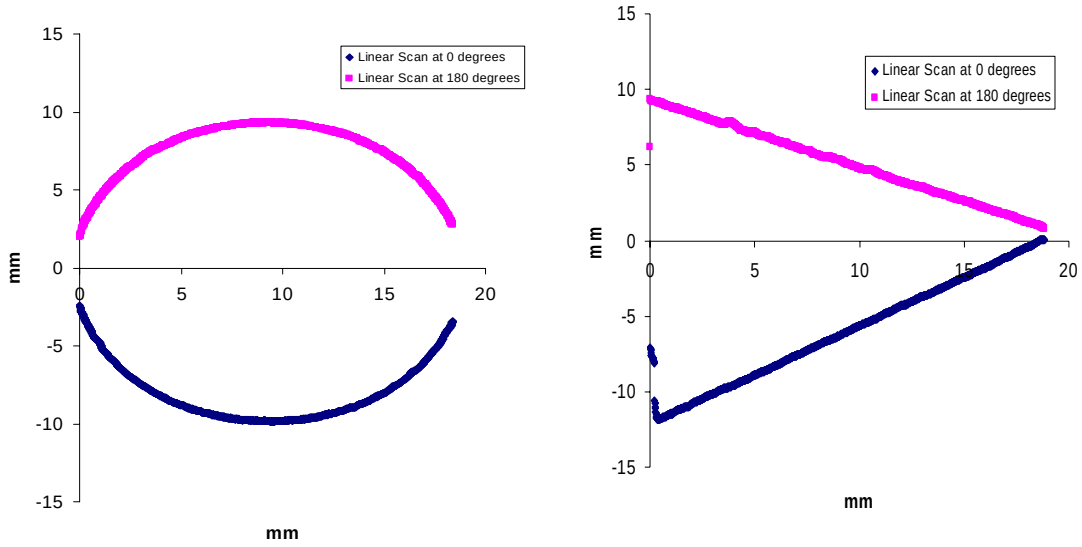

Figure 52: The shape of the circle and triangle were reconstructed using the new configuration of the CCD laser reflectance system (two linear scans). Note: The gaps in the shape reconstructions show that the system could not accurately reconstruct the edges of these shapes possibly due to the extreme angles of incidence of the specimen's surface at the edges relative to the laser sensor.

In order to test the feasibility of this configuration on the MCL, the cross-sectional shape and area of a rabbit and a porcine MCL were measured in this configuration. Although measurements could be obtained for the rabbit MCL, the validity of these measurements is in question because the obtained cross-sectional area (1.4 mm^2) were at least half of what is normally obtained using laser micrometer system (3 - 5 mm^2). However, the new configuration performed better for the porcine MCL and gave a cross-sectional area measurement of 17.7 mm^2, although this value is still very different from the laser micrometer measurement (24.8 mm^2). The cross-sectional shapes obtained for the porcine MCL compared well between the two systems (Figure 53).

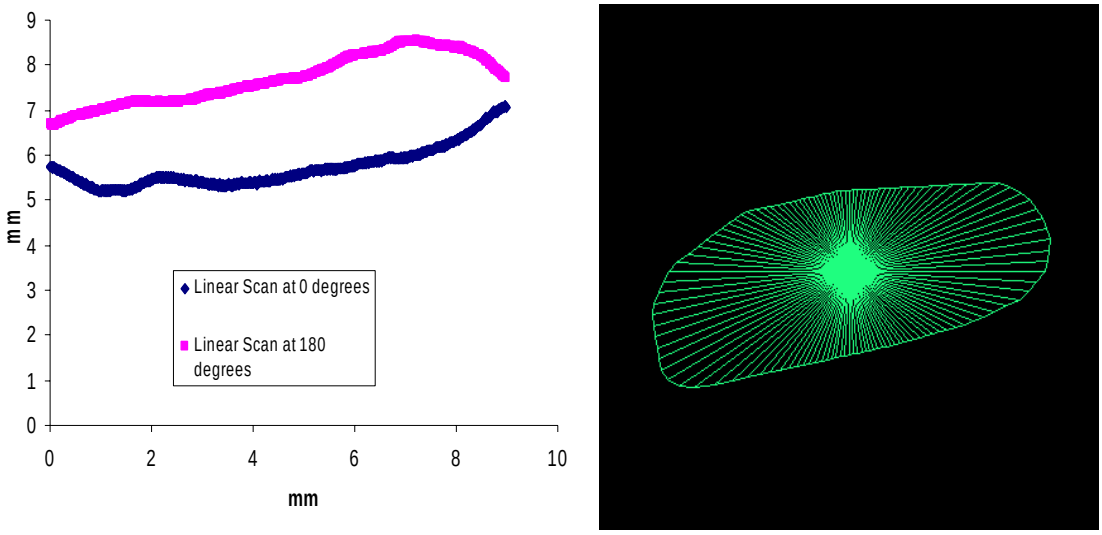

Figure 53: The cross-sectional shape obtained for a porcine MCL using two linear scans in the CCD laser reflectance system is shown on the left and a shape obtained using the laser micrometer system is shown on the right.

Although the performance of this new configuration was poor for the triangle, the results obtained for the circle were promising since ligaments tend to be more rounded in shape. Adding more planes (one or two) may improve the accuracy by allowing for the measurement of the points on the edges of the specimens. In addition, similar factors that were found to be causing errors for the circular configuration may be affecting measurements in this configuration. However, very small and relatively flat specimens could be easily placed in this configuration since the COR was not required to be within the specimen's cross-section in order for measurements to be taken. A more in depth investigation into these alternative configurations would be necessary before they can be put into practice.

5.7 DISCUSSION

A CCD laser reflectance system was developed and used to measure the cross-sectional shape and area of ligaments and tendons. This system successfully satisfies six out of the eight criteria set forth (all criteria except accuracy and cost). One of the requirements it did not meet was accuracy, however this can be improved by machining the device under tighter tolerances (0.01 mm) as shown by the sensitivity analysis. The other requirement it did not meet was cost, since the use of rotary positioning tables makes this device quite expensive. However a simple stepper motor coupled with several gears can be substituted for this positioning table to lower the cost of construction. The laser itself, on the other hand, was relatively inexpensive (purchased for less than $1500).

The circular configuration was selected for both its ease of use and simple subsequent cross-sectional shape and area reconstruction. This system configuration was shown to provide accurate and repeatable measurements on convex objects, as well as objects containing concavities. In order to successfully determine the shape and area of soft tissues using the circular configuration, the COR must be within the cross-section of the specimen. This restriction makes this configuration unreasonable for measuring small and relatively thin tissues such as the MCL because they are difficult to position in this manner. However, other possible configurations of the CCD laser reflectance system may allow for accurate measurements of these types of tissues. Taking two linear scans 180° apart is a promising approach, yet more research and development is required before this methodology can be successfully applied to biomechanical testing protocols. Also, additional scans may be necessary to capture the edges of the specimens for this approach.

It is not necessary to measure relatively flat and thin tissues, such as the MCL with the CCD laser reflectance system because their concavities are relatively shallow and therefore the new system will not significantly improve the accuracy of cross-sectional area measurements compared to the laser micrometer system (Appendix K-1). In addition it is difficult to position the MCL so that the laser beam does not leave the tissue during measurements. Therefore either a new configuration is needed, or the laser micrometer system should continue to be utilized to provide accurate and repeatable measurements for future studies on the MCL. However, this device is well designed to measure the cross-sectional shape and area of soft tissues that contain significant concavities. For example accounting for these concavities in the porcine ACL can result in a significant improvement in the accuracy of the area measurements (Appendix K-2). Another study reported that not accounting for concavities in the posteromedial bundle of the human PCL could result in 10.9% to 29% error [72]. Therefore, the CCD laser reflectance system would be well suited to measuring the cross-sectional shape and area of these tissues.

Future work to further improve this system in the circular configuration will involve the design and construction of a frame precision machined to a tolerance of 0.01 mm. In addition, clamps and fixtures will be designed and made to better fix the specimen and make it easier to adjust the position of the specimen within the frame. If the system is still unable to meet the criteria for accuracy, a more accurate laser with a smaller spot diameter can be utilized, however this will make the system more expensive.

6.0 CONCLUSION

The major objective of this thesis was to evaluate the cross-sectional shape and area of normal and healing ligaments. In order to accomplish this objective, the areas of ligaments with simple and complex geometries were measured using laser based systems. For healing ligaments, the amount of tissue growth and remodeling could be quantified and compared relative to the sham-operated controls. In addition, the effects of treatment with a biological scaffold on the cross-sectional shape and area could also be quantified. Due to limitations in currently available methods, a new and improved CCD laser reflectance system was developed in order to detect concavities in the cross-sectional shape and area of complex ligaments. The CCD laser reflectance system was found to be effective for determining the cross-sectional shape and area of soft tissues with concavities on their surfaces and could be easily adopted by other biomechanics laboratories as standard equipment because it is simple to use and can be constructed inexpensively. A standard cross-sectional area measurement method among different laboratories would also allow for improved comparison of the mechanical properties of different tissues.

However the CCD laser reflectance in its circular configuration was not successful in measuring the cross-sectional shape and area of rabbit MCLs due to their small size and the relatively flat shape of MCLs in general. These characteristics also make the specimen extremely difficult to orient in a position where the laser beam will not leave the tissue's surface

for all 360° of rotation. In addition, the system does not provide much improvement in accuracy for these tissues since the concavities are not very large. But the system, with further refinements, would be an excellent tool for measuring the cross-sectional shape and area of larger tissues with significant concavities on the surface such as the ACL and PCL from porcine and cadaver specimens.

6.1 RECOMMENDATIONS FOR FUTURE STUDIES

This study demonstrated that the accuracy of measurements of cross-sectional shape and area can be dependent on many factors such as surface concavities in the cross-section for the laser micrometer system and the misalignment of the laser sensor and slight miscalculations in the parameters (for the configuration) used to reconstruct shape and calculate area for the CCD laser reflectance system. In addition, it was shown that certain methods of measurement are more suitable for some tissues while not as suitable for others. For instance, the CCD laser reflectance system in its circular configuration seems to be suitable for tissues that are relatively large and rounded since they are easy to orient in a position where the laser beam does not leave the surface of the specimen during measurements. However, for flat and relatively thin tissues, the laser micrometer system is a better method since it is difficult to orient these tissues so that correct measurements can be taken in the circular configuration of the CCD laser reflectance system. Thus, one must take into account the general geometry of the tissue's cross-section before choosing the appropriate method (or system configuration) for cross-sectional shape and area measurement. Factors such as the overall size of the cross-section, the complexity (amount

of surface concavities), and shape (circular or flat) all play a role in deciding which method is appropriate for measuring cross-sectional shape and area of a tissue.

In addition, the sensitivity analysis done for the circular configuration of the CCD laser reflectance system demonstrated that small systematic errors in the configuration setup or possibly the measurements obtained could result in significant errors for the cross-sectional area measurements. The percent errors will also most likely increase as the size of the specimens decreases. Thus future work on developing new methods should also incorporate what effects the size of a specimen may have on its accuracy, as well as, the effects of possible errors in the set up of the device in order to determine the tolerances necessary.

6.2 FUTURE DIRECTIONS

This thesis demonstrated how cross-sectional shape and area measurements can be used to study the morphology of healing tissues. Studies into the effects of scaffolds on the tissue's morphology can further elucidate mechanisms on how they guide tissue growth and healing. Future studies in our research center will look into how scaffolds can be used to treat a variety of ligament and tendon injuries from the MCL and ACL to the patellar tendon.

In addition, other configurations for the CCD laser reflectance system will be investigated in more detail. These other configurations may allow for improved measurements on tissues that the circular configuration is not suitable for such as the rabbit MCL. These improved systems will not only allow for more accurate measurements of cross-sectional shape and area, but will also allow researchers to be able to detect smaller changes in the mechanical

properties of tissues that may occur with different treatment regimens. Furthermore, CCD lasers can be applied for other applications such as anthropometric studies and reconstructing the three-dimensional geometry of ligaments and articular surfaces, with implications for mathematical models.

APPENDIX A

GEOMETRIC CHARACTERISTICS OF CONCAVITIES IN THE RABBIT MCL

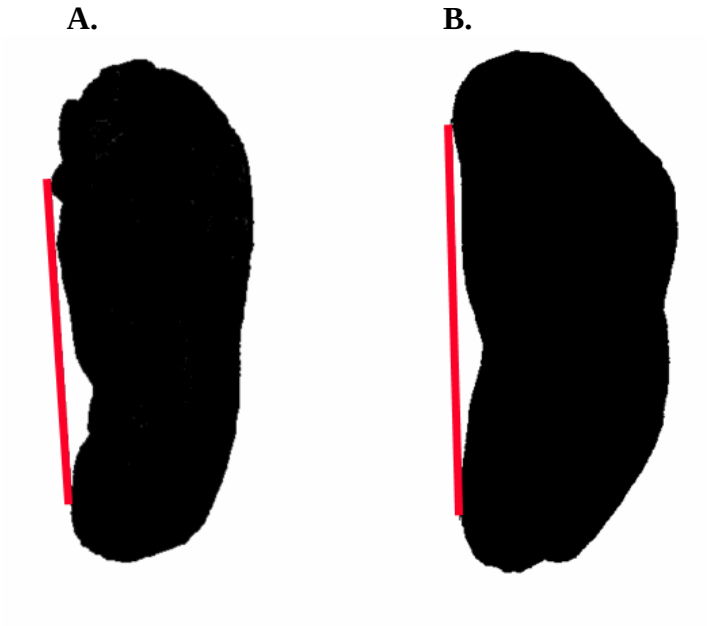

Figure A-1: Examples of the effects of concavities on the cross-sectional area calculations of rabbit MCLs. Not accounting for the concavity enclosed by the red line in specimen (A) would result in a 5.4% error in the cross-sectional area measurement. Not accounting for the concavity enclosed by the red line in specimen (B) would result in a 4.6% error in cross-sectional area measurements.

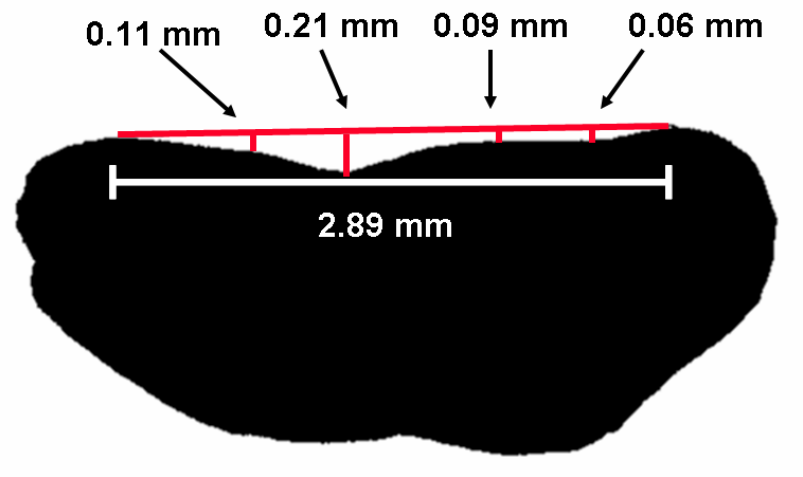

Figure A-2: Profile of a surface concavity in a sample rabbit MCL cross-section.

APPENDIX B

ELECTRONIC SCHEMATIC

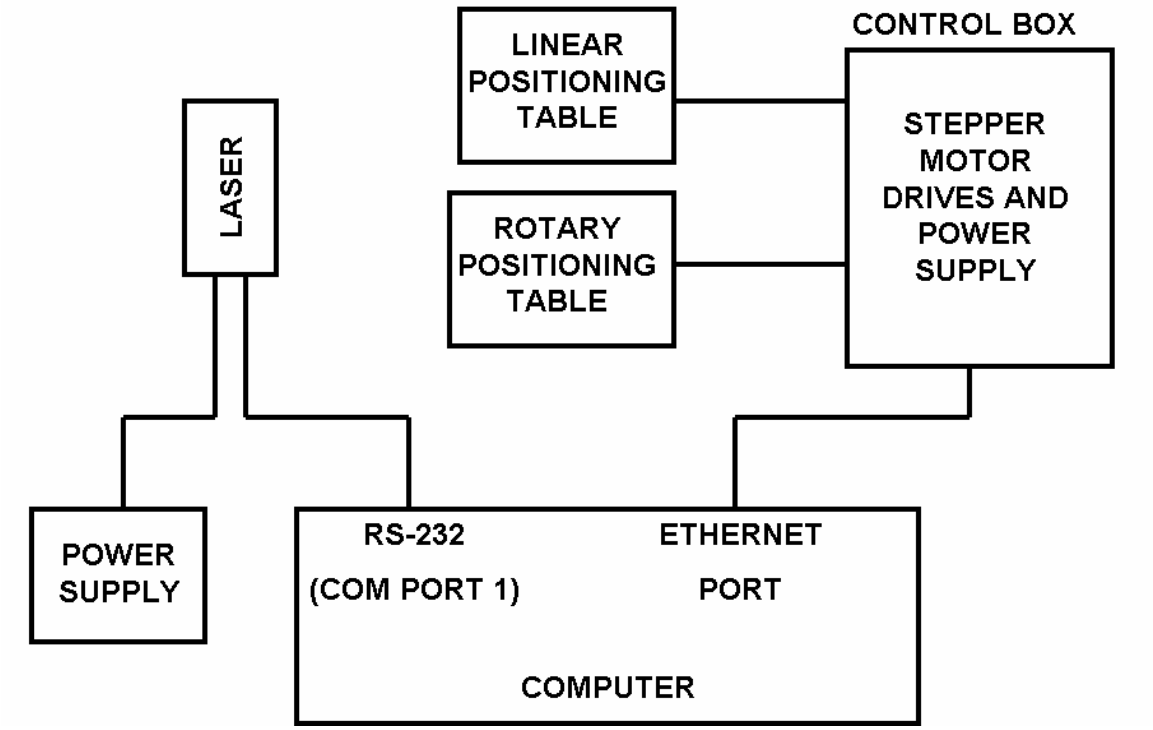

Figure B-1: Schematic detailing the electronic connections for the CCD laser reflectance system

APPENDIX C

EFFECTS OF SURFACE CONDITIONS ON LASER SENSOR

Table C- 1: Gray Surface

The motion table was instructed to move in 1 mm increments (row 1). At each increment, the reading on the laser sensor was recorded (rows 2-4). The average of three trials was taken (row 5). The displacement measured by the laser sensor was determined by finding the difference between the reading at one position and the previous position (row 6).

Motion Table Position (mm)	Laser Sensor Measurements (mm)				Displacement Measured by Laser (mm)
	1	2	3	Average	
0	50.77	50.78	50.78	50.78	-----
1	49.7	49.77	49.76	49.74	1.03
2	48.68	48.68	48.66	48.67	1.07
3	47.69	47.67	47.65	47.67	1.00
4	46.7	46.69	46.67	46.69	0.98
5	45.69	45.67	45.64	45.67	1.02
6	44.65	44.66	44.66	44.66	1.01
7	43.6	43.64	43.63	43.62	1.03
8	42.6	42.67	42.66	42.64	0.98
9	41.65	41.66	41.63	41.65	1.00
10	40.65	40.66	40.65	40.65	0.99
11	39.63	39.65	39.63	39.64	1.02
12	38.62	38.65	38.62	38.63	1.01
13	37.64	37.64	37.62	37.63	1.00
14	36.67	36.66	36.66	36.66	0.97
15	35.63	35.65	35.64	35.64	1.02
16	34.64	34.66	34.66	34.65	0.99
17	33.62	33.61	33.6	33.61	1.04
18	32.59	32.61	32.6	32.60	1.01
19	31.63	31.63	31.63	31.63	0.97
20	30.62	30.61	30.61	30.61	1.02
21	29.63	29.62	29.61	29.62	0.99
22	28.6	28.6	28.6	28.60	1.02

Table C-1 (continued)

Motion Table Position (mm)	Laser Sensor Measurements (mm)				Displacement Measured by Laser (mm)
	1	2	3	Average	
23	27.59	27.6	27.6	27.60	1.00
24	26.61	26.6	26.6	26.60	0.99
25	25.6	25.6	25.6	25.60	1.00
26	24.62	24.61	24.6	24.61	0.99
27	23.61	23.6	23.6	23.60	1.01
28	22.59	22.59	22.6	22.59	1.01
29	21.58	21.61	21.61	21.60	0.99
30	20.62	20.58	20.62	20.61	0.99
31	19.64	19.61	19.64	19.63	0.98
32	18.56	18.56	18.57	18.56	1.07
33	17.56	17.56	17.54	17.55	1.01
34	16.59	16.61	16.58	16.59	0.96
35	15.63	15.64	15.65	15.64	0.95
36	14.61	14.6	14.6	14.60	1.04
37	13.59	13.61	13.58	13.59	1.01
38	12.6	12.59	12.59	12.59	1.00
39	11.6	11.59	11.59	11.59	1.00
40	10.64	10.63	10.62	10.63	0.96
41	9.63	9.62	9.62	9.62	1.01
42	8.62	8.61	8.62	8.62	1.01
43	7.62	7.62	7.62	7.62	1.00
44	6.64	6.64	6.63	6.64	0.98
45	5.64	5.64	5.64	5.64	1.00
46	4.64	4.63	4.64	4.64	1.00
47	3.65	3.64	3.64	3.64	0.99
48	2.66	2.65	2.65	2.65	0.99
49	1.68	1.67	1.68	1.68	0.98
50	0.71	0.71	0.71	0.71	0.97

Table C-2: White Surface

The motion table was instructed to move in 1 mm increments (row 1). At each increment, the reading on the laser sensor was recorded (rows 2-4). The average of three trials was taken (row 5). The displacement measured by the laser sensor was determined by finding the difference between the reading at one position and the previous position (row 6).

Motion Table Position (mm)	Laser Sensor Measurements (mm)				Displacement Measured by Laser (mm)
	1	2	3	Average	
0	50.02	50.72	50.01	50.25	-----
1	48.94	49.67	48.96	49.19	1.06
2	47.91	48.64	47.92	48.16	1.03
3	46.96	47.64	46.95	47.18	0.97
4	45.96	46.67	45.95	46.19	0.99
5	44.93	45.63	44.92	45.16	1.03
6	43.89	44.6	43.88	44.12	1.04
7	42.94	43.6	42.93	43.16	0.97
8	41.94	42.62	41.93	42.16	0.99
9	40.97	41.64	40.96	41.19	0.97
10	39.95	40.61	39.93	40.16	1.03
11	38.93	39.62	38.91	39.15	1.01
12	37.92	38.61	37.91	38.15	1.01
13	36.94	37.6	36.93	37.16	0.99
14	35.95	36.64	35.94	36.18	0.98
15	34.94	35.64	34.94	35.17	1.00
16	33.9	34.63	33.89	34.14	1.03
17	32.9	33.58	32.89	33.12	1.02
18	31.95	32.58	31.94	32.16	0.97
19	30.93	31.61	30.92	31.15	1.00
20	29.91	30.6	29.9	30.14	1.02
21	28.9	29.59	28.88	29.12	1.01
22	27.9	28.59	27.89	28.13	1.00
23	26.91	27.57	26.89	27.12	1.00
24	25.91	26.58	25.9	26.13	0.99
25	24.91	25.58	24.91	25.13	1.00
26	23.91	24.58	23.89	24.13	1.01
27	22.9	23.58	22.88	23.12	1.01
28	21.9	22.56	21.88	22.11	1.01
29	20.9	21.57	20.89	21.12	0.99
30	19.91	20.55	19.9	20.12	1.00
31	18.87	19.6	18.84	19.10	1.02
32	17.85	18.54	17.82	18.07	1.03
33	16.87	17.5	16.83	17.07	1.00
34	15.93	16.57	15.9	16.13	0.93
35	14.89	15.6	14.88	15.12	1.01

Table C-2 (continued)

Motion Table Position (mm)	Laser Sensor Measurements (mm)				Displacement Measured by Laser (mm)
	1	2	3	Average	
36	13.9	14.57	13.87	14.11	1.01
37	12.89	13.57	12.86	13.11	1.01
38	11.91	12.57	11.88	12.12	0.99
39	10.94	11.58	10.92	11.15	0.97
40	9.95	10.63	9.93	10.17	0.98
41	8.95	9.62	8.93	9.17	1.00
42	7.94	8.62	7.92	8.16	1.01
43	6.95	7.62	6.93	7.17	0.99
44	5.97	6.66	5.94	6.19	0.98
45	4.97	5.65	4.94	5.19	1.00
46	3.98	4.65	3.96	4.20	0.99
47	2.97	3.65	2.96	3.19	1.00
48	2	2.66	1.97	2.21	0.98
49	1.03	1.68	1.01	1.24	0.97
50	0.04	0.71	0.0091	0.25	0.99

Table C-3: Black Surface

The motion table was instructed to move in 1 mm increments (row 1). At each increment, the reading on the laser sensor was recorded (rows 2-4). The average of three trials was taken (row 5). The displacement measured by the laser sensor was determined by finding the difference between the reading at one position and the previous position (row 6).

Motion Table Position (mm)	Laser Sensor Measurements				Displacement Measured by Laser (mm)
	1	2	3	Average	
0	50.02	50.72	50.01	50.25	-----
1	48.94	49.67	48.96	49.19	1.06
2	47.91	48.64	47.92	48.16	1.03
3	46.96	47.64	46.95	47.18	0.97
4	45.96	46.67	45.95	46.19	0.99
5	44.93	45.63	44.92	45.16	1.03
6	43.89	44.6	43.88	44.12	1.04
7	42.94	43.6	42.93	43.16	0.97
8	41.94	42.62	41.93	42.16	0.99
9	40.97	41.64	40.96	41.19	0.97
10	39.95	40.61	39.93	40.16	1.03
11	38.93	39.62	38.91	39.15	1.01
12	37.92	38.61	37.91	38.15	1.01
13	36.94	37.6	36.93	37.16	0.99
14	35.95	36.64	35.94	36.18	0.98
15	34.94	35.64	34.94	35.17	1.00
16	33.9	34.63	33.89	34.14	1.03
17	32.9	33.58	32.89	33.12	1.02
18	31.95	32.58	31.94	32.16	0.97
19	30.93	31.61	30.92	31.15	1.00
20	29.91	30.6	29.9	30.14	1.02
21	28.9	29.59	28.88	29.12	1.01
22	27.9	28.59	27.89	28.13	1.00
23	26.91	27.57	26.89	27.12	1.00
24	25.91	26.58	25.9	26.13	0.99
25	24.91	25.58	24.91	25.13	1.00
26	23.91	24.58	23.89	24.13	1.01
27	22.9	23.58	22.88	23.12	1.01
28	21.9	22.56	21.88	22.11	1.01
29	20.9	21.57	20.89	21.12	0.99
30	19.91	20.55	19.9	20.12	1.00
31	18.87	19.6	18.84	19.10	1.02
32	17.85	18.54	17.82	18.07	1.03

Table C-3 (continued)

Motion Table	Laser Sensor Measurements				Displacement Measured
Position (mm)	1	2	3	Average	by Laser (mm)
33	16.87	17.5	16.83	17.07	1.00
34	15.93	16.57	15.9	16.13	0.93
35	14.89	15.6	14.88	15.12	1.01
36	13.9	14.57	13.87	14.11	1.01
37	12.89	13.57	12.86	13.11	1.01
38	11.91	12.57	11.88	12.12	0.99
39	10.94	11.58	10.92	11.15	0.97
40	9.95	10.63	9.93	10.17	0.98
41	8.95	9.62	8.93	9.17	1.00
42	7.94	8.62	7.92	8.16	1.01
43	6.95	7.62	6.93	7.17	0.99
44	5.97	6.66	5.94	6.19	0.98
45	4.97	5.65	4.94	5.19	1.00
46	3.98	4.65	3.96	4.20	0.99
47	2.97	3.65	2.96	3.19	1.00
48	2	2.66	1.97	2.21	0.98
49	1.03	1.68	1.01	1.24	0.97
50	0.04	0.71	0.0091	0.25	0.99

Table C-4: Rabbit Medial Collateral Ligament Surface

The motion table was instructed to move in 1 mm increments (row 1). At each increment, the reading on the laser sensor was recorded (rows 2-4). The average of three trials was taken (row 5). The displacement measured by the laser sensor was determined by finding the difference between the reading at one position and the previous position (row 6).

Motion Table Position (mm)	Laser Sensor Measurements (mm)				Displacement Measured By Laser (mm)
	1	2	3	Average	
0	49.64	49.87	49.88	49.80	-----
1	48.63	48.81	48.8	48.75	1.05
2	47.6	47.79	47.81	47.73	1.01
3	46.61	46.85	46.86	46.77	0.96
4	45.57	45.85	45.83	45.75	1.02
5	44.54	44.79	44.78	44.70	1.05
6	43.51	43.75	43.74	43.67	1.04
7	42.51	42.77	42.76	42.68	0.99
8	41.53	41.77	41.75	41.68	1.00
9	40.51	40.77	40.75	40.68	1.01
10	39.48	39.76	39.73	39.66	1.02
11	38.48	38.73	38.7	38.64	1.02
12	37.48	37.75	37.71	37.65	0.99
13	36.48	36.73	36.69	36.63	1.01
14	35.48	35.74	35.69	35.64	1.00
15	34.48	34.72	34.69	34.63	1.01
16	33.41	33.67	33.62	33.57	1.06
17	32.43	32.66	32.62	32.57	1.00
18	31.46	31.67	31.64	31.59	0.98
19	30.43	30.64	30.6	30.56	1.03
20	29.41	29.64	29.6	29.55	1.01
21	28.4	28.62	28.6	28.54	1.01
22	27.39	27.6	27.56	27.52	1.02
23	26.41	26.61	26.57	26.53	0.99
24	25.43	25.62	25.58	25.54	0.99
25	24.44	24.61	24.57	24.54	1.00
26	23.39	23.6	23.55	23.51	1.03
27	22.38	22.57	22.53	22.49	1.02
28	21.39	21.57	21.54	21.50	0.99
29	20.38	20.55	20.52	20.48	1.02
30	19.41	19.57	19.55	19.51	0.97
31	18.33	18.49	18.5	18.44	1.07
32	17.35	17.5	17.48	17.44	1.00
33	16.4	16.54	16.51	16.48	0.96
34	15.42	15.59	15.55	15.52	0.96
35	14.4	14.54	14.53	14.49	1.03
36	13.37	13.51	13.49	13.46	1.03

Table C-4 (continued)

Motion Table	Laser Sensor Measurements (mm)				Displacement Measured
Position (mm)	1	2	3	Average	By Laser (mm)
37	12.39	12.51	12.49	12.46	0.99
38	11.4	11.54	11.51	11.48	0.98
39	10.4	10.55	10.52	10.49	0.99
40	9.39	9.54	9.51	9.48	1.01
41	8.37	8.56	8.53	8.49	0.99
42	7.34	7.55	7.53	7.47	1.01
43	6.37	6.58	6.54	6.50	0.98
44	5.36	5.58	5.54	5.49	1.00
45	4.35	4.58	4.54	4.49	1.00
46	3.38	3.6	3.56	3.51	0.98
47	2.37	2.6	2.56	2.51	1.00
48	1.41	1.62	1.56	1.53	0.98
49	0.42	0.64	0.59	0.55	0.98

APPENDIX D

EFFECTS OF INCIDENCE ANGLE ON LASER SENSOR

Table D-1: Gray Surface

The motion table was instructed to move in 1 mm increments (row 1: Motion Table Position). At each increment, the reading on the laser sensor was recorded (Laser Meas.). The displacement measured by the laser sensor was determined by finding the difference between the readings at one position and the previous position (Meas. Disp.). These measurements were then compared to the 1 mm displacement by the motion table to assess accuracy of the laser.

	Angle of Incidence (Degrees)									
Motion Table Position (mm)	15 Degrees		30 Degrees		45 Degrees		60 Degrees		75 Degrees	
	Laser Meas. (mm)	Meas. Disp. (mm)	Laser Meas. (mm)	Meas. Disp. (mm)	Laser Meas. (mm)	Meas. Disp. (mm)	Laser Meas. (mm)	Meas. Disp. (mm)	Laser Meas. (mm)	Meas. Disp. (mm)
0	50.02	-----	50.72	-----	50.01	-----	50.72	-----	50.61	-----
1	48.97	1.05	49.71	1.01	48.93	1.08	49.7	1.02	49.63	0.98
2	47.92	1.05	48.69	1.02	47.91	1.02	48.69	1.01	48.65	0.98
3	46.93	0.99	47.68	1.01	46.94	0.97	47.7	0.99	47.66	0.99
4	45.94	0.99	46.71	0.97	45.94	1	46.76	0.94	46.76	0.9
5	44.97	0.97	45.7	1.01	44.94	1	45.74	1.02	45.77	0.99
6	43.93	1.04	44.7	1	43.93	1.01	44.74	1	44.77	1
7	42.94	0.99	43.7	1	42.93	1	43.76	0.98	43.76	1.01
8	41.94	1	42.67	1.03	41.92	1.01	42.76	1	42.82	0.94
9	40.97	0.97	41.71	0.96	40.97	0.95	41.8	0.96	41.87	0.95
10	39.93	1.04	40.7	1.01	39.96	1.01	40.79	1.01	40.89	0.98
11	38.89	1.04	39.68	1.02	38.95	1.01	39.79	1	39.89	1
12	37.93	0.96	38.68	1	37.96	0.99	38.81	0.98	38.88	1.01
13	36.92	1.01	37.68	1	36.97	0.99	37.82	0.99	37.92	0.96
14	35.94	0.98	36.71	0.97	35.98	0.99	36.84	0.98	36.94	0.98
15	34.97	0.97	35.71	1	35.01	0.97	35.85	0.99	35.96	0.98
16	33.9	1.07	34.73	0.98	33.97	1.04	34.89	0.96	35.04	0.92
17	32.92	0.98	33.66	1.07	32.96	1.01	33.83	1.06	33.99	1.05
18	31.95	0.97	32.68	0.98	32.01	0.95	32.84	0.99	33.02	0.97
19	30.93	1.02	31.7	0.98	31	1.01	31.9	0.94	32.11	0.91

Table D-1 (continued)

	Angle of Incidence (Degrees)									
Motion	15 Degrees		30 Degrees		45 Degrees		60 Degrees		75 Degrees	
Table Position (mm)	Laser Meas. (mm)	Meas. Disp. (mm)	Laser Meas. (mm)	Meas. Disp. (mm)	Laser Meas. (mm)	Meas. Disp. (mm)	Laser Meas. (mm)	Meas. Disp. (mm)	Laser Meas. (mm)	Meas. Disp. (mm)
20	29.93	1	30.7	1	30	1	30.91	0.99	31.16	0.95
21	28.89	1.04	29.69	1.01	28.97	1.03	29.91	1	30.2	0.96
22	27.9	0.99	28.66	1.03	27.99	0.98	28.91	1	29.21	0.99
23	26.88	1.02	27.67	0.99	26.99	1	27.92	0.99	28.23	0.98
24	25.93	0.95	26.67	1	26	0.99	26.93	0.99	27.23	1
25	24.91	1.02	25.7	0.97	25	1	25.94	0.99	26.27	0.96
26	23.92	0.99	24.69	1.01	24.02	0.98	24.99	0.95	25.3	0.97
27	22.89	1.03	23.7	0.99	23	1.02	24	0.99	24.33	0.97
28	21.89	1	22.71	0.99	22.01	0.99	22.98	1.02	23.33	1
29	20.89	1	21.72	0.99	21	1.01	21.97	1.01	22.34	0.99
30	19.93	0.96	20.7	1.02	20.04	0.96	20.99	0.98	21.38	0.96
31	18.87	1.06	19.73	0.97	18.99	1.05	20	0.99	20.39	0.99
32	17.88	0.99	18.69	1.04	17.97	1.02	18.96	1.04	19.43	0.96
33	16.88	1	17.66	1.03	17.03	0.94	17.94	1.02	18.39	1.04
34	15.94	0.94	16.73	0.93	16.08	0.95	16.98	0.96	17.4	0.99
35	14.92	1.02	15.73	1	15.08	1	16.03	0.95	16.47	0.93
36	13.9	1.02	14.73	1	14.06	1.02	15.06	0.97	15.5	0.97
37	12.89	1.01	13.71	1.02	13.04	1.02	14.04	1.02		
38	11.93	0.96	12.7	1.01	12.07	0.97	13.02	1.02		
39	10.94	0.99	11.73	0.97	11.1	0.97	12.05	0.97		
40	9.95	0.99	10.77	0.96	10.11	0.99	11.11	0.94		
41	8.96	0.99	9.78	0.99	9.13	0.98	10.13	0.98		
42	7.94	1.02	8.78	1	8.14	0.99	9.14	0.99		
43	6.96	0.98	7.78	1	7.17	0.97	8.17	0.97		
44	5.98	0.98	6.81	0.97	6.19	0.98	7.19	0.98		
45	5	0.98	5.83	0.98	5.19	1	6.23	0.96		
46	4.01	0.99	4.83	1	4.22	0.97	5.26	0.97		
47	3.01	1	3.83	1	3.24	0.98				
48	2.02	0.99	2.84	0.99	2.26	0.98				
49	1.06	0.96	1.86	0.98	1.3	0.96				
50	0.08	0.98	0.91	0.95	0.31	0.99				

Table D- 2: White Surface

The motion table was instructed to move in 1 mm increments (row 1: Motion Table Position). At each increment, the reading on the laser sensor was recorded (Laser Meas.). The displacement measured by the laser sensor was determined by finding the difference between the readings at one position and the previous position (Meas. Disp.). These measurements were then compared to the 1 mm displacement by the motion table to assess accuracy of the laser.

	Angle of Incidence (Degrees)									
Motion Table Position (mm)	15 Degrees		30 Degrees		45 Degrees		60 Degrees		75 Degrees	
	Laser Meas. (mm)	Meas. Disp. (mm)	Laser Meas. (mm)	Meas. Disp. (mm)	Laser Meas. (mm)	Meas. Disp. (mm)	Laser Meas. (mm)	Meas. Disp. (mm)	Laser Meas. (mm)	Meas. Disp. (mm)
0	50.74	-----	50.76	-----	50.59	-----	50.21	-----	50.47	-----
1	49.74	1	49.73	1.03	49.59	1	49.23	0.98	49.85	0.62
2	48.68	1.06	48.7	1.03	48.61	0.98	48.21	1.02	48.91	0.94
3	47.69	0.99	47.71	0.99	47.64	0.97	47.18	1.03	47.97	0.94
4	46.71	0.98	46.76	0.95	46.69	0.95	46.29	0.89	47.04	0.93
5	45.66	1.05	45.76	1	45.66	1.03	45.24	1.05	46.11	0.93
6	44.68	0.98	44.72	1.04	44.66	1	44.31	0.93	45.16	0.95
7	43.67	1.01	43.71	1.01	43.68	0.98	43.3	1.01	44.2	0.96
8	42.68	0.99	42.72	0.99	42.7	0.98	42.36	0.94	43.22	0.98
9	41.69	0.99	41.74	0.98	41.7	1	41.4	0.96	42.27	0.95
10	40.71	0.98	40.75	0.99	40.69	1.01	40.37	1.03	41.37	0.9
11	39.69	1.02	39.75	1	39.68	1.01	39.37	1	40.37	1
12	38.67	1.02	38.74	1.01	38.69	0.99	38.38	0.99	39.42	0.95
13	37.68	0.99	37.75	0.99	37.71	0.98	37.42	0.96	38.45	0.97
14	36.67	1.01	36.78	0.97	36.72	0.99	36.47	0.95	37.53	0.92
15	35.69	0.98	35.79	0.99	35.72	1	35.51	0.96	36.58	0.95
16	34.7	0.99	34.8	0.99	34.76	0.96	34.52	0.99	35.64	0.94
17	33.65	1.05	33.75	1.05	33.7	1.06	33.47	1.05	34.69	0.95
18	32.66	0.99	32.76	0.99	32.72	0.98	32.5	0.97	33.7	0.99
19	31.69	0.97	31.8	0.96	31.77	0.95	31.55	0.95	32.74	0.96
20	30.68	1.01	30.78	1.02	30.76	1.01	30.55	1	31.84	0.9
21	29.67	1.01	29.78	1	29.77	0.99	29.55	1	30.86	0.98
22	28.67	1	28.76	1.02	28.75	1.02	28.55	1	29.92	0.94
23	27.65	1.02	27.76	1	27.77	0.98	27.57	0.98	28.94	0.98
24	26.67	0.98	26.78	0.98	26.79	0.98	26.6	0.97	28.05	0.89
25	25.7	0.97	25.8	0.98	25.83	0.96	25.65	0.95	27.11	0.94
26	24.69	1.01	24.81	0.99	24.84	0.99	24.66	0.99	26.18	0.93
27	23.67	1.02	23.81	1	23.85	0.99	23.66	1	25.23	0.95
28	22.67	1	22.79	1.02	22.84	1.01	22.66	1	24.28	0.95
29	21.7	0.97	21.81	0.98	21.85	0.99	21.71	0.95	23.28	1
30	20.69	1.01	20.83	0.98	20.87	0.98	20.71	1	22.29	0.99
31	19.71	0.98	19.87	0.96	19.88	0.99	19.73	0.98	21.37	0.92
32	18.66	1.05	18.8	1.07	18.85	1.03	18.7	1.03	20.4	0.97

Table D-2 (continued)

	Angle of Incidence (Degrees)									
Motion	15 Degrees		30 Degrees		45 Degrees		60 Degrees		75 Degrees	
Table Position (mm)	Laser Meas. (mm)	Table Position (mm)	Laser Meas. (mm)	Table Position (mm)	Laser Meas. (mm)	Table Position (mm)	Laser Meas. (mm)	Table Position (mm)	Laser Meas. (mm)	Table Position (mm)
33	17.65	1.01	17.79	1.01	17.83	1.02	17.72	0.98	19.45	0.95
34	16.7	0.95	16.83	0.96	16.89	0.94	16.76	0.96	18.42	1.03
35	15.74	0.96	15.89	0.94	15.95	0.94	15.83	0.93	17.44	0.98
36	14.72	1.02	14.86	1.03	14.92	1.03	14.8	1.03	16.54	0.9
37	13.69	1.03	13.86	1	13.91	1.01	13.8	1	15.6	0.94
38	12.7	0.99	12.86	1	12.93	0.98	12.82	0.98	14.63	0.97
39	11.73	0.97	11.88	0.98	11.95	0.98	11.85	0.97	13.67	0.96
40	10.77	0.96	10.91	0.97	11	0.95	10.91	0.94	12.72	0.95
41	9.76	1.01	9.92	0.99	10	1	9.91	1	11.79	0.93
42	8.76	1	8.93	0.99	9.02	0.98	8.93	0.98	10.88	0.91
43	7.77	0.99	7.94	0.99	8.03	0.99	7.96	0.97	9.67	1.21
44	6.79	0.98	6.95	0.99	7.06	0.97	6.98	0.98		
45	5.8	0.99	6	0.95	6.1	0.96	6.01	0.97		
46	4.81	0.99	4.98	1.02	5.11	0.99	5.02	0.99		
47	3.82	0.99	4	0.98	4.14	0.97	4.06	0.96		
48	2.83	0.99	3.01	0.99	3.15	0.99	3.06	1		
49	1.85	0.98	2.04	0.97	2.18	0.97	2.09	0.97		
50	0.88	0.97	1.08	0.96	1.21	0.97	1.13	0.96		

Table D-3: Black Surface

The motion table was instructed to move in 1 mm increments (row 1: Motion Table Position). At each increment, the reading on the laser sensor was recorded (Laser Meas.). The displacement measured by the laser sensor was determined by finding the difference between the readings at one position and the previous position (Meas. Disp.). These measurements were then compared to the 1 mm displacement by the motion table to assess accuracy of the laser.

	Angle of Incidence (Degrees)									
Motion Table Position (mm)	15 Degrees		30 Degrees		45 Degrees		60 Degrees		75 Degrees	
	Laser Meas. (mm)	Meas. Disp. (mm)	Laser Meas. (mm)	Meas. Disp. (mm)	Laser Meas. (mm)	Meas. Disp. (mm)	Laser Meas. (mm)	Meas. Disp. (mm)	Laser Meas. (mm)	Meas. Disp. (mm)
0	50.24	-----	50.22	-----	50.79	-----	50.62	-----	50.45	-----
1	49.24	1	49.29	0.93	49.72	1.07	49.58	1.04	49.6	0.85
2	48.25	0.99	48.29	1	48.65	1.07	48.55	1.03	48.68	0.92
3	47.17	1.08	47.31	0.98	47.73	0.92	47.59	0.96	47.82	0.86
4	46.18	0.99	46.27	1.04	46.8	0.93	46.63	0.96	46.91	0.91
5	45.19	0.99	45.29	0.98	45.8	1	45.65	0.98	45.99	0.92
6	44.16	1.03	44.28	1.01	44.78	1.02	44.66	0.99	45.05	0.94
7	43.2	0.96	43.31	0.97	43.79	0.99	43.68	0.98	44.11	0.94
8	42.21	0.99	42.36	0.95	42.81	0.98	42.69	0.99	43.13	0.98
9	41.27	0.94	41.39	0.97	41.8	1.01	41.74	0.95	42.17	0.96
10	40.23	1.04	40.38	1.01	40.82	0.98	40.72	1.02	41.19	0.98
11	39.17	1.06	39.37	1.01	39.81	1.01	39.72	1	40.19	1
12	38.2	0.97	38.39	0.98	38.79	1.02	38.74	0.98	39.21	0.98
13	37.23	0.97	37.4	0.99	37.82	0.97	37.74	1	38.27	0.94
14	36.21	1.02	36.43	0.97	36.84	0.98	36.79	0.95	37.31	0.96
15	35.24	0.97	35.46	0.97	35.86	0.98	35.81	0.98	36.4	0.91
16	34.23	1.01	34.48	0.98	34.87	0.99	34.83	0.98	35.44	0.96
17	33.18	1.05	33.42	1.06	33.85	1.02	33.8	1.03	34.44	1
18	32.19	0.99	32.42	1	32.82	1.03	32.82	0.98	33.4	1.04
19	31.21	0.98	31.47	0.95	31.88	0.94	31.86	0.96	32.41	0.99
20	30.2	1.01	30.44	1.03	30.56	1.32	30.88	0.98	31.48	0.93
21	29.19	1.01	29.45	0.99	29.86	0.7	29.92	0.96	30.6	0.88
22	28.2	0.99	28.42	1.03	28.83	1.03	28.93	0.99	29.72	0.88
23	27.18	1.02	27.42	1	27.87	0.96	27.93	1	28.74	0.98
24	26.2	0.98	26.42	1	26.89	0.98	26.98	0.95	27.81	0.93
25	25.22	0.98	25.47	0.95	25.89	1	26	0.98	26.86	0.95
26	24.23	0.99	24.45	1.02	24.91	0.98	25.04	0.96	25.9	0.96
27	23.22	1.01	23.47	0.98	23.94	0.97	24.06	0.98	24.96	0.94
28	22.22	1	22.48	0.99	22.94	1	23.11	0.95	23.95	1.01
29	21.2	1.02	21.5	0.98	21.95	0.99	22.08	1.03	23	0.95
30	20.21	0.99	20.5	1	20.97	0.98	21.12	0.96	22.05	0.95

Table D-3 (continued)

	Angle of Incidence (Degrees)									
Motion	15 Degrees		30 Degrees		45 Degrees		60 Degrees		75 Degrees	
Table Position (mm)	Laser Meas. (mm)	Table Position (mm)	Laser Meas. (mm)	Table Position (mm)	Laser Meas. (mm)	Table Position (mm)	Laser Meas. (mm)	Table Position (mm)	Laser Meas. (mm)	Table Position (mm)
31	19.21	1	19.53	0.97	19.97	1	20.15	0.97	21.09	0.96
32	18.2	1.01	18.5	1.03	18.94	1.03	19.13	1.02	20.08	1.01
33	17.2	1	17.49	1.01	17.93	1.01	18.13	1	19.06	1.02
34	16.26	0.94	16.56	0.93	16.97	0.96	17.16	0.97	18.15	0.91
35	15.27	0.99	15.56	1	16.08	0.89	16.2	0.96	17.21	0.94
36	14.28	0.99	14.54	1.02	15.08	1	15.23	0.97	16.28	0.93
37	13.24	1.04	13.54	1	14.05	1.03	14.23	1	15.32	0.96
38	12.26	0.98	12.56	0.98	13.06	0.99	13.21	1.02	14.33	0.99
39	11.28	0.98	11.59	0.97	12.08	0.98	12.23	0.98	13.3	1.03
40	10.27	1.01	10.63	0.96	11.11	0.97	11.28	0.95	12.33	0.97
41	9.3	0.97	9.64	0.99	10.12	0.99	10.29	0.99	11.36	0.97
42	8.31	0.99	8.65	0.99	9.15	0.97	9.33	0.96	10.44	0.92
43	7.3	1.01	7.66	0.99	8.15	1	8.39	0.94	9.45	0.99
44	6.33	0.97	6.69	0.97	7.18	0.97	7.46	0.93		
45	5.36	0.97	5.7	0.99	6.2	0.98	6.51	0.95		
46	4.35	1.01	4.72	0.98	5.24	0.96	5.55	0.96		
47	3.36	0.99	3.72	1	4.25	0.99	4.55	1		
48	2.36	1	2.73	0.99	3.27	0.98	3.59	0.96		
49	1.4	0.96	1.77	0.96	2.31	0.96	2.61	0.98		
50	0.42	0.98	0.81	0.96	1.34	0.97	1.66	0.95		

APPENDIX E

KNOWN GEOMETRIC SHAPES

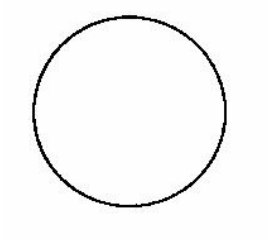

0.75” Diameter Circle

Area = 284.7 mm^2

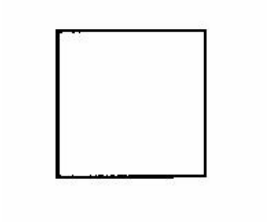

0.5” Diameter Square

Area = 163.2 mm^2

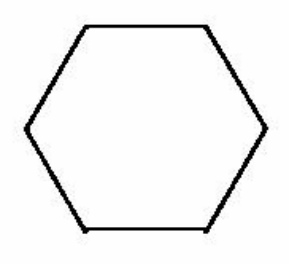

Hexagon

Area = 421.5 mm^2

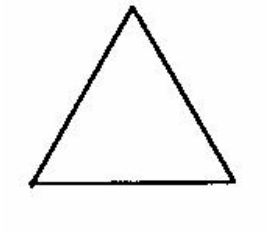

Triangle

Area = 211 mm^2

Figure E-1: Convex Shapes

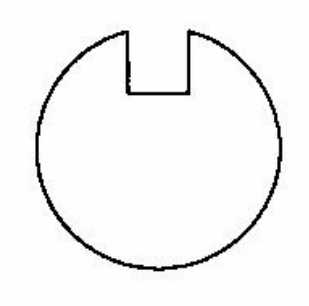

1” Diameter circle with square keyway
Area = 470.1 mm^2

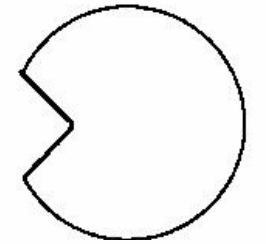

1” Diameter circle with triangle keyway
Area = 465.3 mm^2

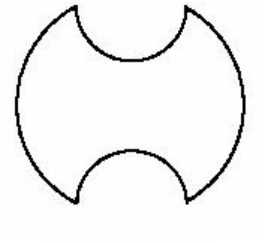

1” Diameter circle with 2 half circle cutouts
Area = 471.1 mm^2

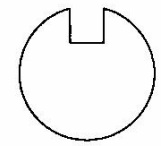

0.5” Diameter circle with square keyway
Area = 115.3 mm^2

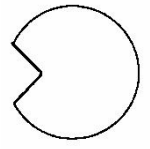

0.5” Diameter circle with triangle keyway
Area = 112.1 mm^2

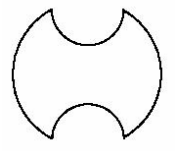

0.5” Diameter circle with 2 half circle cutouts
Area = 121.4 mm^2

Figure E- 2: Shapes with Concavities

APPENDIX F

PERFORMANCE OF CCD LASER REFLECTANCE SYSTEM AND LASER MICROMETER SYSTEM FOR DIFFERENT CROSS-SECTIONS

CCD Laser Reflectance System

Laser Micrometer System

Circle

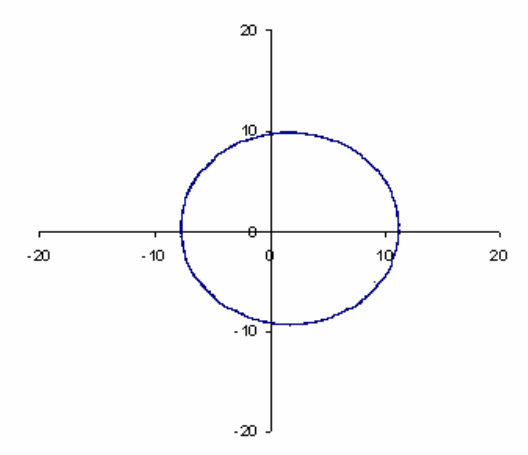

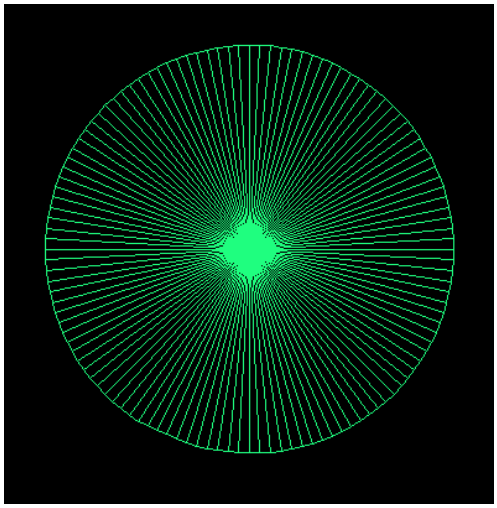

Cross-Sectional Area: 283.9±0.6 mm^2
Percent Error: -0.3%

Cross-Sectional Area: 285.2±0.1 mm^2
Percent Error: 0.2%

CCD Laser Reflectance System

Laser Micrometer System

Hexagon

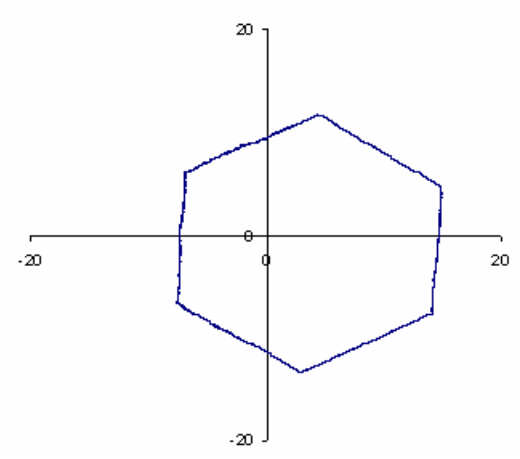

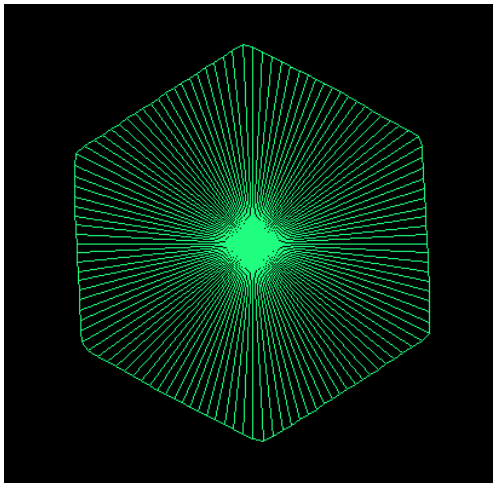

Cross-Sectional Area: 410.7±1.5 mm^2
Percent Error: -1.5%

Cross-Sectional Area: 425.1±1.3 mm^2
Percent Error: 1.3%

Square

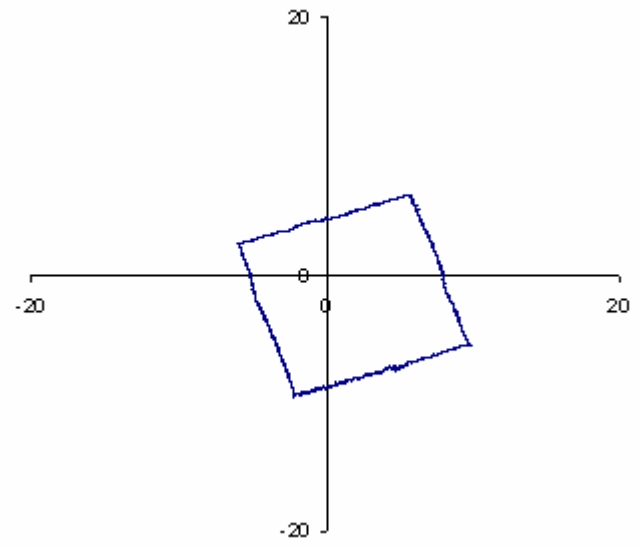

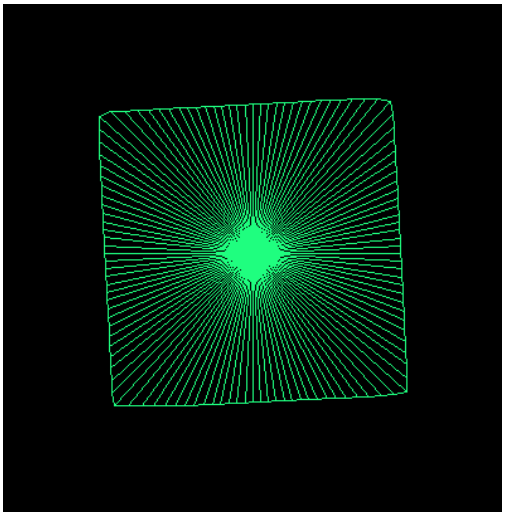

Cross-Sectional Area: 150.7±0.1 mm^2
Percent Error: -7.6%

Cross-Sectional Area: 166.2 ±0.9 mm^2
Percent Error: 1.8%

CCD Laser Reflectance System

Laser Micrometer System

Triangle

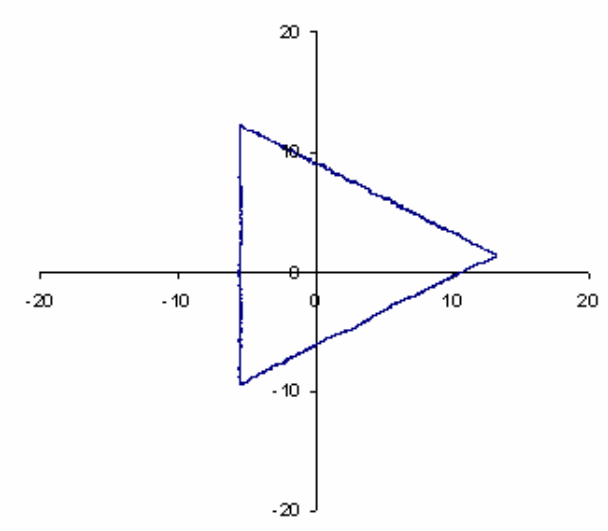

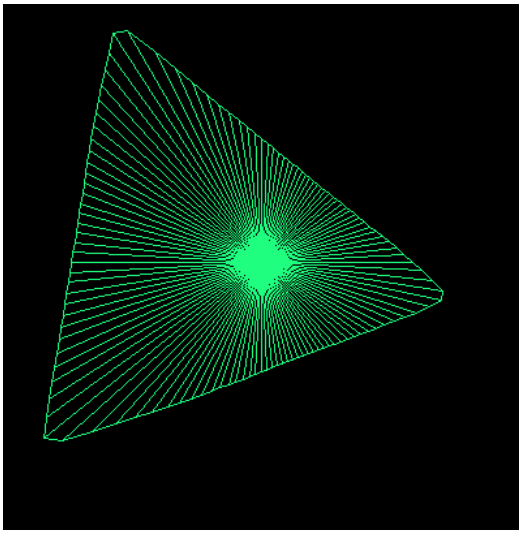

Cross-Sectional Area: 202.5±2.6 mm^2
Percent Error: -4.0%

Cross-Sectional Area: 225.5±3.2 mm^2
Percent Error: 6.9%

1” Diameter Circle with 2 Half Circle Cutouts

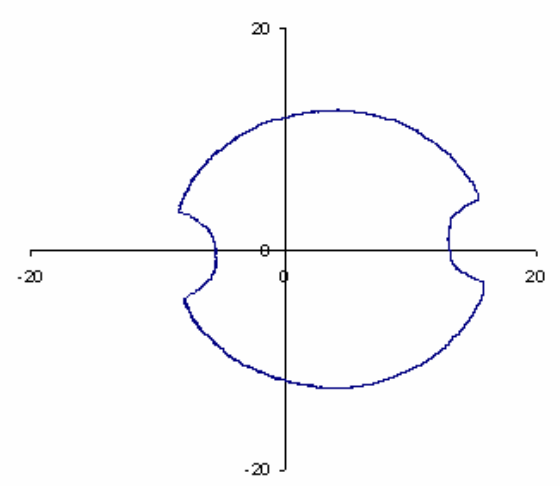

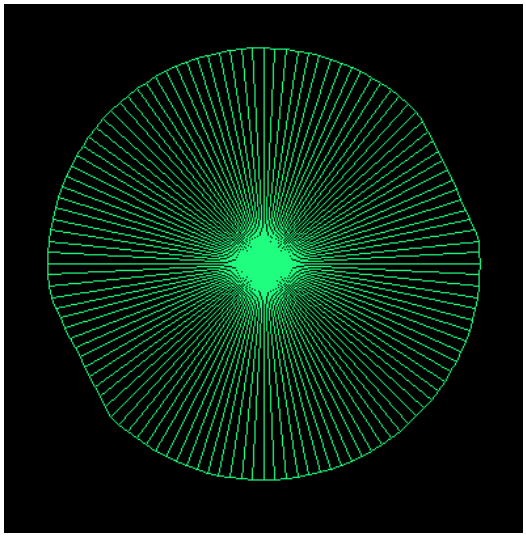

Cross-Sectional Area: 462.0±0.6 mm^2
Percent Error: -1.9%

Cross-Sectional Area: 501.7±0.3 mm^2
Percent Error: 6.5%

CCD Laser Reflectance System **Laser Micrometer System**

0.5” Diameter Circle with 2 Half Circle Cutouts

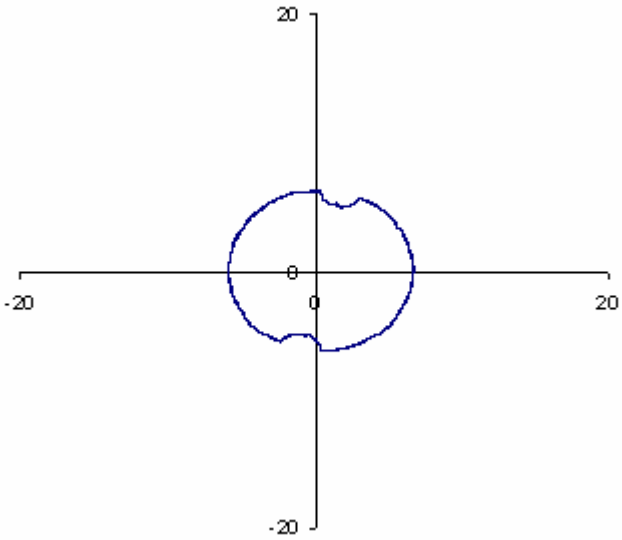

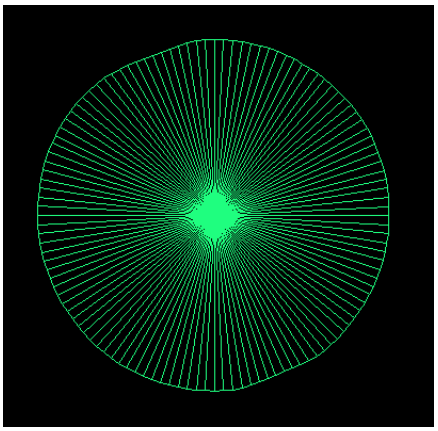

Cross-Sectional Area: 114.2 ±0.4 mm^2
Percent Error: -6.0 %

Cross-Sectional Area: 126.1±0.4 mm^2
Percent Error: 3.9%

1” Diameter Circle with Square Keyway

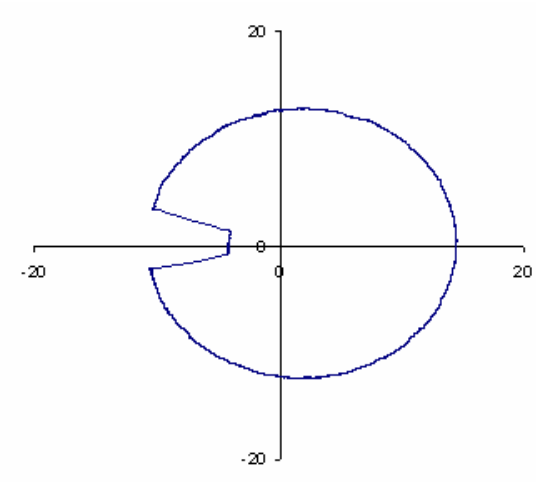

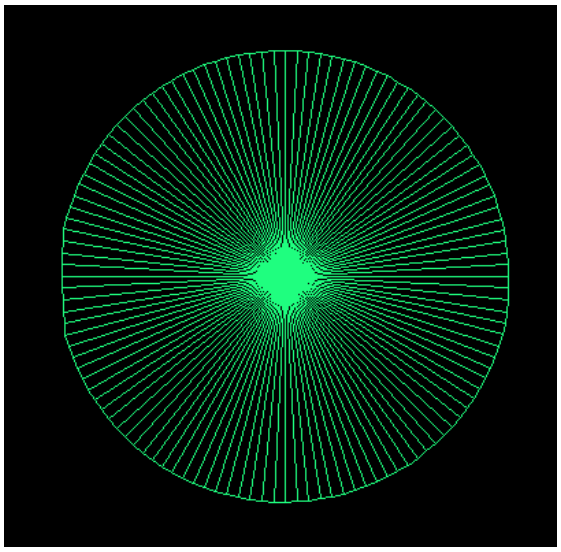

Cross-Sectional Area: 463.4±3.3 mm^2
Percent Error: -1.4%

Cross-Sectional Area: 506.1±0.5 mm^2
Percent Error: 7.7%

CCD Laser Reflectance System

Laser Micrometer System

1” Diameter Circle with Triangle Keyway

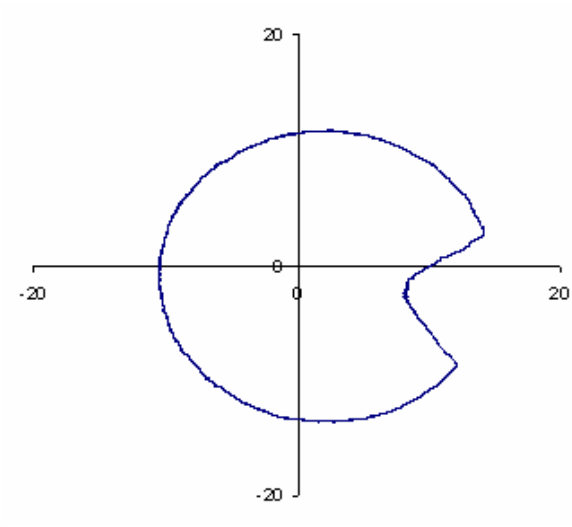

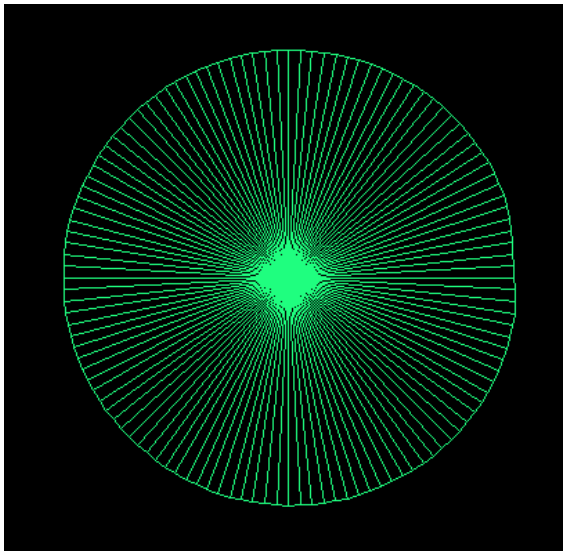

Cross-Sectional Area: 453.1±2.2 mm^2
Percent Error: -2.6%

Cross-Sectional Area: 497.8±0.4 mm^2
Percent Error: 7.0%

0.5” Diameter Circle with Square Keyway

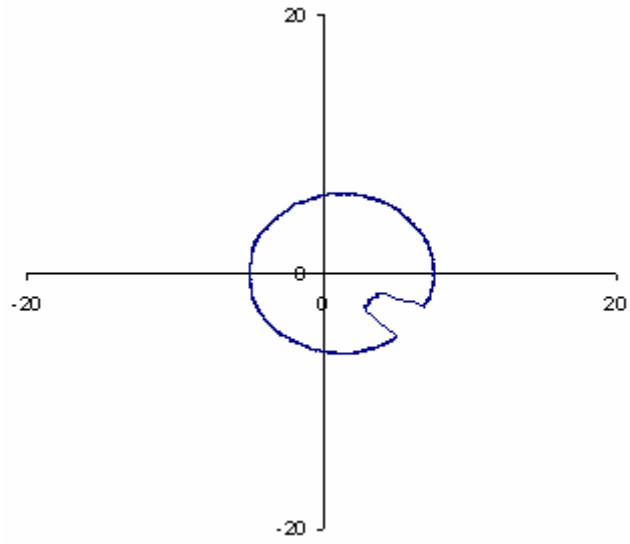

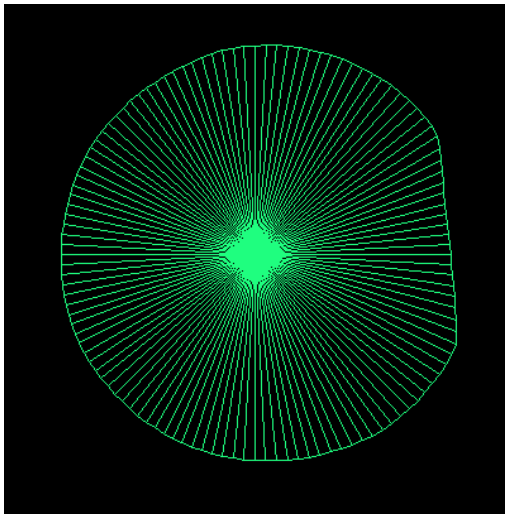

Cross-Sectional Area: 112.0±1.7 mm^2
Percent Error: -2.9%

Cross-Sectional Area: 126.0±0.1 mm^2
Percent Error: 9.3%

CCD Laser Reflectance System **Laser Micrometer System**

0.5” Diameter Circle with Triangle Keyway

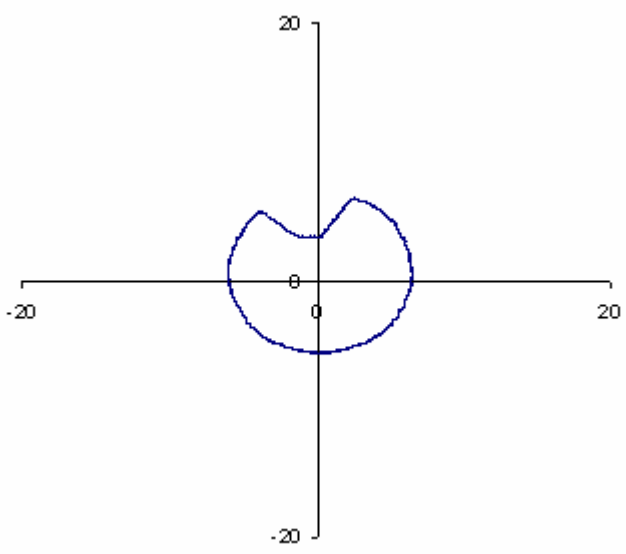

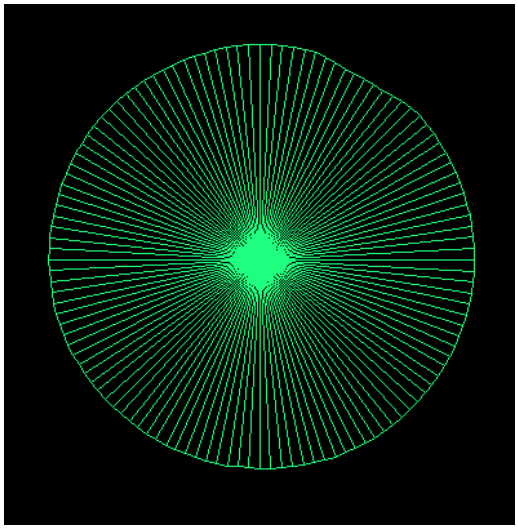

Cross-Sectional Area: 107.2±1.5 mm^2
Percent Error: -4.37%

Cross-Sectional Area: 123.0 ±0.2 mm^2
Percent Error: 9.7%

“Kidney Bean” Shape

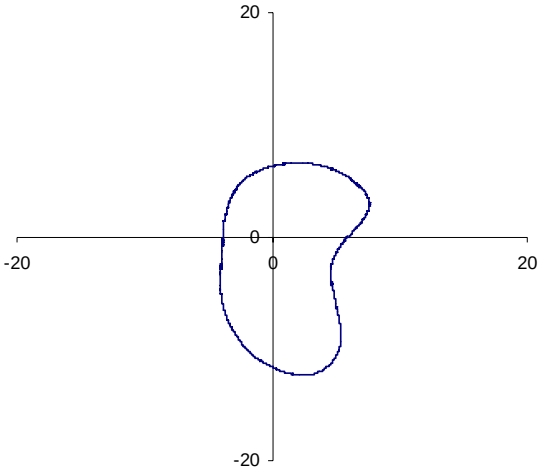

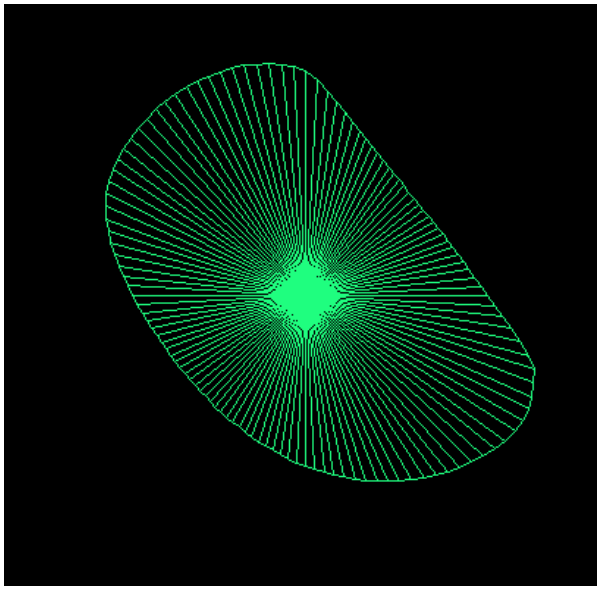

Cross-Sectional Area: 160.7±0.4 mm^2

Cross-Sectional Area: 177.2±0.7 mm^2

CCD Laser Reflectance System

Laser Micrometer System

Porcine ACL

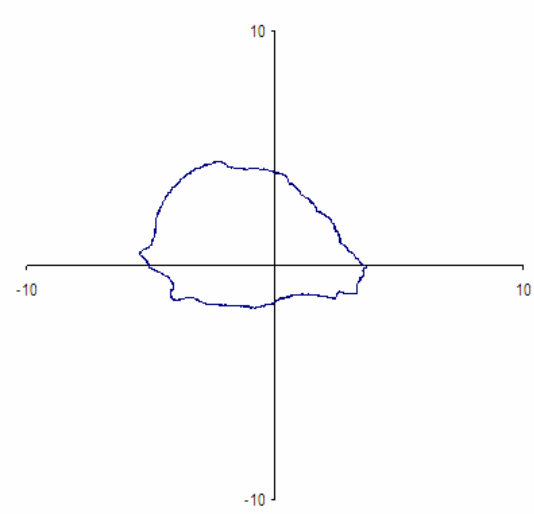

Cross-Sectional Area: 40.7±1.4 mm^2

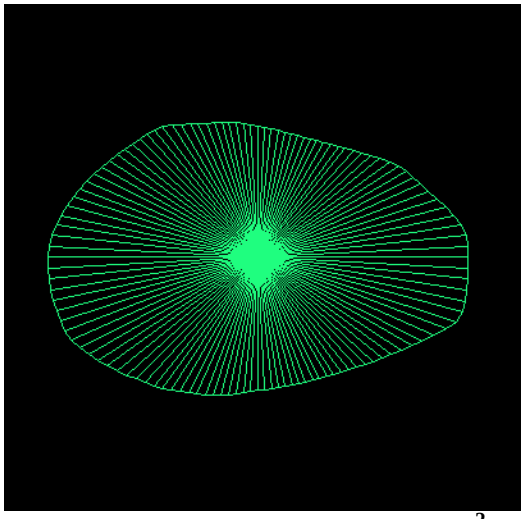

Cross-Sectional Area: 50.8±0.2 mm^2

Porcine PCL

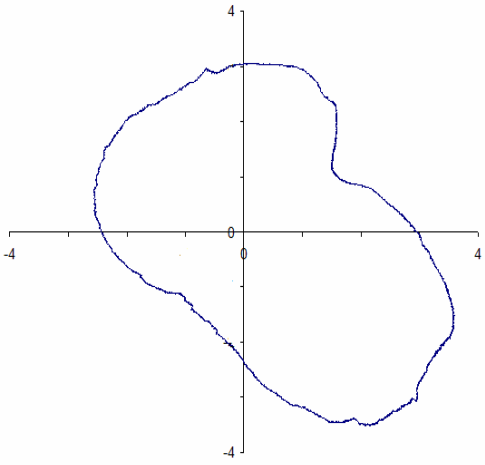

Cross-Sectional Area: 26.3±1.3 mm^2

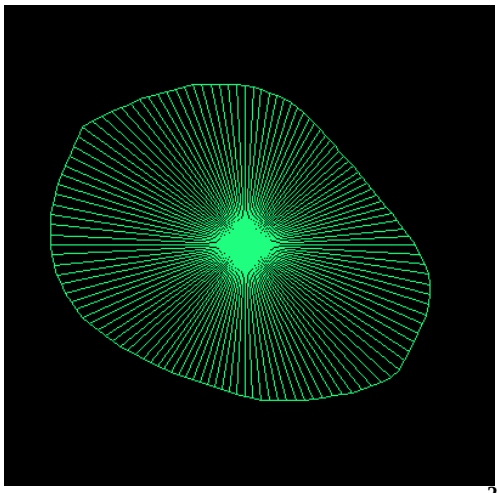

Cross-Sectional Area: 38.6±0.4 mm^2

CCD Laser Reflectance System **Laser Micrometer System**

Porcine Patellar Tendon

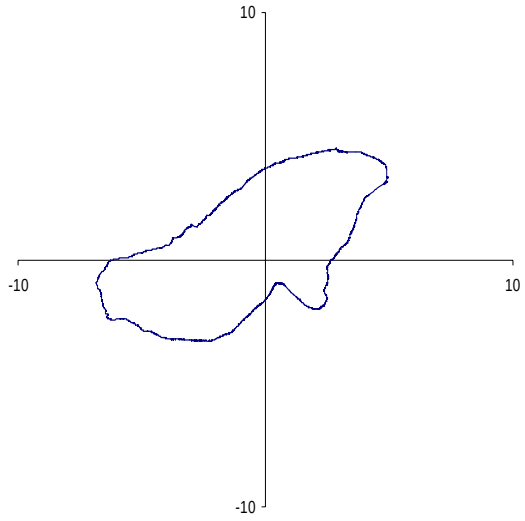

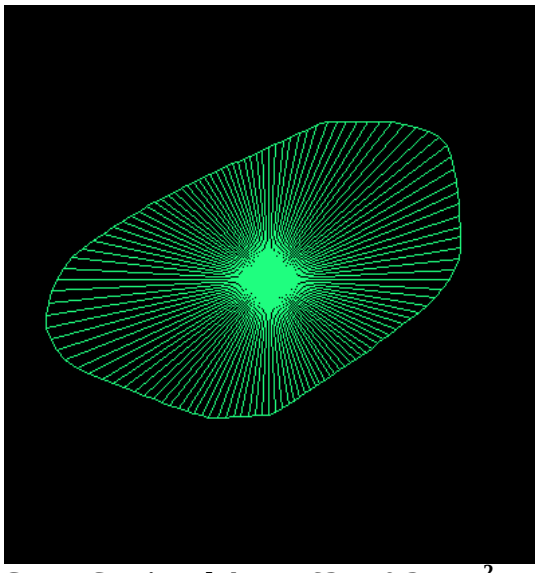

Cross-Sectional Area: 48.6±1.3 mm^2 **Cross-Sectional Area: 63.1±0.3 mm^2**

Figure F-1: Comparison of cross-sectional shapes and areas obtained for all geometric shapes and specimens in the CCD laser reflectance system and the laser micrometer system (mean±SD)

APPENDIX G

SENSITIVITY ANALYSIS FOR CIRCULAR SYSTEM CONFIGURATION: EFFECTS OF MISCALCULATION OF "R" FOR CIRCULAR CROSS-SECTIONS OF VARIOUS SIZES

Table G-1: Effects of Miscalculation of "R" on Circle with Diameter = 2 mm

Offset	Area	% Error
Ideal	3.14 mm^2	0.00%
-0.1 mm	3.80 mm^2	21.00%
+0.1 mm	2.54 mm^2	-19.00%
-0.05 mm	3.46 mm^2	10.25%
+0.05 mm	2.84 mm^2	-9.75%
-0.025 mm	3.30 mm^2	5.06%
+0.025 mm	2.99 mm^2	-4.94%
-0.01 mm	3.20 mm^2	2.01%
+0.01 mm	3.08 mm^2	-1.99%

Table G-2: Effects of Miscalculation of "R" on Circle with Diameter = 4 mm

Offset	Area	% Error
Ideal	12.57 mm^2	0.00%
-0.1 mm	13.85 mm^2	10.25%
+0.1 mm	11.34 mm^2	-9.75%
-0.05 mm	13.20 mm^2	5.06%
+0.05 mm	11.95 mm^2	-4.94%
-0.025 mm	12.88 mm^2	2.52%
+0.025 mm	12.25 mm^2	-2.48%
-0.01 mm	12.69 mm^2	1.00%
+0.01 mm	12.44 mm^2	-1.00%

Table G-3: Effects of Miscalculation of "R" on Circle with Diameter = 8 mm

Offset	Area	% Error
Ideal	50.27 mm^2	0.00%
-0.1 mm	52.81 mm^2	5.06%
+0.1 mm	47.78 mm^2	-4.94%
-0.05 mm	51.53 mm^2	2.52%
+0.05 mm	49.02 mm^2	-2.48%
-0.025 mm	50.90 mm^2	1.25%
+0.025 mm	49.64 mm^2	-1.25%
-0.01 mm	50.52 mm^2	0.50%
+0.01 mm	50.01 mm^2	-0.50%

Table G-4: Effects of Miscalculation of "R" on Circle with Diameter = 12 mm

Offset	Area	% Error
Ideal	113.10 mm^2	0.00%
-0.1 mm	116.90 mm^2	3.36%
+0.1 mm	109.36 mm^2	-3.31%
-0.05 mm	114.99 mm^2	1.67%
+0.05 mm	111.22 mm^2	-1.66%
-0.025 mm	114.04 mm^2	0.84%
+0.025 mm	112.16 mm^2	-0.83%
-0.01 mm	113.47 mm^2	0.33%
+0.01 mm	112.72 mm^2	-0.33%

Table G-5: Effects of Miscalculation of "R" on Circle with Diameter = 16 mm

Offset	Area	% Error
Ideal	201.06 mm^2	0.00%
-0.1 mm	206.12 mm^2	2.52%
+0.1 mm	196.07 mm^2	-2.48%
-0.05 mm	203.58 mm^2	1.25%
+0.05 mm	198.56 mm^2	-1.25%
-0.025 mm	202.32 mm^2	0.63%
+0.025 mm	199.81 mm^2	-0.62%
-0.01 mm	201.56 mm^2	0.25%
+0.01 mm	200.56 mm^2	-0.25%

APPENDIX H

SENSITIVITY ANALYSIS FOR CIRCULAR SYSTEM CONFIGURATION: EFFECTS OF MISCALCULATION OF "R" FOR SQUARE CROSS-SECTIONS OF VARIOUS SIZES

Table H-1: Effects of Miscalculation of "R" on Square with Sides = 2 mm

Offset	Area	% Error
Ideal	4.00 mm^2	0.00%
-0.1 mm	4.74 mm^2	18.40%
+0.1 mm	3.33 mm^2	-16.84%
-0.05 mm	4.36 mm^2	9.01%
+0.05 mm	3.66 mm^2	-8.62%
-0.025 mm	4.18 mm^2	4.46%
+0.025 mm	3.83 mm^2	-4.36%
-0.01 mm	4.07 mm^2	1.77%
+0.01 mm	3.93 mm^2	-1.75%

Table H-2: Effects of Miscalculation of "R" on Square with Sides = 4 mm

Offset	Area	% Error
Ideal	16.00 mm^2	0.00%
-0.1 mm	17.44 mm^2	9.00%
+0.1 mm	14.62 mm^2	-8.63%
-0.05 mm	16.71 mm^2	4.44%
+0.05 mm	15.30 mm^2	-4.38%
-0.025 mm	16.35 mm^2	2.19%
+0.025 mm	15.65 mm^2	-2.19%
-0.01 mm	16.14 mm^2	0.88%
+0.01 mm	15.86 mm^2	-0.88%

Table H-3: Effects of Miscalculation of "R" on Square with Sides = 8 mm

Offset	Area	% Error
Ideal	64.00 mm^2	0.00%
-0.1 mm	66.85 mm^2	4.45%
+0.1 mm	61.21 mm^2	-4.36%
-0.05 mm	65.42 mm^2	2.22%
+0.05 mm	62.60 mm^2	-2.19%
-0.025 mm	64.71 mm^2	1.10%
+0.025 mm	63.30 mm^2	-1.10%
-0.01 mm	64.28 mm^2	0.44%
+0.01 mm	63.72 mm^2	-0.44%

Table H-4: Effects of Miscalculation of "R" on Square with Sides = 12 mm

Offset	Area	% Error
Ideal	144.00 mm^2	0.00%
-0.1 mm	148.25 mm^2	2.95%
+0.1 mm	139.80 mm^2	-2.92%
-0.05 mm	146.12 mm^2	1.47%
+0.05 mm	141.89 mm^2	-1.46%
-0.025 mm	145.06 mm^2	0.74%
+0.025 mm	142.94 mm^2	-0.73%
-0.01 mm	144.42 mm^2	0.29%
+0.01 mm	143.58 mm^2	-0.29%

Table H-5: Effects of Miscalculation of "R" on Square with Sides = 16 mm

Offset	Area	% Error
Ideal	256.00 mm^2	0.00%
-0.1 mm	261.65 mm^2	2.21%
+0.1 mm	250.39 mm^2	-2.19%
-0.05 mm	258.83 mm^2	1.10%
+0.05 mm	253.19 mm^2	-1.10%
-0.025 mm	257.41 mm^2	0.55%
+0.025 mm	254.59 mm^2	-0.55%
-0.01 mm	256.56 mm^2	0.22%
+0.01 mm	255.44 mm^2	-0.22%

APPENDIX I

SENSITIVITY ANALYSIS FOR CIRCULAR SYSTEM CONFIGURATION: EFFECTS OF LASER MISALIGNMENT FOR CIRCULAR CROSS-SECTIONS OF VARIOUS SIZES

Table I-1: Effects of Laser Misalignment on Circle with Diameter = 2 mm

Offset	Area	% Error
Ideal	3.14 mm^2	0.00%
±0.1 mm	3.11 mm^2	-0.96%
±0.05 mm	3.13 mm^2	-0.32%
±0.025 mm	3.14 mm^2	0.00%
±0.01 mm	3.14 mm^2	0.00%

Table I-2: Effects of Laser Misalignment on Circle with Diameter = 4 mm

Offset	Area	% Error
Ideal	12.57 mm^2	0.00%
±0.1 mm	12.53 mm^2	-0.32%
±0.05 mm	12.56 mm^2	-0.08%
±0.025 mm	12.56 mm^2	-0.08%
±0.01 mm	12.57 mm^2	0.00%

Table I-3: Effects of Laser Misalignment on Circle with Diameter = 8 mm

Offset	Area	% Error
Ideal	50.27 mm^2	0.00%
±0.1 mm	50.23 mm^2	-0.08%
±0.05 mm	50.26 mm^2	-0.02%
±0.025 mm	50.26 mm^2	-0.02%
±0.01 mm	50.27 mm^2	0.00%

Table I-4: Effects of Laser Misalignment on Circle with Diameter = 12 mm

Offset	Area	% Error
Ideal	113.1 mm^2	0.00%
±0.1 mm	113.07 mm^2	-0.03%
±0.05 mm	113.09 mm^2	-0.01%
±0.025 mm	113.1 mm^2	0.00%
±0.01 mm	113.1 mm^2	0.00%

Table I-5: Effects of Laser Misalignment on Circle with Diameter = 16 mm

Offset	Area	% Error
Ideal	201.06 mm^2	0.00%
±0.1 mm	201.03 mm^2	-0.01%
±0.05 mm	201.05 mm^2	0.00%
±0.025 mm	201.06 mm^2	0.00%
±0.01 mm	201.06 mm^2	0.00%

APPENDIX J

SENSITIVITY ANALYSIS FOR CIRCULAR SYSTEM CONFIGURATION: EFFECTS OF LASER MISALIGNMENT FOR SQUARE CROSS-SECTIONS OF VARIOUS SIZES

Table J-1: Effects of Laser Misalignment on Square with Sides = 2 mm

Offset	Area	% Error
Ideal	4.00 mm^2	0.00%
±0.1 mm	3.68 mm^2	-8.00%
±0.05 mm	3.84 mm^2	-4.00%
±0.025 mm	3.92 mm^2	-2.00%
±0.01 mm	3.97 mm^2	-0.75%

Table J-2: Effects of Laser Misalignment on Square with Sides = 4 mm

Offset	Area	% Error
Ideal	16.00 mm^2	0.00%
±0.1 mm	15.35 mm^2	-4.06%
±0.05 mm	15.67 mm^2	-2.06%
±0.025 mm	15.83 mm^2	-1.06%
±0.01 mm	15.93 mm^2	-0.44%

Table J-3: Effects of Laser Misalignment on Square with Sides = 8 mm

Offset	Area	% Error
Ideal	64.00 mm^2	0.00%
±0.1 mm	62.68 mm^2	-2.06%
±0.05 mm	63.34 mm^2	-1.03%
±0.025 mm	63.67 mm^2	-0.52%
±0.01 mm	63.87 mm^2	-0.20%

Table J-4: Effects of Laser Misalignment on Square with Sides = 12 mm

Offset	Area	% Error
Ideal	144.00 mm^2	0.00%
±0.1 mm	142.02 mm^2	-1.37%
±0.05 mm	143.01 mm^2	-0.69%
±0.025 mm	143.50 mm^2	-0.35%
±0.01 mm	143.8 mm^2	-0.14%

Table J-5: Effects of Laser Misalignment on Square with Sides = 16 mm

Offset	Area	% Error
Ideal	256.00 mm^2	0.00%
±0.1 mm	253.36 mm^2	-1.03%
±0.05 mm	254.68 mm^2	-0.52%
±0.025 mm	255.34 mm^2	-0.26%
±0.01 mm	255.74 mm^2	-0.10%

APPENDIX K

THE EFFECT OF ACCOUNTING FOR CONCAVITIES ON THE ACCURACY OF CROSS-SECTIONAL AREA MEASUREMENTS FOR THE MCL AND ACL

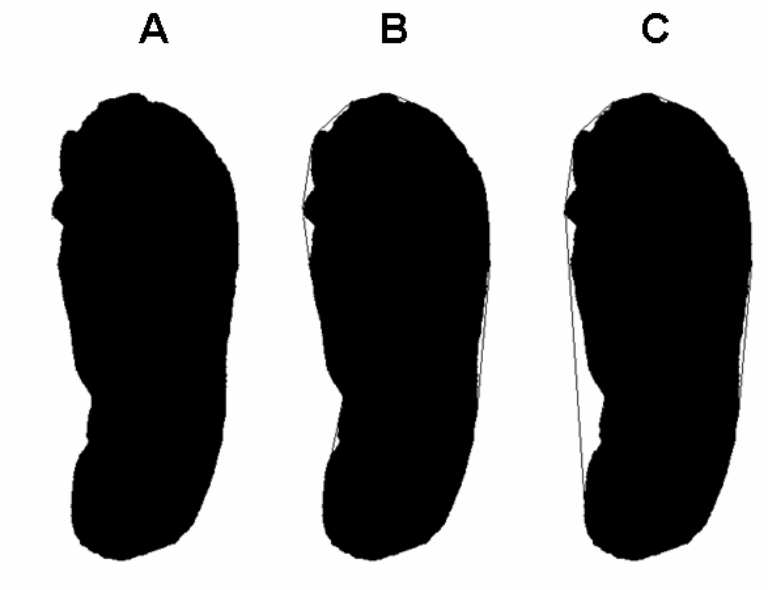

Figure K-1: **(A) A sample cross-section of a normal MCL. If the CCD laser reflectance system were to be unable to detect small concavities (B), then the resulting error in the cross-sectional area measurement would be approximately 2.3%. If none of the concavities are accounted for (C), then a 6.5% error in the cross-sectional area measurement would result.**

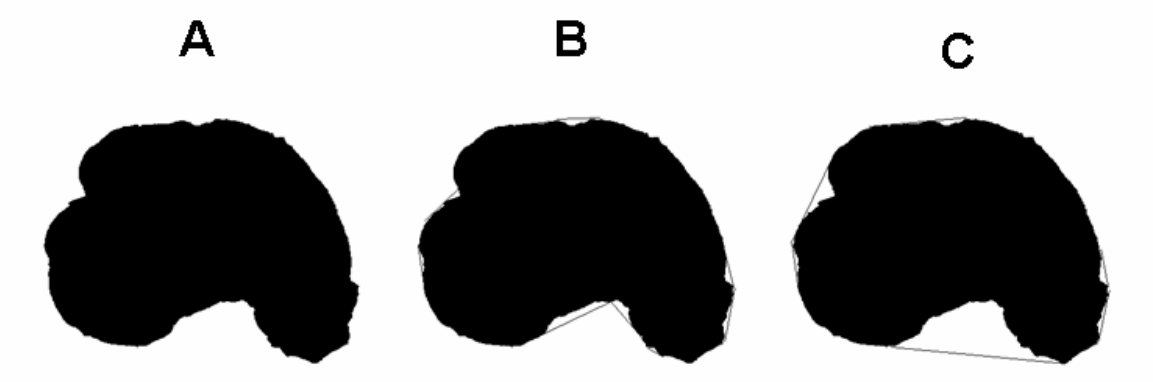

Figure K-2: **(A) A sample cross-section of a porcine ACL. If the CCD laser reflectance were to be unable to detect small concavities (B), then the resulting error in the cross-sectional area measurement would be approximately 2.3%. If none of the concavities are accounted for (C), then a 10.1% error in the cross-sectional area measurement would result.**

BIBLIOGRAPHY

1. Miyasaka, KC, DM Daniel, ML Stone, and P Hirshman, *The incidence of knee ligament injuries in the general population.* Am J Knee Surg, 1991. **4**: p. 3-8.

2. Beaty, J, ed. *Knee and leg: soft tissue trauma*. Orthopaedic knowledge update. Vol. 6. 1999, American Academy of Orthopaedic Surgeons: Rosemont, IL. 533.

3. Indelicato, PA, *Non-operative treatment of complete tears of the medial collateral ligament of the knee.* J Bone Joint Surg Am, 1983. **65**(3): p. 323-9.

4. Jokl, P, N Kaplan, P Stovell, and K Keggi, *Non-operative treatment of severe injuries to the medial and anterior cruciate ligaments of the knee.* J Bone Joint Surg Am, 1984. **66**(5): p. 741-4.

5. Kannus, P, *Long-term results of conservatively treated medial collateral ligament injuries of the knee joint.* Clin Orthop, 1988(226): p. 103-12.

6. Frank, C, SL-Y Woo, D Amiel, F Harwood, M Gomez, and W Akeson, *Medial collateral ligament healing. A multidisciplinary assessment in rabbits.* Am J Sports Med, 1983. **11**(6): p. 379-89.

7. Gomez, MA, SL-Y Woo, M Inoue, D Amiel, FL Harwood, and L Kitabayashi, *Medial collateral ligament healing subsequent to different treatment regimens.* J Appl Physiol, 1989. **66**(1): p. 245-52.

8. Ohland, KJ, SL-Y Woo, JA Weiss, S Takai, and MS Shelley. *Healing of combined injuries of the rabbit medial collateral ligament and its insertions: A long term study on the effects of conservative vs. surgical treatment*. in *ASME Adv Bioeng*. 1991.

9. Weiss, JA, SL-Y Woo, KJ Ohland, S Horibe, and PO Newton, *Evaluation of a new injury model to study medial collateral ligament healing: Primary repair versus nonoperative treatment.* J Orthop Res, 1991. **9**(4): p. 516-28.

10. Woo, SL-Y, M Inoue, E McGurk-Burleson, and MA Gomez, *Treatment of the medial collateral ligament injury. II: Structure and function of canine knees in response to differing treatment regimens.* Am J Sports Med, 1987. **15**(1): p. 22-9.

11. Fetto, JF and JL Marshall, *The natural history and diagnosis of anterior cruciate ligament insufficiency.* Clin Orthop, 1980(147): p. 29-38.

12. Kannus, P and M Jarvinen, *Conservatively treated tears of the anterior cruciate ligament. Long-term results.* J Bone Joint Surg Am, 1987. **69**(7): p. 1007-12.

13. Parolie, JM and JA Bergfeld, *Long-term results of nonoperative treatment of isolated posterior cruciate ligament injuries in the athlete.* Am J Sports Med, 1986. **14**(1): p. 35-8.

14. Aglietti, P, R Buzzi, F Giron, AJ Simeone, and G Zaccherotti, *Arthroscopic-assisted anterior cruciate ligament reconstruction with the central third patellar tendon. A 5-8-year follow-up.* Knee Surg Sports Traumatol Arthrosc, 1997. **5**(3): p. 138-44.

15. McCormick, WC, RJ Bagg, CW Kennedy, Jr., and CA Leukens, *Reconstruction of the posterior cruciate ligament: preliminary report of a new procedure.* Clin Orthop, 1976(118): p. 30-1.

16. Woo, SL-Y, A Kanamori, J Zeminski, M Yagi, C Papageorgiou, and FH Fu, *The effectiveness of reconstruction of the anterior cruciate ligament with hamstrings and patellar tendon . A cadaveric study comparing anterior tibial and rotational loads.* J Bone Joint Surg Am, 2002. **84-A**(6): p. 907-14.

17. Yagi, M, EK Wong, A Kanamori, RE Debski, FH Fu, and SL Woo, *Biomechanical analysis of an anatomic anterior cruciate ligament reconstruction.* Am J Sports Med, 2002. **30**(5): p. 660-6.

18. Aune, AK, I Holm, MA Risberg, HK Jensen, and H Steen, *Four-strand hamstring tendon autograft compared with patellar tendon-bone autograft for anterior cruciate ligament reconstruction. A randomized study with two-year follow-up.* Am J Sports Med, 2001. **29**(6): p. 722-8.

19. Anderson, AF, RB Snyder, and AB Lipscomb, Jr., *Anterior cruciate ligament reconstruction. A prospective randomized study of three surgical methods.* Am J Sports Med, 2001. **29**(3): p. 272-9.

20. Bach, BR, Jr., S Tradonsky, J Bojchuk, ME Levy, CA Bush-Joseph, and NH Khan, *Arthroscopically assisted anterior cruciate ligament reconstruction using patellar tendon autograft. Five- to nine-year follow-up evaluation.* Am J Sports Med, 1998. **26**(1): p. 20-9.

21. Jomha, NM, LA Pinczewski, A Clingeleffer, and DD Otto, *Arthroscopic reconstruction of the anterior cruciate ligament with patellar-tendon autograft and interference screw fixation. The results at seven years.* J Bone Joint Surg Br, 1999. **81**(5): p. 775-9.

22. Ritchie, JR and RD Parker, *Graft selection in anterior cruciate ligament revision surgery.* Clin Orthop, 1996(325): p. 65-77.

23. Linsenmayer, TF, E Gibney, F Igoe, MK Gordon, JM Fitch, LI Fessler, and DE Birk, *Type V collagen: molecular structure and fibrillar organization of the chicken α1(V) NH2-terminal domain, a putative regulator of corneal fibrillogenesis.* J Cell Biol, 1993. **121**(5): p. 1181-9.

24. Niyibizi, C, K Kavalkovich, T Yamaji, and SL-Y Woo, *Type V collagen is increased during rabbit medial collateral ligament healing.* Knee Surg Sports Traumatol Arthrosc, 2000. **8**(5): p. 281-5.

25. Smutz, WP, M Drexler, LJ Berglund, E Growney, and KN An, *Accuracy of a video strain measurement system.* J Biomech, 1996. **29**(6): p. 813-7.

26. Woo, SL-Y, MA Gomez, Y Seguchi, CM Endo, and WH Akeson, *Measurement of mechanical properties of ligament substance from a bone-ligament-bone preparation.* J Orthop Res, 1983. **1**(1): p. 22-9.

27. Harner, CD, GA Livesay, S Kashiwaguchi, H Fujie, NY Choi, and SL Woo, *Comparative study of the size and shape of human anterior and posterior cruciate ligaments.* J Orthop Res, 1995. **13**(3): p. 429-34.

28. Wright, DGaR, D.C., *A Study of the Elastic Properties of Plantar Fascia.* Journal of Bone and Joint Surgery, 1984. **46-A**: p. 482-492.

29. Butler, DL, ES Grood, FR Noyes, RF Zernicke, and K Brackett, *Effects of structure and strain measurement technique on the material properties of young human tendons and fascia.* J Biomech, 1984. **17**(8): p. 579-96.

30. Race, A and AA Amis, *The mechanical properties of the two bundles of the human posterior cruciate ligament.* J Biomech, 1994. **27**(1): p. 13-24.

31. Ellis, DG, *Cross-Sectional Area Measurements for Tendon Specimens: A Comparison of Several Methods.* Journal of Biomechanics, 1969. **2**: p. 175-186.

32. Lee, TQ and SL Woo, *A new method for determining cross-sectional shape and area of soft tissues.* J Biomech Eng, 1988. **110**(2): p. 110-4.

33. Woo, SL-Y, MI Danto, KJ Ohland, TQ Lee, and PO Newton, *The use of a laser micrometer system to determine the cross-sectional shape and area of ligaments: a comparative study with two existing methods.* J Biomech Eng, 1990. **112**(4): p. 426-31.

34. Odensten, M and J Gillquist, *Functional anatomy of the anterior cruciate ligament and a rationale for reconstruction.* J Bone Joint Surg Am, 1985. **67**(2): p. 257-62.

35. Woo, SL-Y, KN An, SP Arnoczky, JS Wayne, DC Fithian, and M B.S., *Anatomy, biology, and biomechanics of tendon, ligament, and meniscus*, in *Orthopaedic Basic Science*, S.R. Simon, Editor. 1994, Am Acad Orthop Surg: Rosemont, IL. p. 45-87.

36. Kastelic, J, A Galeski, and E Baer, *The multicomposite structure of tendon.* Connect Tissue Res, 1978. **6**(1): p. 11-23.

37. Kastelic, J and E Baer, *Deformation in tendon collagen.* Symp Soc Exp Biol, 1980. **34**: p. 397-435.

38. Woo, SL-Y, MA Gomez, and WH Akeson, *The time and history-dependent viscoelastic properties of the canine medical collateral ligament.* J Biomech Eng, 1981. **103**(4): p. 293-8.

39. Johnson, GA, GA Livesay, SL-Y Woo, and KR Rajagopal, *A single integral finite strain viscoelastic model of ligaments and tendons.* J Biomech Eng, 1996. **118**(2): p. 221-6.

40. Woo, SL, MA Gomez, and WH Akeson, *The time and history-dependent viscoelastic properties of the canine medical collateral ligament.* J Biomech Eng, 1981. **103**(4): p. 293-8.

41. Sakane, M, GA Livesay, RJ Fox, TW Rudy, TJ Runco, and SL Woo, *Relative contribution of the ACL, MCL, and bony contact to the anterior stability of the knee.* Knee Surg Sports Traumatol Arthrosc, 1999. **7**(2): p. 93-7.

42. Sakane, M, RJ Fox, SL-Y Woo, GA Livesay, G Li, and FH Fu, *In situ forces in the anterior cruciate ligament and its bundles in response to anterior tibial loads.* J Orthop Res, 1997. **15**(2): p. 285-93.

43. Wong, EK, *In-Situ Forces in the Bundles of the ACL during Simulated Joint Motions: An Experimental and Computational Approach*, in *Bioengineering*. 2000, University of Pittsburgh: Pittsburgh. p. 1-77.

44. Girgis, FG, JL Marshall, and A Monajem, *The cruciate ligaments of the knee joint. Anatomical, functional and experimental analysis.* Clin Orthop, 1975(106): p. 216-31.

45. Lyon, RM, WH Akeson, D Amiel, LR Kitabayashi, and SL Woo, *Ultrastructural differences between the cells of the medical collateral and the anterior cruciate ligaments.* Clin Orthop, 1991(272): p. 279-86.

46. Schmidt, CC, HI Georgescu, CK Kwoh, GL Blomstrom, CP Engle, LA Larkin, CH Evans, and SL Woo, *Effect of growth factors on the proliferation of fibroblasts from the medial collateral and anterior cruciate ligaments.* J Orthop Res, 1995. **13**(2): p. 184-90.

47. Frank, C, D McDonald, D Bray, R Bray, R Rangayyan, D Chimich, and N Shrive, *Collagen fibril diameters in the healing adult rabbit medial collateral ligament.* Connect Tissue Res, 1992. **27**(4): p. 251-63.

48. Musahl, V, SD Abramowitch, TW Gilbert, JH-C Wang, E Tsuda, and SL-Y Woo, *The use of porcine SIS to enhance the healing of the MCL: A functional tissue engineering study in rabbits.* J Orthop Res, 2002. **In revision**.

49. Inoue, M, E McGurk-Burleson, JM Hollis, and SL Woo, *Treatment of the medial collateral ligament injury. I: The importance of anterior cruciate ligament on the varus-valgus knee laxity.* Am J Sports Med, 1987. **15**(1): p. 15-21.

50. Engle, CP, M Noguchi, KJ Ohland, FJ Shelley, and SL Woo, *Healing of the rabbit medial collateral ligament following an O'Donoghue triad injury: effects of anterior cruciate ligament reconstruction.* J Orthop Res, 1994. **12**(3): p. 357-64.

51. Ohno, K, AS Pomaybo, CC Schmidt, RE Levine, KJ Ohland, and SL-Y Woo, *Healing of the medial collateral ligament after a combined medial collateral and anterior cruciate ligament injury and reconstruction of the anterior cruciate ligament: Comparison of repair and nonrepair of medial collateral ligament tears in rabbits.* J Orthop Res, 1995. **13**(3): p. 442-9.

52. Altman, GH, RL Horan, HH Lu, J Moreau, I Martin, JC Richmond, and DL Kaplan, *Silk matrix for tissue engineered anterior cruciate ligaments.* Biomaterials, 2002. **23**(20): p. 4131-41.

53. Badylak, SF, R Tullius, K Kokini, KD Shelbourne, T Klootwyk, SL Voytik, MR Kraine, and C Simmons, *The use of xenogeneic small intestinal submucosa as a biomaterial for Achilles tendon repair in a dog model.* J Biomed Mater Res, 1995. **29**(8): p. 977-85.

54. Badylak, S, S Arnoczky, P Plouhar, R Haut, V Mendenhall, R Clarke, and C Horvath, *Naturally occurring extracellular matrix as a scaffold for musculoskeletal repair.* Clin Orthop, 1999. **367 Suppl**: p. S333-43.

55. Gomez, MA, SL-Y Woo, D Amiel, F Harwood, L Kitabayashi, and JR Matyas, *The effects of increased tension on healing medial collateral ligaments.* Am J Sports Med, 1991. **19**(4): p. 347-54.

56. Huang, D, TR Chang, A Aggarwal, RC Lee, and HP Ehrlich, *Mechanisms and dynamics of mechanical strengthening in ligament-equivalent fibroblast-populated collagen matrices.* Ann Biomed Eng, 1993. **21**(3): p. 289-305.

57. Eastwood, M, VC Mudera, DA McGrouther, and RA Brown, *Effect of precise mechanical loading on fibroblast populated collagen lattices: morphological changes.* Cell Motil Cytoskeleton, 1998. **40**(1): p. 13-21.

58. Guido, S and RT Tranquillo, *A methodology for the systematic and quantitative study of cell contact guidance in oriented collagen gels. Correlation of fibroblast orientation and gel birefringence.* J Cell Sci, 1993. **105 (Pt 2)**: p. 317-31.

59. Dunn, GA and SW Paddock, *Analysing the motile behaviour of cells: a general approach with special reference to pairs of cells in collision.* Philos Trans R Soc Lond B Biol Sci, 1982. **299**(1095): p. 147-57.

60. Dow, JA, P Clark, P Connolly, AS Curtis, and CD Wilkinson, *Novel methods for the guidance and monitoring of single cells and simple networks in culture.* J Cell Sci Suppl, 1987. **8**: p. 55-79.

61. Wang, JH and ES Grood, *The strain magnitude and contact guidance determine orientation response of fibroblasts to cyclic substrate strains.* Connect Tissue Res, 2000. **41**(1): p. 29-36.

62. Wang, JH-C, F Jia, TW Gilbert, and SL Woo, *Cell orientation determines the alignment of cell-produced collagenous matrix.* J Biomech, 2003. **36**(1): p. 97-102.

63. Dejardin, LM, SP Arnoczky, BJ Ewers, RC Haut, and RB Clarke, *Tissue-engineered rotator cuff tendon using porcine small intestine submucosa. Histologic and mechanical evaluation in dogs.* Am J Sports Med, 2001. **29**(2): p. 175-84.

64. Cook, JL, JL Tomlinson, JM Kreeger, and CR Cook, *Induction of meniscal regeneration in dogs using a novel biomaterial.* Am J Sports Med, 1999. **27**(5): p. 658-65.

65. Sacks, MS and DC Gloeckner, *Quantification of the fiber architecture and biaxial mechanical behavior of porcine intestinal submucosa.* J Biomed Mater Res, 1999. **46**(1): p. 1-10.

66. Conkrite, AE, *The Tensile Strength of Human Tendons.* The Anatomical Record, 1936. **64**: p. 173-185.

67. Haut, RCaL, R.W., *Rheological Properties of Canine Anterior Cruciate Ligaments.* Journal of Biomechanics, 1969. **2**: p. 289-298.

68. Chan, SS, *M.S. Thesis: The Development and Evaluation of a Laser Reflectance System to Determine the Complex Cross-Sectional Shape and Area of Soft Tissues*, in *Bioengineering*. 1995, University of Pittsburgh: Pittsburgh. p. 97.

69. Walker, LB, Harris, E.H. and Benedict, J.V., *Stress-Strain Relationship in Human Cadaveric Plantaris Tendon: A Preliminary Study.* Medical Electronics and Biological Engineering, 1964. **2**(1964): p. 31-38.

70. Woo, SL, WH Akeson, and GF Jemmott, *Measurements of nonhomogeneous, directional mechanical properties of articular cartilage in tension.* J Biomech, 1976. **9**(12): p. 785-91.

71. Allard, P, PS Thiry, A Bourgault, and G Drouin, *Pressure dependence of "the area micrometer" method in evaluation of cruciate ligament cross-section.* J Biomed Eng, 1979. **1**(4): p. 265-7.

72. Race, A and AA Amis, *Cross-sectional area measurement of soft tissue. A new casting method.* J Biomech, 1996. **29**(9): p. 1207-12.

73. Shrive, NG, TC Lam, E Damson, and CB Frank, *A new method of measuring the cross-sectional area of connective tissue structures.* J Biomech Eng, 1988. **110**(2): p. 104-9.

74. Gupta, BN, Subramanian, K.N., Brinker, W.O. and Gupta, A.N., *Tensile Strength of Canine Cranial Cruciate Ligaments.* American Journal of Veterinary Research, 1971. **32**: p. 183-190.

75. Njus, GOaN, N.M. *A Noncontact Method for Determining Cross-Sectional Area of Soft Tissues*. in *32nd Annual Meeeting, Orthopaedic Research Society*. 1986.

76. Iaconis, F, R Steindler, and G Marinozzi, *Measurements of cross-sectional area of collagen structures (knee ligaments) by means of an optical method.* J Biomech, 1987. **20**(10): p. 1003-10.

77. Noguchi, M, T Kitaura, K Ikoma, and Y Kusaka, *A method of in-vitro measurement of the cross-sectional area of soft tissues, using ultrasonography.* J Orthop Sci, 2002. **7**(2): p. 247-51.

78. Narici, MV, H Hoppeler, B Kayser, L Landoni, H Claassen, C Gavardi, M Conti, and P Cerretelli, *Human quadriceps cross-sectional area, torque and neural activation during 6 months strength training.* Acta Physiol Scand, 1996. **157**(2): p. 175-86.

79. Scheffler, SU, TD Clineff, CD Papageorgiou, RE Debski, C Benjamin, and SL-Y Woo, *Structure and function of the healing medial collateral ligament in a goat model.* Ann Biomed Eng, 2001. **29**(2): p. 173-80.

80. Woo, SL-Y, CA Orlando, JF Camp, and WH Akeson, *Effects of postmortem storage by freezing on ligament tensile behavior.* J Biomech, 1986. **19**(5): p. 399-404.

81. Haut, TL, ML Hull, and SM Howell, *A high-accuracy three-dimensional coordinate digitizing system for reconstructing the geometry of diarthrodial joints.* J Biomech, 1998. **31**(6): p. 571-7.